Universität Bremen

Synthesis and Characterization of Fluorescent Iron Oxide Nanoparticles to Study Uptake and Intracellular Trafficking of Nanoparticles in Neural Cells

Dissertation

Zur Erlangung des akademischen Grades in den Naturwissenschaften (Dr. rer. nat.)

Fachbreich 2 (Biologie/Chemie)

Universität Bremen

Wiebke Willmann (née Rastedt)

2018

Erster Gutachter:	Professor Dr. Heinrich Hofmann
Zweiter Gutachter:	Professor Dr. Lucio Colombi Ciacchi

Table of Content

I. Acknowledgements

First of all, I would like to gratefully thank Prof. Dr. Ralf Dringen for giving me the opportunity to work on my doctoral thesis under his supervision and for his constant support, for his valuable advices for the practical work as well was for the writing of the manuscripts and of his never ending optimism and motivation. I admire his open door policy and the discussion with him were always very valuable and helpful to keep the focus for the important things and for the completion of this work.

Secondly I would like to thank Prof. Dr. Heinrich Hofmann and Prof. Dr. Lucio Colombi Ciacchi for being the reviewers of my thesis. I would like to direct a special thanks to Prof. Dr. Heinrich Hofmann for taken the effort to come the long way to Bremen to take part at my colloquium and to Prof. Dr. Lucio Colombi for giving me the opportunity to gain some insights into the work with the AFM.

Thanks to all recent and former members of the neurobiochemistry group for the warm and friendly welcome they provided me, the nice working atmosphere, the coffee and lunch breaks and all the little moments that made working in this group so pleasant. I am really thankful for all the scientific discussion, all the constructive words and help during my work and all the sweets and chocolate to cheer me up in the right moment. I thank my coffee buddies for the liters of coffee you drank with me in our seminar room but also in front of the building if I had decided that it was about time to catch some sunrays. Thanks to all my colleagues for all the patient with me. We had a great time together within the lab but also during various other occasions. Especially I would like to thank Felix who took his time - even after leaving the lab - to support me, and Eva for all her help and advice, her not ending support, even so she is now in Scotland -too far away for a quick coffee in the sun.

I would like to thank my family for all the support and all the encouragement that brought me so far in the first place. Thank you for making all this possible! Last but not least I owe my deepest thanks to my husband Jan! You not just encouraged and supported me the whole way, but also distracted me in your special way with the one or other crazy activity and gave me the strength to keep going. Thanks!

II. Structure of the thesis

This thesis is divided into three main chapters: The introduction (1), the results (2) and the summarizing discussion (3).

(1) The introduction gives an insight into the field of nanoparticle research with the focus on iron oxide nanoparticles including the synthesis and characterization of these materials and their interaction with cells. The section of cell-interaction also contains a short description on the uptake mechanisms of nanoparticles in cells.

(2) The results chapter of this thesis describes the data obtained and investigations made during the laboratory work of this thesis. This part is sub-divided into three chapters that are presented as publications/manuscripts. The first chapter contains a published article describing the synthesis and characterization of fluorescent iron oxide nanoparticles as well as their accumulation in C6 glioma cells. The second chapter represents a submitted manuscript on a study investigating the uptake and intracellular trafficking of fluorescent iron oxide nanoparticles using nanoparticle pulse-chase experiments in C6 glioma cells. The third chapter comprises the submitted manuscript of a review article, which sums up the special challenges of nanoparticle uptake studies in neural cells. The manuscript contains some data collected from experiments studying the effects of an exposure of neural cells to fluorescent iron oxide nanoparticles. The published article is inserted as portable document format. The submitted manuscripts are adapted to the style of the thesis with figures, tables and their legends directly placed after the result chapter or after the conclusion.

(3) The summarizing discussion chapter consolidates the key-findings of the thesis, brings them in the current context of research and presents an outlook on future perspectives regarding the use of the synthesized fluorescent iron oxide nanoparticles.
In addition to the publication and manuscripts as part of this thesis, I have made substantial contribution to the following four publications which are not included in this thesis:

- **Rastedt W**, Blumrich EM & Dringen R (2017). Metabolism of mannose in cultured primary rat neurons. *Neurochem Res*, 42: 2282-2293.

- Stapelfeldt K, Ehrke E, Steinmeier J, **Rastedt W** & Dringen R (2017). Menadione-mediated WST1 reduction assay for the determination of metabolic activity of cultured neural cells. *Anal Biochem,* 538: 42-52.

- Joshi A, **Rastedt W**, Faber K, Schultz AG, Bulcke F & Dringen R (2016). Uptake and toxicity of copper oxide nanoparticles in C6 glioma cells. *Neurochem Res,* 41: 3004-3019.

- Zhang YQ, Dringen R, Petters C, **Rastedt W**, Köser J, Filser J & Stolte S (2016). Toxicity of dimercaptosuccinate-coated and un-functionalized magnetic iron oxide nanoparticles towards aquatic organisms. *Environmental Science-Nano,* 3: 754-767.

III. Summary

Iron oxide nanoparticles (IONPs) have promising features for biomedical applications and are already used for some therapeutic and diagnostic approaches. As IONPs can reach the brain it is important to study the potential consequences of an exposure to IONPs on brain cells. In the presented thesis, fluorescent IONPs were synthesized by functionalizing the coating material dimercaptosuccinate (DMSA) of the IONPs with either the green dye Oregon Green (OG) or the red dye tetramethylrhodamine (TMR). Comparison to previously used BODIPY-labeled DMSA-coated IONPs, OG- and TMR-IONPs revealed higher fluorescence signal intensities and improved stability, while these fluorescent IONPs had almost identical physicochemical properties and colloidal stability as the corresponding non-fluorescent DMSA-coated IONPs. To investigate the accumulation of IONPs in brain cells, C6 glioma cells were used as model system. IONPs exposure studies revealed that these cells accumulate fluorescent and non-fluorescent IONPs in a time-, concentration- and temperature-dependent manner. Due to the strong fluorescence observed in cells that had been exposed to OG- or TMR-IONPs and due to the slow bleaching of cellular fluorescence, these fluorescent IONPs were considered as suitable tools for further studies of cellular uptake and intracellular trafficking of internalized IONPs.

To monitor the intracellular trafficking of fluorescent nanoparticles with improved temporal and spatial resolution, single and double nanoparticle pulse-chase experiments were established for OG- and TMR-IONPs. As IONPs efficiently adsorb to the cell membrane but are not internalized at 4°C, the fluorescent IONPs were bound to the cells by a 10 min pulse at 4°C. Subsequently, unbound nanoparticles were removed by washing before an increase of the incubation temperature to 37°C started a synchronized internalization of the IONPs by the cells. Double nanoparticle pulse-chase experiment with the two types of fluorescent IONPs allowed to even monitor the sequential uptake of OG- and TMR-IONPs. The usage of nanoparticle pulse-chase experiments in the presence of inhibitors of the cytoskeleton integrity revealed an actin-dependent formation of IONPs-containing vesicles and a microtubules-dependent transport of these vesicles to the perinuclear area. Additionally, the separation of the fluorescent DMSA coat and the iron oxide core during the intracellular trafficking was observed in nanoparticle pulse-

chase experiments. Finally, limitations, requirements and special challenges of studies on the exposure of in cultured neural cells with fluorescent IONPs were investigated, and are described and discussed.

In conclusion, the data presented in this thesis revealed that the synthesized fluorescent IONPs are suitable tools to study the uptake and intracellular fate of DMSA-coated IONPs by microscopical approaches and that the established nanoparticles pulse-chase setup allows to study internalization and mechanisms involved in intracellular IONPs trafficking with improved resolution.

IV. Zusammenfassung

Eisenoxidnanopartikel (*iron oxide nanoparticles*, IONPs) besitzen vielversprechende Eigenschaften im Hinblick auf eine biomedizinische Anwendung und werden bereits heute in therapeutischen und diagnostischen Verfahren verwendet. Da IONPs in das Gehirn gelangen können, ist es wichtig die potentiellen Konsequenzen einer Exposition mit IONPs auf Gehirnzellen zu untersuchen. Für die vorliegende Arbeit wurden Fluoreszenz-markierte IONPs durch die Funktionalisierung des Hüllmaterials Dimercaptobernsteinsäure (DMSA) der IONPs mit dem grünen Fluoreszenzfarbstoff *Oregon Green* (OG) oder dem roten Fluoreszenzfarbstoff Tetramethylrhodamine (TMR) synthetisiert. Der Vergleich zu bereits verwendeten BODIPY-markierten DMSA-umhüllten IONPs zeigte eine höhere Fluoreszenzintensität und eine erhöhte Signalstabilität der OG- und TMR-IONPs, wobei physikochemische Eigenschaften und kolloidale Stabilität identisch waren im Vergleich zu entsprechenden nicht-fluoreszierenden DMSA-IONPs. Um die Akkumulation der IONPs in Gehirnzellen zu untersuchen, wurden C6 Gliomzellen als Modelsystem verwendet. IONPs-Expositionsstudien zeigten, dass diese Zellen nicht-fluoreszierende und fluoreszierende IONPs in einer zeit-, konzentrations- und temperaturabhängigen Weise akkumulieren. Die beobachteten starken Fluoreszenzsignale in Zellen, die OG- oder TMR-IONPs ausgesetzt waren, und die auffällig langsame Abschwächung der zellulären Fluoreszenzintensität zeigen, dass diese fluoreszierenden IONPs als geeignetes Werkzeug zur Untersuchung der zellulären Aufnahme und den intrazellulären Transport von aufgenommenen IONPs genutzt werden können.

Um den intrazellulären Transport dieser fluoreszierenden Nanopartikel mit verbesserter zeitlicher und räumlicher Auflösung zu beobachten, wurden Einzel- und Doppel-Nanopartikel-*Pulse*-*Chase*-Experimente etabliert. Aufgrund der Tatsache, dass IONPs bei 4°C effizient an die Zellmembran adsorbieren, aber nicht in den Zellen aufgenommen werden, wurden IONPs zunächst durch eine 10-minütige Nanopartikel-*Pulse*-Inkubation bei 4°C an die Zellmembrane gebunden. Danach wurden nicht-gebundene Nanopartikel durch Waschen entfernt und durch Erhöhung der Inkubationstemperatur auf 37°C eine synchronisierte Aufnahme der IONPs in die Zellen initiiert. Doppel-Nanopartikel-*Pulse*-*Chase*-Experimente mit den zwei verschiedenen fluoreszierenden IONPs ermöglichte die

Beobachtung der sequentiellen Aufnahme von OG- und TMR-IONPs. Die Durchführung dieser Nanopartikel-*Pulse*-*Chase*-Experimente in der Gegenwart von Inhibitoren der Zytoskelettintegrität führte zum Nachweis einer Aktin-abhängige Bildung von IONPs-enthaltenden Vesikeln und eines Mikrotubuli-abhängigen Transport dieser Vesikel zum perinukleären Bereich der Zellen. Zusätzlich konnte die Auftrennung der fluoreszierenden DMSA-Mantels und des Eisenoxidkernes der fluoreszierenden IONPs während der intrazellulären Aufnahme mit Hilfe der Nanopartikel-*Pulse*-*Chase*-Experimente beobachtet werden. Abschließend wurden einige Limitierungen, Anforderungen und spezielle Herausforderungen der Expositionsstudien von kultivierten neuralen Zellen mit fluoreszierenden IONPs untersucht, beschrieben und diskutiert.

Zusammenfassend zeigen die Daten der vorliegenden Dissertationsarbeit, dass die synthetisierten fluoreszierenden IONPs geeignete Werkzeuge sind, um die Aufnahme und den intrazellulären Verbleib von DMSA-umhüllten IONPs mit Hilfe von mikroskopischen Methoden zu untersuchen, und, dass das die etablierten Nanopartikel-*Pulse*-*Chase*-Protokolle die Untersuchung der Aufnahme und der Mechanismen des intrazellulären Transports von IONPs mit verbesserter Auflösung ermöglichen.

V. Abbreviations and symbols

%	percent
°C	degree Celsius
µL	microliter
µM	micromol
a.u.	arbitrary units
AAS	atomic absorption spectroscopy
AFM	atomic force microscopy
$AgNO_3$	silver nitrat
AgNP(s)	silver nanoparticle(s)
ANOVA	analysis of variance
BBB	blood-brain barrier
BP, BODIPY	4,4-difluoro-1,3,5,7,8-pentamethyl-4-bora-3a,4a-diaza-*s*-indacene
BP-IONP(s)	BODIPY-labeled DMSA-coated IONP(s)
BSA	bovine serum albumin
CNS	central nervous system
CuONP(s)	copper oxide nanoparticle(s)
cytoD	cytochalasin D
DAPI	4',6-diamidino-2-phenylindole
DLS	dynamic light scattering
DMEM	Dulbecco's modified Eagle's medium
DMSA	dimercaptosuccinate
EDC	1-ethyl-3-(3-dimethylaminopropyl)carbodiimide
ed(s).	editor(s)
EDX	energy dispersive X-ray spectrometry
EEA1	early endosome antigen 1
ELS	electrophoretic light scattering
FCS	fetal calf serum
FDA	Food and Drug Administration
Fig.	figure
GCM	glia condition medium
GFAP	glial fibrillary acidic protein
GSH	glutathione

h	hour
H33342	Hoechst 33342
HCL	hydrochloride acid
HEPES	4-(2-hydroxyethyl)-1-piperazineethane sulfonic acid
HNO_3	nitric acid
i.e.	that is (Latin: *id est*)
IB	incubation buffer
ICP-MS	inductively coupled plasma mass spectrometry
IONP(s)	iron oxide nanoparticle(s)
LAMP1	lysosomal associated membrane protein 1
LDH	lactate dehydrogenase
LED	light emitting diode
M	molar (mol per liter)
mg	milligramm
min	minutes
mM	millimollar
MRI	magnetic resonance imaging
mV	millivolt
n.d.	not detectable
NaCl	sodium chloride
NADH	nicotinamide adenine dinucleotide (reduced)
NaOH	sodium hydroxide
née	born as/ Maiden name
nf	non-fluorescent
nm	nanometer
NP(s)	nanoparticle(s)
OG	Oregon Green
OG-IONP(s)	Oregon Green-labeled-DMSA-coated IONP(s)
PBS	phosphate-buffered saline
PDI	polydispersity index
PEG	polyethylene glycol
PFA	paraformaldehyde
phalloidin	CytoPainter Phalloidin-iFluor
PI	propidium iodide
Ref.	reference

RT	room temperature
SD	standard deviation
s	second
SPION(s)	superparamagnetic IONP(s)
t	time
TEM	transmission electron microscopy
TMR	tetramethylrhodamine
TMR-IONP(s)	TMR-labeled DMSA-coated IONP(s)
Tris	Tris(hydroxymethyl)-aminomethane
UV	ultraviolet
w/v	weight per volume
ζ	zeta

1. Introduction

1. Introduction

1.1 Nanoparticles

Nanoparticles (NPs) are defined as particles that possess sizes between 1 and 100 nm (Auffan *et al.*, 2009) and that differ in at least some of their chemical and physical properties in comparison to non-nanoscale particles or the bulk material of the same composition (Auffan *et al.*, 2009, Bobo *et al.*, 2016) resulting in their unique physical, chemical and biological properties. NPs have been used already for thousands of years such as in lead-based cosmetics in ancient Egypt and in nanocrystal-containing hair dyes in Greco-Roman times (Walter *et al.*, 2006). The first idea of nanotechnology was placed 1959 by the physicist Richard Feynman with his presentation "There's Plenty of Room at the Bottom" in which Feynman suggested that it is possible to manipulate materials at the level of their atoms and molecules (Santamaria, 2012). Due to their unique properties, NPs are gaining more and more interest during the last two decades in industry and science as indicated by the huge increase in the number of publications on NPs (Fig. 1.1). As a consequence, NPs are also getting more and more access to our daily live (Heiligtag and Niederberger, 2013, Khan *et al.*, 2017, Mohammed *et al.*, 2017).

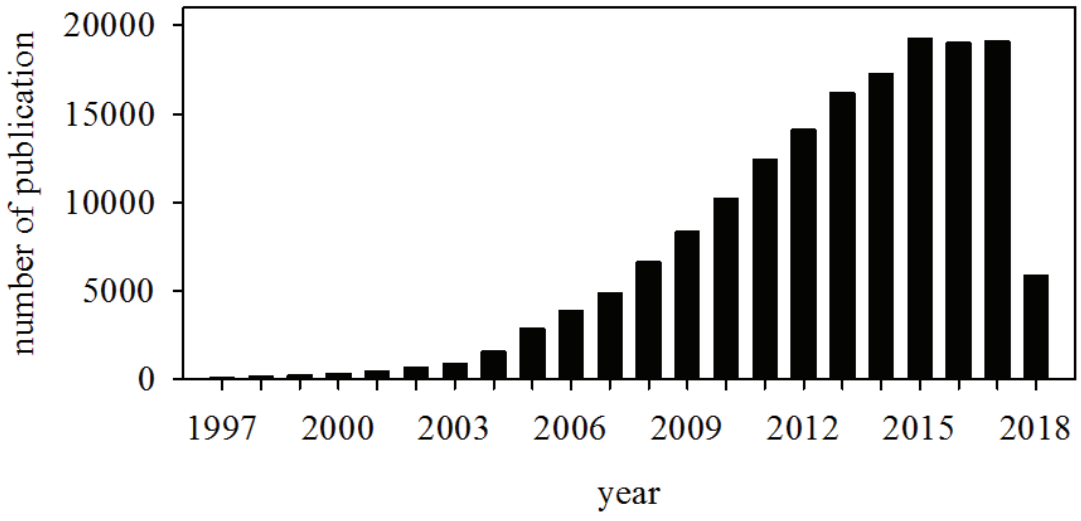

Fig. 1.1 Publications on NPs. The number of publications per year was obtained in a PubMed search for the term: "Nanoparticle" (done on 04 April 2018).

NPs can be composed of and engineered from various materials including inorganic and/or organic materials such as carbon, metals, metal oxides, silica, liposomes and

polymers (Algar *et al.*, 2011, Colombo *et al.*, 2012, De la Fuente and Grazu, 2012). Table 1.1 provides an overview on some frequently used types of NPs and lists their unique properties which make them valuable for industrial or biomedical applications.

Table 1.1 Properties and applications of selected types of NPs

Nanoparticles	Properties	Applications
Carbon-based NPs		
Fullerenes	Safe, inert, semiconductor/superconductor, transmits light based on intensity	Polymer industry, automobiles
Carbon Nano Tubes	High electrical and thermal conductivity, tensile strength, flexible and elastic	Electronic equipment, biosensors, water filters
Metal-based NPs		
Silver	Absorbs and scatters light, stable, anti-bacterial, disinfectant	Cosmetic products, paint industry, food packaging, antimicrobial agents, wound dressings, electronics
Gold	Interactive with visible light, reactive	Fuel cell, catalyst industry, medical diagnostics, photothermal therapy
Copper	Ductile, very high thermal and electrical conductivity, highly flammable solids	Catalyst, biosensor, electrochemical sensors
Zinc	Antibacterial, anti-corrosive, antifungal, UV filtering	Coating industry, antimicrobial agents
Metal oxide-based NPs		
Titanium oxide	High surface area, inhibits bacterial growth	Cosmetic products, coating industry, antimicrobial agents, biosensors
Iron oxide	Magnetic, highly reactive	Cosmetic products, biomedical applications (see chapter 1.2)
Silicon dioxide	Stable, less toxic, able to be functionalized many molecules, biocompatible	Cosmetic products, paint industry, drug delivery, biosensors
Zinc oxide	Antibacterial, anti-corrosive, antifungal and UV filtering	Cosmetic products, paint industry, antimicrobial agents, bioimaging
Cerium oxide	Antioxidant, low reduction potential, switch between oxidation states	Fuel cell, catalyst industry, biosensors, anticancer agent
Quantum dots/ Semiconductor NPs		
CdSe/ZnS	High quantum yield, low photobleaching, high photochemical stability	Bioimaging, photovoltaic, LED

Information was taken from (Phogat *et al.*, 2016, Anu and Saravanakumar, 2017, Khan *et al.*, 2017, McNamara and Tofail, 2017)

The production of NPs accounts for 10,000 t/year worldwide in the case of titanium oxide and between 100 and 1000 t/year in the case of cerium oxide, iron oxide, aluminum oxide, zinc oxide and carbon nanotubes (Piccinno *et al.*, 2012). NPs can be precisely engineered for specific approaches by adapting their size, shape and surface properties and thousands

of nanomaterial-containing products are already available on the market (Bencsik *et al.*, 2018). A number of these NPs are directly encountered by humans via inhalation, dermal exposure, oral ingestion or intravenous routes (Mu *et al.*, 2014, Zhang *et al.*, 2015b) (Fig. 1A). Such exposures are associated with the risks that NPs may enter human cells resulting in major toxicological consequences (Piccinno *et al.*, 2012) which raises concerns on the health and safety aspects of NPs (Zhang *et al.*, 2015b).

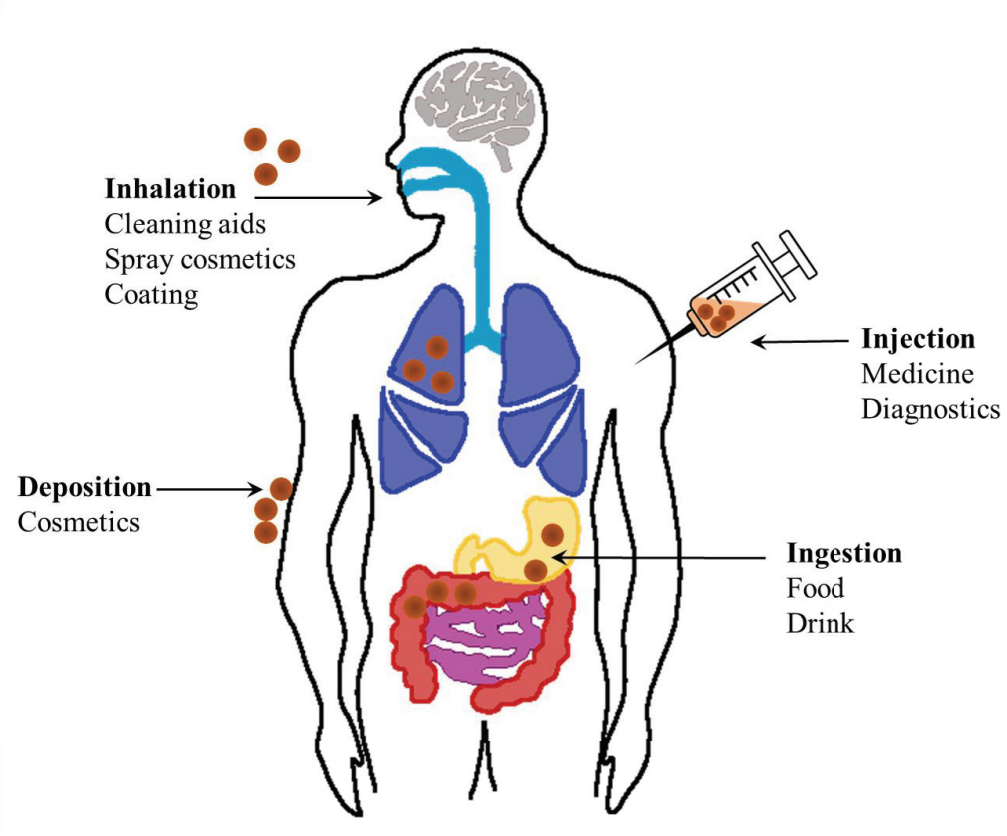

Fig. 1.2 Exposure of the human body to NPs according to (Zhang *et al.*, 2015b, Bencsik *et al.*, 2018).

The increased production and usage of NPs in industry and for cosmetic products such as shampoos and sunscreens has led to an increased release of NPs into the wastewater. As some types of NPs are persistent and slowly degraded in the environment, and as some NPs can be stored in plants, microbes, and animal organs, humans can be exposed to NPs through the consumption of natural products (Mu *et al.*, 2014, Phogat *et al.*, 2016). Several studies stated that continuous high exposure to NPs is associated with severe damage of the respiratory and cardiovascular system (Pieters *et al.*, 2012, Robertson *et al.*, 2012, Patel *et al.*, 2013, Xu *et al.*, 2013, Mu *et al.*, 2014, Bencsik *et al.*, 2018).

The physicochemical properties of NPs have been demonstrated to influence the toxic manifestations of these NPs (Gatoo *et al.*, 2014). A critical factor influencing the potential toxicity of NPs is the parameter size, as it has been observed that smaller NPs have a higher toxic potential than larger NPs due to the greater reactivity caused by the higher surface area to volume ratio (Mu *et al.*, 2014, De Matteis, 2017). Furthermore, the size of the NPs defines how they are taken up, distributed and eliminated in the human body (Gatoo *et al.*, 2014).

Besides the size of NPs, there are many other factors such as shape, surface charge, morphology and coating, chemical composition and agglomeration state that influence and define NPs in their chemical and physical properties (Fig. 1.3), and thereby dictate their uptake, fate and toxic potential within the human body (Gatoo *et al.*, 2014, Mu *et al.*, 2014). The surface charge that depends on the composition and coating of the NPs also has a huge impact on the toxic potential of NPs as it highly influences the interactions with the biological system, the colloidal behavior of the NPs, the binding to biological compounds such as proteins, the transmembrane permeability and the effect of NPs on the blood-brain barrier (BBB) integrity (Gatoo *et al.*, 2014).

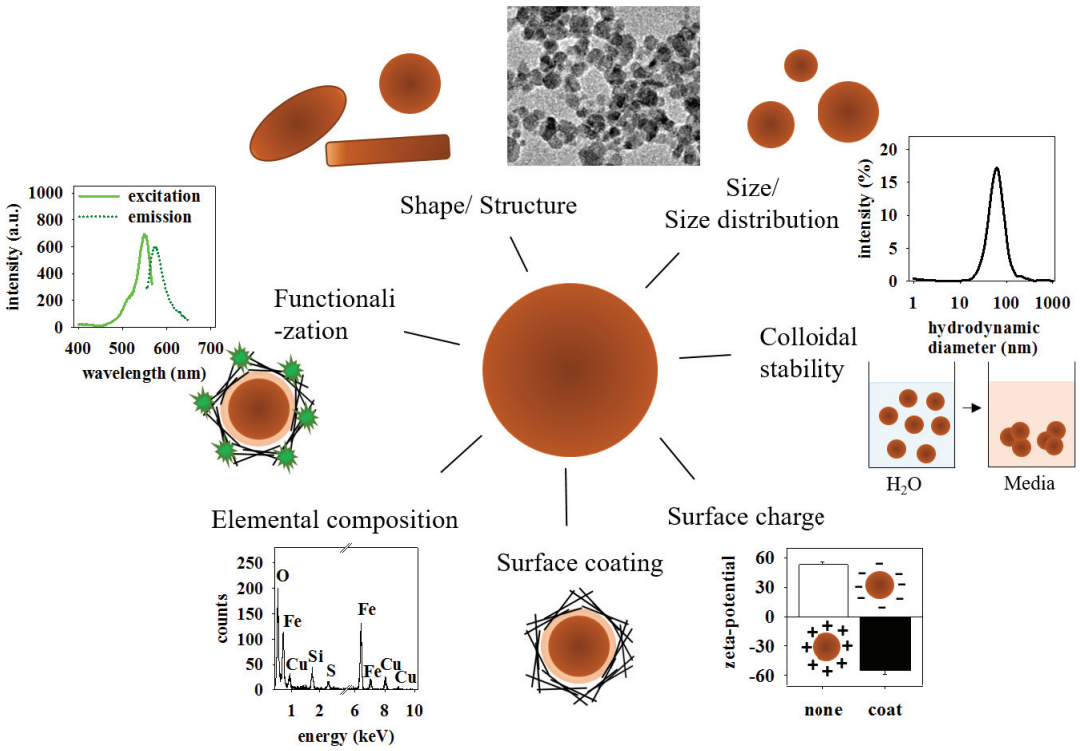

Fig. 1.3 Factors influencing the physicochemical properties of NPs.

NPs are complex materials (Christian *et al.*, 2008, Khan *et al.*, 2017) and as they possess unique properties relative to the bulk counterpart, a prediction of toxicity from their physicochemical properties is not possible (Rivera-Gil *et al.*, 2013, Gatoo *et al.*, 2014). Even in the simplest case of NPs composed of a single component such as silver or gold, the surface shell of the NPs will behave different from the core material due to the high surface to volume ratio and the resulting high reactivity of the surface (Christian *et al.*, 2008). To further complicate the situation, in most cases NPs are composed of more than one component, either due to further functionalization of the core material or simply due to adsorption of organic material, which happens as soon as NPs enter biological systems, or due to a combination of both (Rivera-Gil *et al.*, 2013, Nazarenus *et al.*, 2014). Therefore, NPs in biological environments can consist of various layers as schematically illustrated in Fig. 1.4. The core material (Fig. 1.4A) defines the functional physical properties of NPs such as plasmonic, superparamagnetic or fluorescent properties (Feliu *et al.*, 2016). The shell layer (Fig 1.4B) represents either just the outer layer of the core material or a second layer with a completely different structure than the core material (Christian *et al.*, 2008, Khan *et al.*, 2017). The engineered surface coating (Fig. 1.4C) is generated by functionalization of the NPs surface with small molecules, surfactants or polymers (Sapsford *et al.*, 2013) and the organic coating (Fig. 1.4D) is formed as soon as NPs are entering a biological environment (Rivera-Gil *et al.*, 2013, Nazarenus *et al.*, 2014). The outer-most surface defines the physicochemical properties of the NPs in relation to their surrounding environment (Christian *et al.*, 2008).

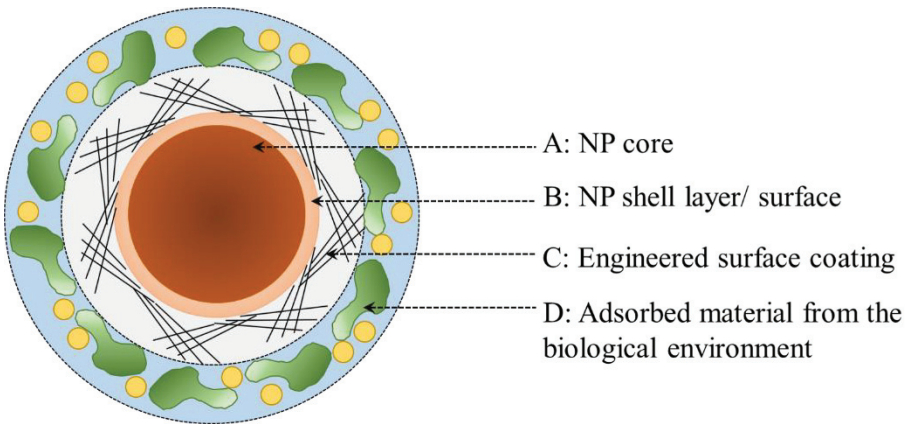

Fig. 1.4 Composition of NPs in biological environment. The simplest NPs are composed of a NP core (A) and a NP shell layer (B). Additional layers can be formed by adding an engineered surface coat(C) and by the adsorption of material such as proteins and ions from the biological environment (D).

1.2 Iron oxide nanoparticles

Superparamagnetic iron oxide NPs (IONPs) have a core made of maghemite (γ-Fe_2O_3) or magnetite (Fe_3O_4) (Wu *et al.*, 2008). Due to their biocompatibility, their magnetic properties and the simple and cost-effective synthesis, IONPs are promising candidates for biomedical application and clinical praxis (Gupta and Gupta, 2005, Ali *et al.*, 2016, Mohammed *et al.*, 2017) as listed in Table 1.2.

Table 1.2 Biomedical and biological applications of IONPs

Application	References
Magnetic resonance imaging (MRI)	(Wang, 2015) (Weinstein *et al.*, 2010)
Cancer treatment by induced hyperthermia	(Baetke *et al.*, 2015) (Shi *et al.*, 2015)
Targeted Drug-delivery to specific tissues including across the blood brain barrier	(El-Boubbou, 2018) (Ivask *et al.*, 2018)
Cell labeling and tracking	(Kolosnjaj-Tabi *et al.*, 2013) (Jasmin *et al.*, 2017)
Cell labeling and magnetic separation	(Gordon *et al.*, 2011) (Thimiri Govinda Raj and Khan, 2016)
Magnetotransfection	(Jenkins *et al.*, 2011) (Scherer *et al.*, 2002)

The majority of IONPs formulations that were approved by the U.S. Food and Drug Administration (FDA) such as Venofer®, Ferrlecit®, INFed®, Dexferrum® and Ferraheme® are used in iron replacement therapies, for example for the treatment of iron deficiency in chronic kidney diseases (Bobo *et al.*, 2016). An emerging field in the biomedical application of IONPs is the use as contrast enhancement reagents for magnetic resonance imaging (Bobo *et al.*, 2016) as well as the use of IONPs for treatment of glioblastomas using magnetically induced hyperthermia (Baetke *et al.*, 2015). For the latter the superparamagnetic properties of the IONPs are essential. IONPs consist of single magnetic domains and can be magnetized by the application of an external field. The magnetization will be lost as soon as the external field is removed (Corr *et al.*, 2008). Suspensions of superparamagnetic IONPs behave as ferrofluids (Sapsford *et al.*, 2013). For the hyperthermia treatment, the ferrofluid will be directly injected into the tumor and an oscillating external magnetic field will be applied leading to the vibration of the particles that results in a local heating (Laurent *et al.*, 2011, Banobre-Lopez *et al.*, 2013).

Nanotherm™, a formulation of aminosilane-coated IONPs, is in the late stage of clinical trials in the US. Hyperthermia treatment of glioblastoma with this formulation was associated with an increased overall survival of patients for up to 12 months (Thiesen and Jordan, 2008, Maier-Hauff *et al.*, 2011, Bobo *et al.*, 2016). The superparamagnetism of the IONPs also allows to direct the IONPs to selected tissues by the application of external magnetic fields (Akbarzadeh *et al.*, 2012).

Furthermore, IONPs have been applied for cell labeling, cell tracking and magnetic separation (Gordon *et al.*, 2011, Kolosnjaj-Tabi *et al.*, 2013). In the field of cell labeling, the focus has recently switched to materials that possesses both fluorescent and magnetic properties to allow the tracking of the NP-labeled cells by magnetic resonance imaging as well as by fluorescent spectroscopy (Corr *et al.*, 2008, Chekina *et al.*, 2011). The combination of magnetic and optical imaging provides additional information about the cell structure imaged (Chekina *et al.*, 2011, Perillo *et al.*, 2017).

1.2.1 Synthesis

IONP can be synthesized by chemical, physical or biological methods (Table 1.2). The chemical preparation methods are most commonly used, with a proportion of 90%, due to low production cost, high yield and high reproducibility (Ali *et al.*, 2017). A simple and effective approach among the numerous chemical approaches, is the chemical co-precipitation (Ali *et al.*, 2016) that was also performed in this thesis. This method was originally developed in 1982 by René Massart (Massart, 1981). Ferrous and ferric ions in a molar ratio of 1:2 are precipitated under alkaline conditions to magnetite (Fe_3O_4) NPs (equation 1). Due to the instability and sensitivity of magnetite to oxidation, further reaction to maghemite (Fe_2O_3) or ferric hydroxide ($Fe(OH)_3$) takes place in the presence of oxygen (Gupta and Gupta, 2005, Laurent *et al.*, 2008, Ali *et al.*, 2016) (equation 2 and 3). IONPs synthesized with this method often contain mixtures of magnetite and maghemite (Maity and Agrawal, 2007).

(1) $$Fe^{2+} + 2\,Fe^{3+} + 8\,OH^- \rightarrow Fe_3O_4 + 4\,H_2O$$

(2) $$Fe_3O_4 + 2\,H^+ \rightarrow \gamma\text{-}Fe_2O_3 + Fe^{2+} + H_2O$$

(3) $$Fe_3O_4 + 0.25\,O_2 + 4.5\,H_2O \rightarrow 3\,Fe(OH)_3$$

Large amounts of IONPs can easily be synthesized this way and the size and shape can be adjusted by modifications of pH, ionic strength, temperature, the type of iron salts and the ratio of ferrous to ferric iron (Laurent *et al.*, 2008). Depending on the conditions applied, the resulting particle size can range from 2-15 nm (Laurent *et al.*, 2008) ensuring the superparamagnetic properties. A disadvantages of the chemical co-precipitation is the resulting broad size distribution of the synthesized particles (Laurent *et al.*, 2008, Sapsford *et al.*, 2013). For the synthesis of a narrow size distribution other methods e.g. thermal decomposition are more appropriate (Sapsford *et al.*, 2013, Ruiz *et al.*, 2014) (Table 1.2).

Table 1.2 IONPs synthesis methods with advantages and disadvantages of the procedures

Method	Advantages	Disadvantages
Chemical		
Co-precipitation	Easy, effective, low cost	Low shape control, broader size distribution
Hydrothermal	Particle size and shape easy to control, highly efficient	High pressure and high reaction temperature
Sol-gel and polyol	Easy, precisely controlled size and internal structure	High pressure, complicated
Microemulsion	Precisely control of size and size distribution and high surface area	Complicated, low yield
Sonochemical	Simple, narrow size distribution	No shape control, medium yield
Thermal decomposition	Monodispersed NPs, very good shape control	Dissolved in non-polar solvents
Electrochemical decomposition	Control of particle size	Lack in reproducibility, rough products, amorphous impurities
Physical		
Aerosol	Relatively narrow size distribution	Complicated
Gas phase deposition	Easy	Low size control
Electron beam lithography	Well-controlled interparticle spacing	Expensive and highly complex equipment
Biological		
Bacteria-mediated	Good reproducibility and scalability, high yield, low cost	Slow, laborious

Information was taken from (Campos *et al.*, 2015, Wu *et al.*, 2015, Ali *et al.*, 2016, Ali *et al.*, 2017).

1.2.2 Coating

The application of IONPs for biomedical attempts requires the colloidal stability of the IONPs in physiological environments (Akbarzadeh *et al.*, 2012). Uncoated IONPs are usually not colloidal stable in biological media (Lodhia *et al.*, 2010, Ali *et al.*, 2016) due to strong magnetic attraction between the particles, van der Waals forces and their high energy surface (Ali *et al.*, 2016). A common approach to prevent agglomeration of IONPs, and thereby also to increase the biocompatibility of the particles in physiological environments, is a coating of IONPs with various inorganic and organic coating materials (Gupta and Gupta, 2005, Valdiglesias *et al.*, 2015, Ali *et al.*, 2016, Mohammed *et al.*, 2017). A selective list of common used coating materials is given in Table 1.3 which includes also information on the core size of the particle measured by transmission electron microscopy (TEM), the average hydrodynamic diameter and the surface charge of the IONPs dispersed in water. As size and surface charge are important factors determining the uptake of NPs in biological systems (Verma and Stellacci, 2010, Nazarenus *et al.*, 2014) it is highly important to characterize engineered IONPs in detail.

Table 1.3 Selective list of inorganic- and organic-coated IONPs including the size of the core and the average hydrodynamic diameter and the surface charge of the IONPs dispersed in water

Coating	Size (TEM, nm)	Average hydrodynamic diameter (nm)	Surface charge	Reference
Inorganic				
Gold	10	22-25	negative	(Lim *et al.*, 2009, Banerjee *et al.*, 2011)
Silicia	7.6	150-200	negative	(Sun *et al.*, 2005)
Organic				
Citric acid	9-25	53-133	negative	(Li *et al.*, 2013)
Dimercaptosuccinate	4-20	30-60	negative	(Bertorelle *et al.*, 2006, Petters *et al.*, 2014a)
Polyvinylalcohol	4.5-5	13-57	positive	(Amiri *et al.*, 2011)
Phosphorylcholine	4.5	<10	positive	(Denizot *et al.*, 1999)
Polyethylengylcol	15	40-50	neutral	(Gupta and Wells, 2004)
Dextran	4.2-4.8	80-150	neutral	(Soenen *et al.*, 2011)
Carboxydextran	4.2	62	negative	(Soenen *et al.*, 2011)
Alginate	11	50-55	negative	(Castello *et al.*, 2015)
Chitosan	11	100	negative	(Castello *et al.*, 2015)

The introduction of the coating material is either performed during the synthesis or directly after preparation of the bare IONPs and the colloidal stabilization by such molecular layers can be of electrostatic or of steric nature (Turro *et al.*, 2002, Sapsford *et al.*, 2013). An additional advantage of the surface coating is the opportunity to further biofunctionalization of the engineered shell (Sapsford *et al.*, 2013, Ali *et al.*, 2016). This opens up a range of possible functionalization approaches and specific applications (Table 1.4) such as insertion of target-specific antibodies for a directed transport of IONPs and/or the addition of drugs for specific treatments (Tietze *et al.*, 2015, El-Boubbou, 2018). The possibility to combine magnetic with fluorescent properties by the synthesis of fluorescently labeled IONPs increases the potential of IONPs for biomedical applications even further (Kaewsaneha *et al.*, 2015, Shi *et al.*, 2015).

Table 1.4 Functionalization of the engineered coating of IONPs for precise application

Coating	Functionalization		Application/ Function	References
	Molecule	Function		
DMSA	BODIPY	Fluorophore	Optical detection of IONPs in cellular uptake studies	(Luther *et al.*, 2013, Petters *et al.*, 2016)
DMSA	Fluorescein	Fluorophore	Fluorescent and magnetic cell labeling	(Bertorelle *et al.*, 2006)
PEG	Cy5.5 Chlorotoxin	Fluorophore Neurotoxin	Specific targeting of glioma cells for magnetical and optical detection	(Veiseh *et al.*, 2005)
PEG	anti-TAG-72 5-FAM Doxorubicin	Antibody Fluorophore Anti-cancer drug	Targeted drug delivery of IONPs to colon cancer cells for simultaneous MRI and fluorescent imaging	(Zou *et al.*, 2010)
Dextran	Hsp70	Antibody	Selective binding to glioma specific CD40 receptor and enhancement of MRI contrast	(Shevtsov *et al.*, 2014)
Dextran	CD11b-TAC	Antibody	Purification of microglia preparations by selective binding of IONPs to the microglia marker protein CD11b followed by magnetic separation	(Gordon *et al.*, 2011)
Dextran	Anti-ferritin	Antibody	Detection of ferritin accumulation in Alzheimer's Disease	(Fernandez *et al.*, 2018)
Chitosan	Ciprofloxacin	Antibiotic drug	Drug delivery system with controllable drug release	(Kariminia *et al.*, 2016)

DMSA: Dimercaptosuccinate; Hsp70: heat shock protein 70, MRI: magnetic resonance imaging; PEG: polyethylenglycol; TAC: tetrameric antibody complexes, TAG: tumor-associated glycoprotein-72

For IONP-cell interaction studies, the small organic molecule *meso*-2,3-dimercaptosuccinate (DMSA) has frequently been used as coating material for IONPs (Fauconnier *et al.*, 1997, Villanueva *et al.*, 2009, Valois *et al.*, 2010, Geppert *et al.*, 2011,

Petters *et al.*, 2014b, Zhang and Liu, 2017). DMSA is an FDA approved agent, which is commonly orally administered as metal chelator and shows low toxicity in various biological systems (Ercal *et al.*, 1996, Rooney, 2007, Flora and Pachauri, 2010). DMSA forms a cage-like structure around the iron core of IONPs through interaction of the terminal carboxylate groups with the iron core and additional intermolecular disulfide-bridges between bound DMSA molecules (Fauconnier *et al.*, 1997, Chen *et al.*, 2008, Valois *et al.*, 2010, Soler *et al.*, 2011). The free carboxylate groups of DMSA lead to a stabilization of the particles in physiological media and even in solutions that range in pH values between 3 to 11 (Fauconnier *et al.*, 1997). Additionally, DMSA accelerates the internalization of IONPs in comparison to IONPs coated with uncharged materials like dextran, most likely due to the high nonspecific binding of DMSA-IONPs to the cell membrane due to the negative surface charges induced by the DMSA coat (Wilhelm *et al.*, 2003, Villanueva *et al.*, 2009). DMSA or the DMSA coat around the NPs can be further functionalized by adding fluorophores (Luther *et al.*, 2013, Petters *et al.*, 2014a, Petters *et al.*, 2016) or drugs, antibodies and other compounds to free thiol- or carboxyl-groups of the coat which allows to study cell interactions of IONPs in more detail or allows a more directed and specific cellular uptake (Shevtsov *et al.*, 2014, Shevtsov *et al.*, 2015, Liu *et al.*, 2016, Galli *et al.*, 2017).

In addition to the defined coating during or after the synthesis of the IONPs, it has to be considered that, as soon as NPs enter biological environments a variety of molecules will adsorb onto the surface of the NPs (Nel *et al.*, 2009, Sakulkhu *et al.*, 2014), and thereby modify surface properties. This process depends on the surface chemistry of the particles and the composition of the medium that may contain ions, lipids, metabolites, sugars, other biomolecules and proteins (Rivera-Gil *et al.*, 2013, Nazarenus *et al.*, 2014, Feliu *et al.*, 2016). As proteins are the most abundant biomolecules in biological fluids (Pelaz *et al.*, 2013), the formation of a so called protein-corona around the IONPs has been intensively studied, showing a huge impact on the size, stability, surface chemistry and, thereby, on the interaction and uptake of IONPs in cells (Doak *et al.*, 2009, Wiogo *et al.*, 2011, Geppert *et al.*, 2013, Mahmoudi *et al.*, 2014, Feliu *et al.*, 2016). The surface coating of the IONPs can strongly influence the formation of the protein corona as interaction of the proteins with the IONP surface are driven by hydrogen bonds, solvation forces, hydrophobic and electrostatic interactions (Saptarshi *et al.*, 2013). For example, the protein-coronas formed around negatively charged carboxylated dextran-coated IONPs

and positive amino dextran-coated IONPs differ strongly in their composition (Amiri *et al.*, 2013), while coating of IONPs with polyethylenegylcol could prevent the formation of a protein corona (Torrisi *et al.*, 2014).

1.2.3 Characterization

The combination of different synthesis methods and various coating options, generates a huge variety of different types of IONPs. As several factors and already minor changes in environmental composites can cause severe alterations in the physicochemical properties of the IONPs and consequently may have a severe impact on the interaction, effects and toxic potential of IONPs on biological systems, it is essential to carefully characterize the physicochemical properties of the NPs for the conditions applied (Rivera-Gil *et al.*, 2013, Nazarenus *et al.*, 2014, Mohammed *et al.*, 2017). Table 1.5 lists important physicochemical parameters of IONPs and commonly used techniques to investigate these parameters.

Table 1.5 Methods to determine physicochemical parameters of IONPs

Parameter investigated	**Method**
Core size, shape, size distribution	Electron microscopy
Elemental composition	Energy dispersive X-ray spectroscopy
Discrimination between Fe^{2+} and Fe^{3+}	Mossbauer spectroscopy
Determination of the iron content	Atomic absorption spectroscopy
Crystal structure	X-ray diffraction
Functional groups (Verification of the coating)	Infrared spectroscopy
Size and size distribution in dispersion	Dynamic light scattering
Surface charge (ζ-potential), colloidal stability	Electrical light scattering
Magnetic properties	Vibrating sample magnetometer

1.3 The brain and iron oxide nanoparticles

1.3.1 The blood-brain barrier and the major cell types in the brain

The blood-brain barrier (BBB) provides a stable environment for neural functions, prevents many macromolecules from entering the brain and protects the central nervous system (CNS) from neurotoxic substances circulating in the blood. The BBB possesses specific transporter systems to ensure an adequate supply of the brain cells with many essential water-soluble nutrients and metabolites (Abbott *et al.*, 2010). The BBB is formed by the endothelial cells of the brain capillaries, pericytes and the basal lamina covered by the endfeets of astrocytes (Abbott *et al.*, 2010, Grabrucker *et al.*, 2016) (Sofroniew and Vinters, 2010, Cabezas *et al.*, 2014) (Fig. 1.5).

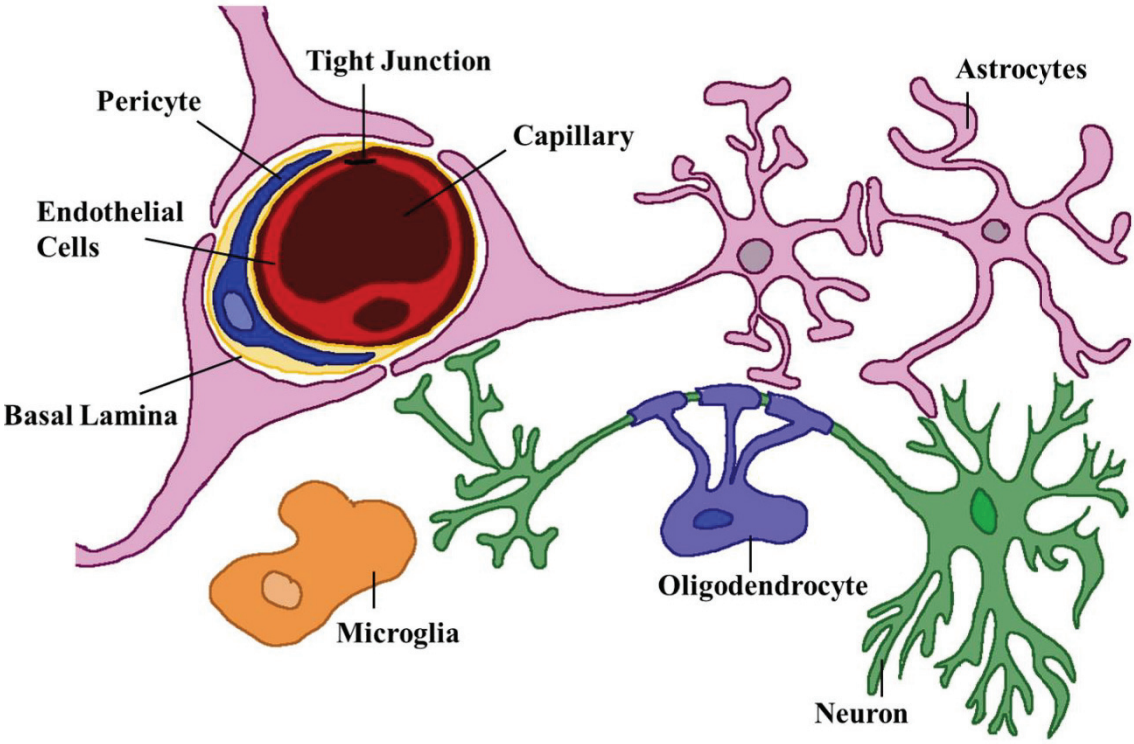

Fig. 1.5 The blood-brain barrier and the four major cell types in the brain.

Astrocytes are the most abundant glial cell type in the CNS and play an important role in the BBB maintenance and permeability (Colombo and Farina, 2016). Due to their location, astrocytes are the first neural cells that encounter compounds passing the BBB from blood (Colombo and Farina, 2016). Furthermore, astrocytes regulate brain homeostasis as they supply metabolites and growth factors to neurons, maintain the extracellular balance of ions, water, metals and neurotransmitters, support synapse

formation and plasticity and detoxify xenobiotics (Dringen *et al.*, 2015, Colombo and Farina, 2016, Gorshkov *et al.*, 2018, Hirase and Koizumi, 2018) (Fig. 1.5).

Beside astrocytes, the main cell types in the brain are neurons, oligodendrocytes and microglia (Fig. 1.5). Neurons are important for signal transduction by the transmission of information along their axons and are characterized by the excitability and the release of neurotransmitters (Scalettar, 2006, Peters and Connor, 2014). Microglia and oligodendrocytes belong together with astrocytes to the glial cells (Peters and Connor, 2014). Microglia comprise around 10-15% of all glial cells and are the immune competent cells of the CNS. Upon activation they clear via phagocytic activity the brain from invading pathogens or from cell debris generated by apoptosis or necrosis of neuronal cells (Saura *et al.*, 2003, Nayak *et al.*, 2014, Murgoci *et al.*, 2018). Oligodendrocytes support and isolate the axons in the CNS by myelination (Bradl and Lassmann, 2010, Michalski and Kothary, 2015).

1.3.2 Consequences of iron oxide nanoparticle exposure to the brain

Over one and a half billion people worldwide suffer from central neural system (CNS) disorders, but the treatment of these diseases is heavily limited due to the poor access of therapeutic drugs and genetic material across the BBB into the CNS (Posadas *et al.*, 2016). The efficient crossing of the BBB is limited to small polar molecules and highly hydrophobic molecules that are not recognized by the multidrug resistance proteins expressed in the brain endothelial cells of the BBB (Thomsen *et al.*, 2015). As small IONPs are capable pf rapidly crossing the BBB (Shubayev *et al.*, 2009, Shi *et al.*, 2016, Vinzant *et al.*, 2017) and possess a high biocompatibility as iron ions released from IONPs are added to natural/cellular iron deposits (Posadas *et al.*, 2016), the interest in IONPs for potential applications in the neurobiomedical field is heavily increasing. They are being especially considered for their use as drug-delivery system through the BBB (Yang, 2010, Pilakka-Kanthikeel *et al.*, 2013, Vinzant *et al.*, 2017) and for direct treatment of brain tumors by hyperthermia (Liu *et al.*, 2016). Besides the direct application of IONPs to the brain by injection in tumoral brain tissues (Fig. 1.6A), IONPs can enter the brain via several other routes (Petters *et al.*, 2014b, Bencsik *et al.*, 2018). After inhalation, IONPs can reach the brain via the olfactory bulb accessible from the nasal cavity (Wang *et al.*, 2007, Petters *et al.*, 2014b, Bencsik *et al.*, 2018) (Fig. 1B).

Alternatively, IONPs can reach the brain via the bloodstream as soon as IONPs have crossed the first barrier such as lung, gastrointestinal tract or skin (Bencsik *et al.*, 2018)(Fig.1C-D). Depending on the size and surface charge of the NPs they may cross the intact BBB either by absorptive transcytosis (Fig. 1.6C), receptor/carrier-mediated transport through the endothelial cells (Fig. 1.6D) or by passive diffusion (Fig. 1.6E) (Yan *et al.*, 2013, Grabrucker *et al.*, 2016, Bencsik *et al.*, 2018), whereby the latter is highly limited due to the structure of the BBB (Grabrucker *et al.*, 2016). Another entry mechanism of IONPs into the brain is the passage through damaged region of the BBB (Fig1.6F) (Mejias *et al.*, 2010, Petters *et al.*, 2014b), as it occurs in various brain diseases such as stroke, nerve trauma or multiple sclerosis (Suh *et al.*, 2009, Weise and Stoll, 2012, Krol *et al.*, 2013).

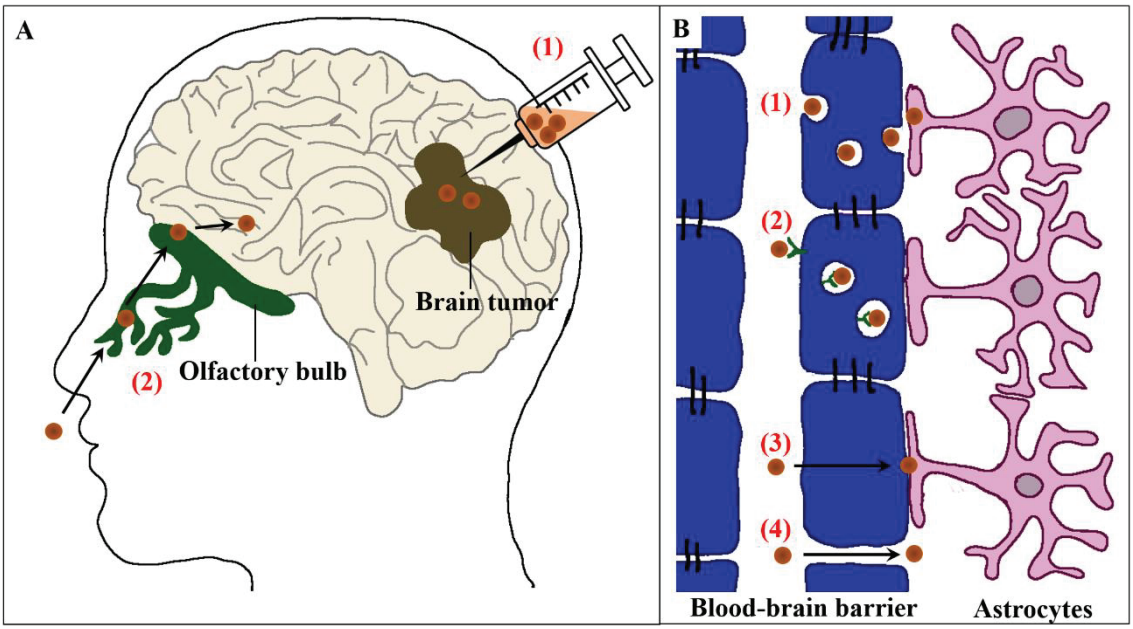

Fig. 1.6 Enty routes of IONPs into the brain. (A) Direct injection for clinical treatment (1) and via the olfactory bulb after inhalation (2). (B) From the blood stream via trancytosis (1), by receptor/carrier-mediated transport (2), by diffussion through the endothelial cells (3) or trough damaged regions of the BBB (4).

Although a lot of effort has been made to design IONPs specific for the use in biomedical application with beneficial outcome for the diagnosis and treatment of CNS diseases, is has to be noted that IONPs can induce neurotoxic effects or accelerate existing brain damage (Valdiglesias *et al.*, 2015, Valdiglesias *et al.*, 2016, Bencsik *et al.*, 2018). In this context it has to be considered that IONPs can be metabolized and easily release iron ions

(Valdiglesias *et al.*, 2015). Iron plays an important role in many metabolic processes in the CNS, for example in myelin synthesis, oxidative phosphorylation, neurotransmitter production and nitric oxide metabolism. But, on the other hand, a disturbance in the iron homeostasis can cause toxic effects by iron-mediated formation of oxygen radical species (ROS) and oxidative stress (Yarjanli *et al.*, 2017). Alterations of the iron homeostasis in the brain have been linked to various neurodegenerative diseases (Hare *et al.*, 2013, Rouault, 2013, Petters *et al.*, 2014b, Morris *et al.*, 2018). Thus, the increase usage of IONPs in biomedical applications makes it highly important to investigate the potential cytotoxicity of IONPs on brain cells (Shi *et al.*, 2016) and to understand the uptake mechanisms and the intracellular fate of IONPs in brain cells.

1.3.3 Uptake and metabolism of iron oxide nanoparticles in brain cells

As soon as IONPs have crossed the BBB, neurons, astrocytes and microglia will encounter these particles. Several studies have shown that IONPs can be found in all these brain cell types after they have crossed the BBB (van Landeghem *et al.*, 2009, Ku *et al.*, 2010, Yan *et al.*, 2013). Although a large number of studies and reviews are available dealing with the interaction of IONPs with peripheral mammalian cells (Nazarenus *et al.*, 2014, Oh and Park, 2014), more work is needed to understand the IONP-cell interactions, uptake and fate of IONPs in neural cells (Kura *et al.*, 2014, Petters *et al.*, 2014b, Costa *et al.*, 2016, Dante *et al.*, 2017).

The first step in cellular uptake of IONPs is the interaction of the particle with the cell membrane (Wilhelm *et al.*, 2003, Mahmoudi *et al.*, 2014). This interaction has a huge impact on the further uptake, internalization and fate of the particles and depends on a variety of factors. As the engineered coating or the absorbed biomaterial defines the interaction of the NPs with the cells (Pelaz *et al.*, 2013), the surface charge and surface chemistry of the IONPs, that depends on the composition of the coating (Table 1.3), plays a crucial role in the interactions with the cell membrane (Nel *et al.*, 2009, Lesniak *et al.*, 2013, Dante *et al.*, 2017). As the plasma membrane is globally negatively charged (Forest *et al.*, 2015), positively charged IONPs are taken up more efficiently than negatively charge IONPs. Nevertheless, negatively charge IONPs can interact, for example, with cationic lipid domains in the lipid raft of the cell membrane and are subsequently internalized (Wilhelm *et al.*, 2003, Adjei *et al.*, 2014, Nazarenus *et al.*, 2014). Such

IONPs show a higher uptake rate than neutral dextran-coated IONPs (Wilhelm *et al.*, 2003). The size of the IONPs is also crucial for uptake as it will influence the amount of potential binding sites (e.g. specific receptors) between the particle and cells, which may even lead to activation of different endocytotic pathways for cellular uptake. In addition, the characteristics of the cell membrane the like lipid composition, shape, thickness and stiffness, but also membrane protein-expression influence the adhesion of NPs to the cell membrane (Laurent *et al.*, 2013, Mahmoudi *et al.*, 2014).

As mentioned above, as soon as IONPs enter a biological environment, the formation of a protein corona around the particle is unavoidable (Nel *et al.*, 2009, Sakulkhu *et al.*, 2014). This can result, for example, in a reduced cellular adhesion and consequently reduced cellular uptake (Geppert *et al.*, 2013, Lesniak *et al.*, 2013). The altered uptake of protein-coated IONPs could be caused by more specific interactions between the protein-coated IONPs and the cell membrane that may involve and activate different uptake mechanisms (Wilhelm *et al.*, 2003, Lesniak *et al.*, 2013, Mahmoudi *et al.*, 2014)

As reported for other cell types, there are several ways how brain cells are able to take up IONPs: (1) Diffusion through the cell membrane, (2) transport through ion channels, (3) endocytosis and (4) direct translocation e.g. by the insertion of cell penetrating peptides into the coat or by electroporation, magnetofection or microinjection (Mahmoudi *et al.*, 2014). The first two uptake principles are restricted to very small IONPs with a size of just a few nanometers (Mahmoudi *et al.*, 2014). As red blood cells do not possess any endocytotic machinery, but are capable of internalizing NPs (Rothen-Rutishauser *et al.*, 2006, Wang *et al.*, 2012) such endocytotic independent uptake seems to be possible. Nonetheless, it is widely accepted that IONPs enter cells mainly via endocytic mechanisms (Iversen *et al.*, 2011, Oh and Park, 2014, Petters *et al.*, 2014b, Zhang *et al.*, 2015a).

1.3.4 Endocytosis of iron oxide nanoparticles

Endocytosis is a fundamental energy-dependent process of cells to internalize ions and biomolecules (Canton and Battaglia, 2012, Oh and Park, 2014). Bacteria and viruses also use the cellular endocytosis mechanisms to enter cells (Cossart and Helenius, 2014). A

lot of effort has been taken to understand the mechanisms and the complexity of cellular endocytosis pathways. Here, only the most common routes will be shortly described. Depending on the size of the molecules taken up and the cell type, two main categories of endocytotic uptake mechanisms can be separated: Phagocytosis, which is limited to specialized cells like immune cells including microglia cells, and pinocytosis which is ubiquitously used by almost all eukaryotic cells and can be sub-categorized into macropinocytosis, clathrin- or caveolae-mediated endocytosis and clathrin-/caveolae independent mechanisms (Soldati and Schliwa, 2006, Canton and Battaglia, 2012) (Fig. 1.7).

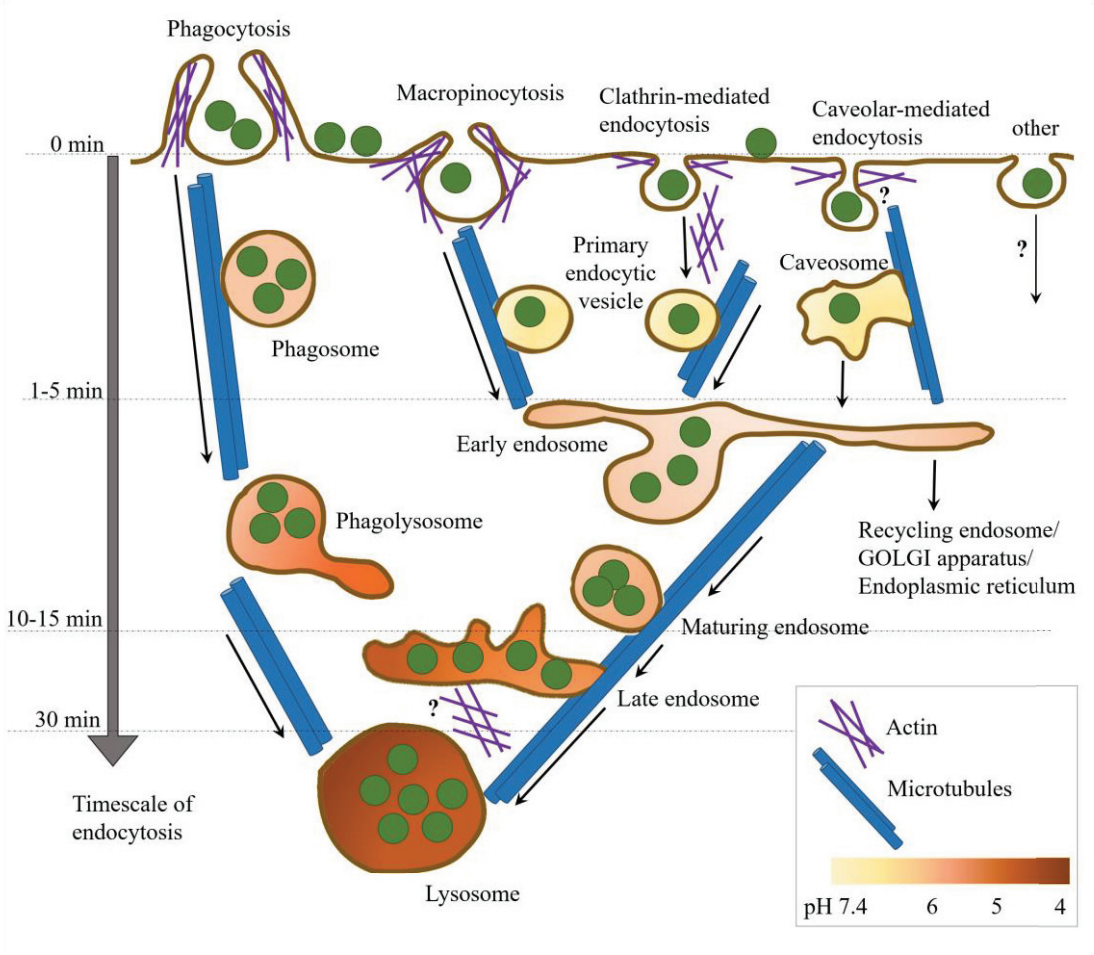

Fig. 1.7 Simplified scheme of the cellular endocytosis and the postulated role of actin filaments and microtubules in these processes

Endocytotic mechanisms can be described as a sequence of four essential steps: (1) initial binding to the cell surface membrane, (2) vesicle formation by plasma membrane deformation, (3) detachment of the vesicle from the membrane and (4) trafficking of

vesicles to specific subcellular organelles (Qualmann *et al.*, 2000). The time scale of these processes is relatively short. Engulfment of biomolecules or NPs and vesicle formation is a rapid process and already after 1-5 min vesicles reach the first endosomal compartment (Durrbach *et al.*, 1996), namely the early endosome. After 10-15 min the internalized molecules arrive in the late endosomes and after additional 15 min lysosomal compartments are reached (Canton and Battaglia, 2012, Thimiri Govinda Raj and Khan, 2016) (Fig. 1.7). During the endocytotic transport the compartments involved are getting more and more acidic. While early endosomes still have a more or less neutral pH (7.4-6.2), all the later compartments are more acidic reaching a pH of finally 5-4.4 in the lysosomes (Fig. 1.7) (Durrbach *et al.*, 1996, Canton and Battaglia, 2012, Cossart and Helenius, 2014).

Depending on the endocytotic pathway the vesicles are derived from, the destination of the vesicles may vary. Vesicle formed by phagocytosis (so-called phagosomes) fuse directly with late endosomes or lysosomes, leading their cargo quickly into the acidic environment (Doherty and McMahon, 2009, Canton and Battaglia, 2012). Vesicle derived from macropinocytosis or clathrin/caveolin-mediated endocytosis evolve first to early endosomes, from where the cargo is either transported to the late endosome and lysosome or sorted to the Golgi apparatus, the endoplasmic reticulum or to recycling endosomes (Lai *et al.*, 2007, Doherty and McMahon, 2009, Canton and Battaglia, 2012).

For cultured astrocytes, microglia and oligodendrocytes, DMSA-coated IONPs were postulated to be taken up by macropinocytosis and clathrin-mediated endocytosis (Geppert *et al.*, 2013, Luther *et al.*, 2013, Petters *et al.*, 2014a), whereas in neurons the uptake of DMSA-coated IONPs seems to depend on clathrin-mediated endocytosis, but not on macropinocytosis (Petters and Dringen, 2015). These endocytotic pathways were connetcted to the uptake of protein-coated IONPs, whereas the strong uptake of IONPs applied in protein-free medium could not be prevented by known pharmacological endocytosis inhibitors (Lamkowsky *et al.*, 2012, Geppert *et al.*, 2013, Petters, 2015). Depending on the cell type and the route of internalization, IONPs have distinct toxic potential on brain cells (Petters *et al.*, 2014b). In the case of the phagocytic microglia, IONPs are rapidly transported to the lysosome which leads to severe toxicity due to the quick release of iron ions (Pickard and Chari, 2010, Luther *et al.*, 2013, Petters *et al.*, 2016), consistent with data reporting that IONPs are dissolved under conditions present

in the lysosomal compartments (Skotland *et al.*, 2002, Levy *et al.*, 2010, Mazuel *et al.*, 2016). In contrast, for cultured astrocytes IONPs have no toxic potential (Geppert *et al.*, 2011, Geppert *et al.*, 2013, Hohnholt *et al.*, 2013, Petters *et al.*, 2016) and the lysosomal release of iron ions from the internalized IONPs is low and taken care of by a strong upregulation of the iron storage protein ferritin (Geppert *et al.*, 2012).

The endocytosis processes require a complex protein machinery for the formation of vesicles, especially during the receptor-mediated endocytosis, and the control of these processes (Qualmann *et al.*, 2000). The cytoskeleton plays a crucial role in endocytosis (Fig. 1.7). Microtubules are important for long distance transport (Soldati and Schliwa, 2006, Granger *et al.*, 2014), but also support short-range movements of vesicles (Granger *et al.*, 2014), whereas the flexible actin filaments support the engulfment of membrane segments, the formation of vesicles, separation and transport of the vesicles from the membrane (Durrbach *et al.*, 1996, Kumari *et al.*, 2010, Mooren *et al.*, 2012). The role of actin in certain endocytosis pathways is still under debate. However, there is an agreement that actin places an obligatory role in phagocytosis (Granger *et al.*, 2014). It is also widely accepted that actin is mandatory for clathrin-mediated endocytosis in yeast, but for mammalian cells this picture is not as clear and contradictory results and opinions have been reported (Lamaze *et al.*, 1997, Fujimoto *et al.*, 2000, Qualmann *et al.*, 2000, Soldati and Schliwa, 2006, Granger *et al.*, 2014). Commonly, accepted is that actin plays at least a supportive role in endocytotic vesicle formation, especially if larger force is required for budding due to high membrane rigidity or if larger cargoes are ingested (Boulant *et al.*, 2011). There is also evidence for the role of actin in the transport of newly formed vesicles away from the plasma membrane, at least during clathrin-mediated endocytosis (Soldati and Schliwa, 2006, Granger *et al.*, 2014). However, the major role, in the transport of the nascent vesicles from the actin-rich cell periphery to their specific compartment appears to be played by microtubules, as the switch from the actin-based movement to a microtubules-based movement occurs after forming and release of the vesicle from the plasma membrane (Granger *et al.*, 2014). Uptake studies for polystyrene NPs in various cell lines including brain astrocytoma 1321N1 cells but also tumor epithelial HeLa, lung carcinoma A549 and macrophages revealed that the role of actin polymerization and microtubules formation in NP-uptake highly depends on the cell type investigated (Rejman *et al.*, 2004, Geiser *et al.*, 2005, dos Santos *et al.*, 2011, Kasten *et al.*, 2014). Furthermore, the role of the cytoskeleton in the uptake of NPs depends

strongly on the size of the NPs (Rejman *et al.*, 2004, dos Santos *et al.*, 2011). For brain cells no information is currently available on the role of the cytoskeleton in IONPs uptake and trafficking.

1.4 Cell cultures as model systems for glial cells

To understand the uptake and cellular trafficking of IONPs and the consequences of IONP exposure in biological systems, cell cultures are suitable *in vitro* tools to gain first knowledge on IONP-cell interactions. (Calero *et al.*, 2014, Bencsik *et al.*, 2018). Although, cell cultures models cannot capture the whole complexity of living organisms due to the lack of three dimensional organization of tissues, the connection to other cell types, the lack of the immune system and the altered environment, they are indispensable for exploring the basal cytotoxicity and uptake mechanisms of NPs before more complex *in vivo* experiments are performed (Lange *et al.*, 2012, Calero *et al.*, 2014).

1.4.1 Cultured astrocytes

Astrocytes can be used as primary or secondary culture (Lange *et al.*, 2012, Petters and Dringen, 2014). Primary astrocytes are probably the closest *in vitro* model for *in vivo* situations (Bregoli *et al.*, 2013) and have been frequently used to study properties and functions of brain astrocytes (Lange *et al.*, 2012, Petters *et al.*, 2014b, Tulpule *et al.*, 2014). Cultured astrocytes are most commonly prepared from brain tissue of mice or rats (Hamprecht and Loffler, 1985, Tulpule *et al.*, 2014). These cultures can contain contaminations of other types of brain cells such as microglia, neurons, oligodendrocytes, endothelial cells and neuronal stem cells (Hamprecht and Loffler, 1985, Lange *et al.*, 2012, Tulpule *et al.*, 2014). For example, in uptake studies of IONPs using astrocyte primary cultures the presence of microglial cells (Petters and Dringen, 2014, Tulpule *et al.*, 2014) should be considered and analyzed as co-culture studies observed that IONPs are taken up more strongly by microglial cells in co-cultures of microglia and astrocytes (Fleige *et al.*, 2001, Pickard and Chari, 2010). The presence of different cell types in primary cultures can be investigated by immunocytochemical staining for cell type specific markers (Petters and Dringen, 2014, Tulpule *et al.*, 2014). For astrocytes the expression of the glial fibrillary acid protein (GFAP) is commonly used marker for immunocytochemical characterization (Sofroniew and Vinters, 2010) (Fig. 1.8). GFAP

expression *in vivo* is more or less restricted to reactive astrocytes that are responding to CNS injuries (Sofroniew and Vinters, 2010), whereas in culture astrocytes vary in the intensity of GFAP-positive staining depending on the culturing conditions.

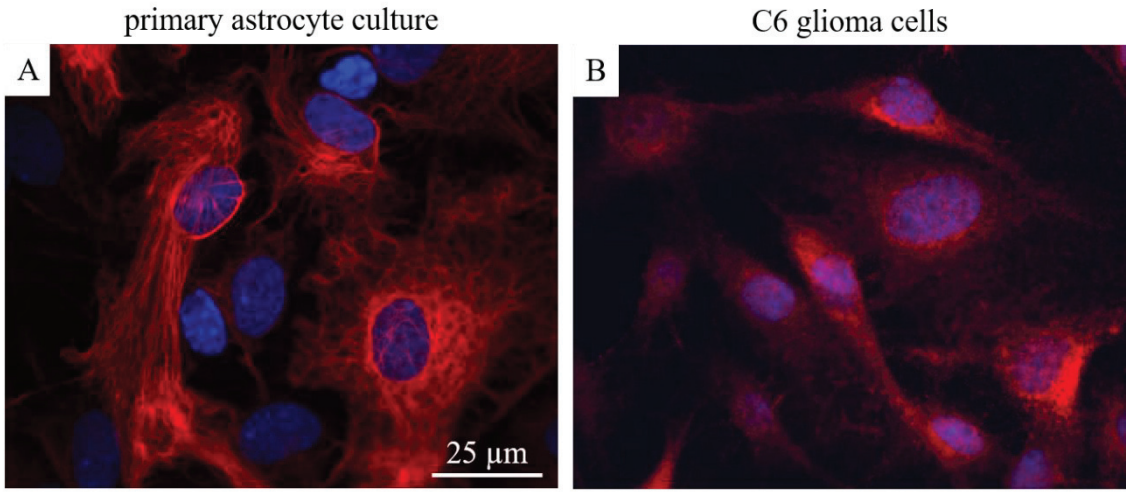

Fig. 1.8 GFAP-expression in primary astrocyte cultures and C6 glioma cells. Primary astrocyte cultures and C6 glioma cells were washed twice with cold phosphate-buffered saline, fixed with 3.5% (w/v) paraformaldehyde and stained as described (Stapelfeldt *et al*., 2017) for glial fibrillary acidic protein (GFAP, red) by using an rabbit α-GFAP antibody. The nuclei were stained with DAPI (blue).

1.4.2 C6 glioma cells

C6 glioma cells are widely used as model to study glial cells (Mangoura *et al.*, 1989) and brain glioma cells (Grobben *et al.*, 2002). Due to the expression of the glial fibrillary acidic protein (GFAP) (Fig. 3.8) and the glutamine synthetase, C6 glioma cells are often used as an astrocyte model system (Kumar *et al.*, 1986, Mangoura *et al.*, 1989, Goswami *et al.*, 2015). However results obtained in such cell lines as model systems should be carefully interpreted for their relevance for normal tissue cells as cell lines are mostly transformed, possess lost growth control and genetic and chromosomal changes compared to the genuine brain cells (Bregoli *et al.*, 2013). Furthermore, differentiation states of the cell culture can change the protein expression patterns. In fact, C6 glioma cells express also oligodendroglial marker proteins such as glycerol phosphate dehydrogenase and cyclic nucleotide phosphohydrogenase (Bissell *et al.*, 1975, Kumar *et al.*, 1986, Mangoura *et al.*, 1989) and should therefore be considered as glia precursor cells (Koch *et al.*, 2007). Nevertheless, the advantages of such cell lines are the easy

handling and continuous availability of a large number of cells (Bregoli *et al.*, 2013). Another advantage of C6 glioma cells as model system is the homogeneity of these cells in culture in contrast to primary cultures, where always a small contamination with other cells is possible due to the preparation methods (Lange *et al.*, 2012, Petters and Dringen, 2014). Due to these advantages cell lines are often used for first screening tests, even though the primary cultures are more precise in reflecting properties of the respective brain cells (Kaur and Dufour, 2012, Bregoli *et al.*, 2013, Gordon *et al.*, 2013).

1.5 Aim of the thesis

Dimercaptosuccinate (DMSA)-coated IONPs have previously been functionalized with the fluorescence dye BODIPY (BP) to study the cellular uptake and intracellular localization of IONPs in brain cells by fluorescence microscopy (Luther *et al.*, 2013, Petters *et al.*, 2014a, Petters *et al.*, 2016). However, a strong disadvantage of these BP-IONPs is a rapid photo bleaching which limited the possible applications of these particles for studies on the intracellular fate of IONPs in neural cells.

The aim of the present thesis is to generate more stable fluorescent IONPs by attaching fluorescence dyes to the SH groups of the DMSA. To improve fluorescence intensity and stability of the fluorescent IONPs, the DMSA coat will be functionalized with Oregon Green (OG) or tetramethylrhodamine (TMR) as these dyes are available as iodoacetamides for easy coupling to the SH-group of the DMSA (Fig. 1.9) and possess suitable absorption and emission maxima matching the settings of the available wide-field epifluorescence microscope.

OG-DMSA-coated and TMR-DMSA-coated IONPs will be synthesized, characterized for their physicochemical properties (size, shape, size distribution, charge and fluorescence) and compared to non-fluorescent and BODIPY-labeled IONPs. Additionally, the fluorescent IONPs will be compared to non-fluorescent IONPs regarding interaction with cells to investigate whether the insertion of the fluorescence dyes has any effect on the binding and the cellular accumulation using C6 glioma cells.
To study the internalization and intracellular fate of fluorescent IONPs nanoparticle pulse-chase set up will be established to improve cellular resolution of these IONPs in

C6 glioma cells and other neural cell cultures. Finally, these optimized settings for nanoparticle pulse-chase will be used to analyze the role of the cytoskeleton in the uptake and intracellular trafficking of IONPs and to investigate the intracellular separation of the coating material and the core of the internalized fluorescent IONPs.

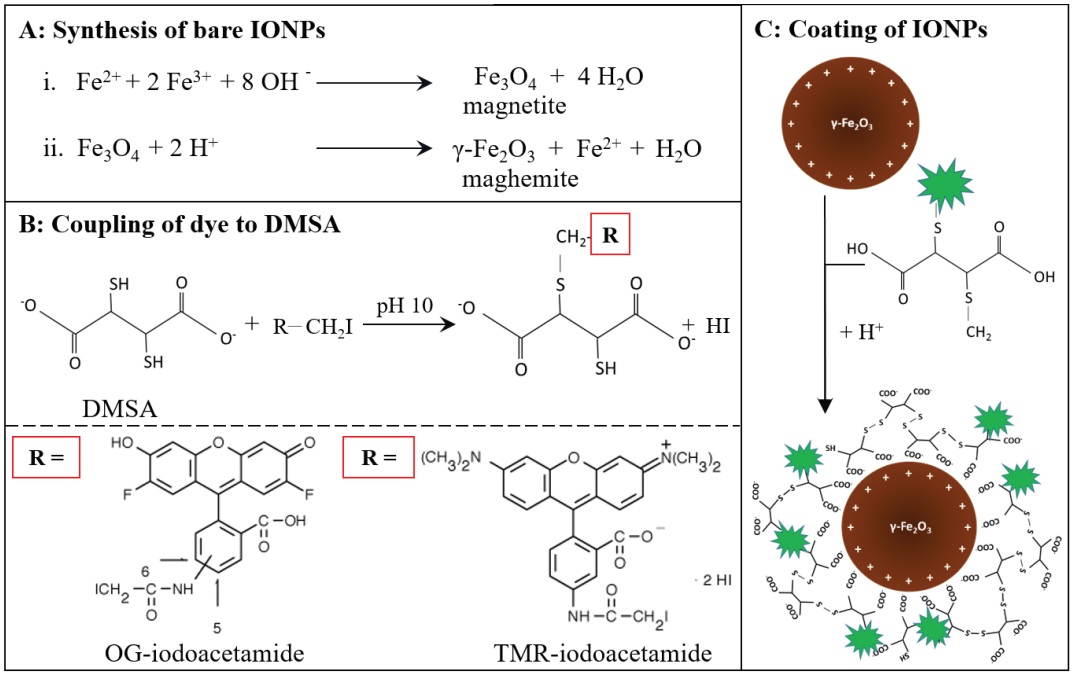

Fig. 1.9 Synthesis of fluorescently labeled IONPs. The synthesis of fluorescent IONPs is a three step process: (A) The synthesis of bare IONPs via the chemical coprecipitation method, (B) synthesis of fluorescent DMSA by formation of a thioether-bound between the iodoacetamide group of the fluorescence dye and the SH-group of the DMSA and (C) coating of the bare IONPs with the fluorescent DMSA.

1.6 References

Abbott NJ, Patabendige AA, Dolman DE, Yusof SR & Begley DJ (2010). Structure and function of the blood-brain barrier. *Neurobiol Dis,* 37: 13-25.

Adjei IM, Sharma B & Labhasetwar V (2014). Nanoparticles: Cellular uptake and cytotoxicity. *Adv Exp Med Biol,* 811: 73-91.

Akbarzadeh A, Samiei M & Davaran S (2012). Magnetic nanoparticles: Preparation, physical properties, and applications in biomedicine. *Nanoscale Res Lett,* 7: 144.

Algar WR, Prasuhn DE, Stewart MH, Jennings TL, Blanco-Canosa JB, Dawson PE & Medintz IL (2011). The controlled display of biomolecules on nanoparticles: A challenge suited to bioorthogonal chemistry. *Bioconjug Chem,* 22: 825-58.

Ali A, Zafar H, Zia M, Ul Haq I, Phull AR, Ali JS & Hussain A (2016). Synthesis, characterization, applications, and challenges of iron oxide nanoparticles. *Nanotechnol Sci Appl,* 9: 49-67.

Ali K, Javed Y & Jamil Y (2017). Size and shape control synthesis of ion oxide-based nanoparticles: current status and future possibility. In*:* Sharma SK (ed.) Complex magnetic nanostructures. Springer, Cham pp. 39-81

Amiri H, Bordonali L, Lascialfari A, Wan S, Monopoli MP, Lynch I, Laurent S & Mahmoudi M (2013). Protein corona affects the relaxivity and MRI contrast efficiency of magnetic nanoparticles. *Nanoscale,* 5: 8656-65.

Amiri H, Mahmoudi M & Lascialfari A (2011). Superparamagnetic colloidal nanocrystal clusters coated with polyethylene glycol fumarate: A possible novel theranostic agent. *Nanoscale,* 3: 1022-30.

Anu ME & Saravanakumar MP (2017). A review on the classification, characterisation, sythesis of nanoparticles and their application. *IOP Conf Ser Mater Sci Eng,* 263: 032019.

Auffan M, Rose J, Bottero JY, Lowry GV, Jolivet JP & Wiesner MR (2009). Towards a definition of inorganic nanoparticles from an environmental, health and safety perspective. *Nat Nanotechnol,* 4: 634-41.

Baetke SC, Lammers T & Kiessling F (2015). Applications of nanoparticles for diagnosis and therapy of cancer. *Br J Radiol,* 88: 1054.

Banerjee S, Raja SO, Sardar M, Gayathri N, Ghosh B & Dasgupta A (2011). Iron oxide nanoparticles coated with gold: Enhanced magnetic moment due to interfacial effects. *J Appl Phys,* 109.

Banobre-Lopez M, Teijeiro A & Rivas J (2013). Magnetic nanoparticle-based hyperthermia for cancer treatment. *Rep Pract Oncol Radiother,* 18: 397-400.

Bencsik A, Lestaevel P & Guseva Canu I (2018). Nano- and neurotoxicology: An emerging discipline. *Prog Neurobiol,* 160: 45-63.

Bertorelle F, Wilhelm C, Roger J, Gazeau F, Menager C & Cabuil V (2006). Fluorescence-modified superparamagnetic nanoparticles: Intracellular uptake and use in cellular imaging. *Langmuir,* 22: 5385-91.

Bissell MG, Eng LF, Herman MM, Bensch KG & Miles LE (1975). Quantitative increase of neuroglia-specific GFA protein in rat C-6 glioma cells in vitro. *Nature,* 255: 633-4.

Bobo D, Robinson KJ, Islam J, Thurecht KJ & Corrie SR (2016). Nanoparticle-based medicines: A review of FDA-approved materials and clinical trials to date. *Pharm Res,* 33: 2373-87.

Boulant S, Kural C, Zeeh JC, Ubelmann F & Kirchhausen T (2011). Actin dynamics counteract membrane tension during clathrin-mediated endocytosis. *Nat Cell Biol,* 13: 1124-31.

Bradl M & Lassmann H (2010). Oligodendrocytes: Biology and pathology. *Acta Neuropathol,* 119: 37-53.

Bregoli L, Benetti F, Venturini M & Sabbioni E (2013). ECSIN's methodological approach for hazard evaluation of engineered nanomaterials. *J Phys Conf Ser,* 429: 012017.

Cabezas R, Avila M, Gonzalez J, El-Bacha RS, Baez E, Garcia-Segura LM, Jurado Coronel JC, Capani F, Cardona-Gomez GP & Barreto GE (2014). Astrocytic modulation of blood brain barrier: Perspectives on Parkinson's disease. *Front Cell Neurosci,* 8: 211.

Calero M, Gutierrez L, Salas G, Luengo Y, Lazaro A, Acedo P, Morales MP, Miranda R & Villanueva A (2014). Efficient and safe internalization of magnetic iron oxide nanoparticles: two fundamental requirements for biomedical applications. *Nanomedicine (Lond),* 10: 733-43.

Campos EA, Pinto DVBS, de Oliveira JIS, Mattos ED & Dutra RDL (2015). Synthesis, characterization and applications of iron oxide nanoparticles - a short review. *J Aerosp Technol Man,* 7: 267-276.

Canton I & Battaglia G (2012). Endocytosis at the nanoscale. *Chem Soc Rev,* 41: 2718-39.

Castello J, Gallardo M, Busquets MA & Estelrich J (2015). Chitosan (or alginate)-coated iron oxide nanoparticles: A comparative study. *Colloid Surface A,* 468: 151-158.

Chekina N, Horak D, Jendelova P, Trchova M, Benes MJ, Hruby M, Herynek V, Turnovcova K & Sykova E (2011). Fluorescent magnetic nanoparticles for biomedical applications. *J Mater Chem,* 21: 7630-7639.

Chen ZP, Zhang Y, Zhang S, Xia JG, Liu JW, Xu K & Gu N (2008). Preparation and characterization of water-soluble monodisperse magnetic iron oxide nanoparticles via surface double-exchange with DMSA. *Colloids and Surfaces a-Physicochemical and Engineering Aspects,* 316: 210-216.

Christian P, Von der Kammer F, Baalousha M & Hofmann T (2008). Nanoparticles: structure, properties, preparation and behaviour in environmental media. *Ecotoxicology,* 17: 326-43.

Colombo E & Farina C (2016). Astrocytes: Key regulators of neuroinflammation. *Trends Immunol,* 37: 608-20.

Colombo M, Carregal-Romero S, Casula MF, Gutierrez L, Morales MP, Bohm IB, Heverhagen JT, Prosperi D & Parak WJ (2012). Biological applications of magnetic nanoparticles. *Chem Soc Rev,* 41: 4306-34.

Corr SA, Rakovich YP & Gun'ko YK (2008). Multifunctional magnetic-fluorescent nanocomposites for biomedical applications. *Nanoscale Res Lett,* 3: 87-104.

Cossart P & Helenius A (2014). Endocytosis of viruses and bacteria. *Cold Spring Harb Perspect Biol,* 6.

Costa C, Brandao F, Bessa MJ, Costa S, Valdiglesias V, Kilic G, Fernandez-Bertolez N, Quaresma P, Pereira E, Pasaro E, Laffon B & Teixeira JP (2016). In vitro cytotoxicity of superparamagnetic iron oxide nanoparticles on neuronal and glial cells. Evaluation of nanoparticle interference with viability tests. *J Appl Toxicol,* 36: 361-72.

Dante S, Petrelli A, Petrini EM, Marotta R, Maccione A, Alabastri A, Quarta A, De Donato F, Ravasenga T, Sathya A, Cingolani R, Zaccaria RP, Berdondini L, Barberis A & Pellegrino T (2017). Selective targeting of neurons with inorganic nanoparticles: Revealing the crucial role of nanoparticle surface charge. *ACS Nano,* 11: 6630-6640.

De la Fuente JM & Grazu V (2012). Nanobiotechnology: Inorganic nanoparticles vs organic nanoparticles, United Kingdom, Elsevier.

De Matteis V (2017). Exposure to inorganic nanoparticles: Routes of entry, immune response, biodistribution and in vitro/in vivo toxicity evaluation. *Toxics,* 5.

Denizot B, Tanguy G, Hindre F, Rump E, Jacques Le Jeune J & Jallet P (1999). Phosphorylcholine coating of iron oxide nanoparticles. *J Colloid Interface Sci,* 209: 66-71.

Doak SH, Griffiths SM, Manshian B, Singh N, Williams PM, Brown AP & Jenkins GJS (2009). Confounding experimental considerations in nanogenotoxicology. *Mutagenesis,* 24: 285-293.

Doherty GJ & McMahon HT (2009). Mechanisms of endocytosis. *Annu Rev Biochem,* 78: 857-902.

dos Santos T, Varela J, Lynch I, Salvati A & Dawson KA (2011). Effects of transport inhibitors on the cellular uptake of carboxylated polystyrene nanoparticles in different cell lines. *PLoS One,* 6: e24438.

Dringen R, Brandmann M, Hohnholt MC & Blumrich EM (2015). Glutathione-dependent detoxification processes in astrocytes. *Neurochem Res,* 40: 2570-82.

Durrbach A, Louvard D & Coudrier E (1996). Actin filaments facilitate two steps of endocytosis. *J Cell Sci,* 109: 457-65.

El-Boubbou K (2018). Magnetic iron oxide nanoparticles as drug carriers: clinical relevance. *Nanomedicine (Lond),* https://doi.org/10.2217/nnm-2017-0336.

Ercal N, Treeratphan P, Hammond TC, Matthews RH, Grannemann NH & Spitz DR (1996). In vivo indices of oxidative stress in lead-exposed C57BL/6 mice are reduced by treatment with meso-2,3-dimercaptosuccinic acid or N-acetylcysteine. *Free Radic Biol Med,* 21: 157-61.

Fauconnier N, Pons JN, Roger J & Bee A (1997). Thiolation of maghemite nanoparticles by dimercaptosuccinic acid. *J Colloid Interface Sci,* 194: 427-33.

Feliu N, Docter D, Heine M, Del Pino P, Ashraf S, Kolosnjaj-Tabi J, Macchiarini P, Nielsen P, Alloyeau D, Gazeau F, Stauber RH & Parak WJ (2016). In vivo degeneration and the fate of inorganic nanoparticles. *Chem Soc Rev,* 45: 2440-57.

Fernandez T, Martinez-Serrano A, Cusso L, Desco M & Ramos-Gomez M (2018). Functionalization and characterization of magnetic nanoparticles for the detection of ferritin accumulation in Alzheimer's disease. *ACS Chem Neurosci*.

Fleige G, Nolte C, Synowitz M, Seeberger F, Kettenmann H & Zimmer C (2001). Magnetic labeling of activated microglia in experimental gliomas. *Neoplasia,* 3: 489-99.

Flora SJ & Pachauri V (2010). Chelation in metal intoxication. *Int J Environ Res Public Health,* 7: 2745-88.

Forest V, Cottier M & Pourchez J (2015). Electrostatic interactions favor the binding of positive nanoparticles on cells: A reductive theory. *Nano Today,* 10: 677-680.

Fujimoto LM, Roth R, Heuser JE & Schmid SL (2000). Actin assembly plays a variable, but not obligatory role in receptor-mediated endocytosis in mammalian cells. *Traffic,* 1: 161-71.

Galli M, Guerrini A, Cauteruccio S, Thakare P, Dova D, Orsini F, Arosio P, Carrara C, Sangregorio C, Lascialfari A, Maggioni D & Licandro E (2017). Superparamagnetic iron oxide nanoparticles functionalized by peptide nucleic acids. *Rsc Advances,* 7: 15500-15512.

Gatoo MA, Naseem S, Arfat MY, Dar AM, Qasim K & Zubair S (2014). Physicochemical properties of nanomaterials: implication in associated toxic manifestations. *Biomed Res Int,* 2014: 498420.

Geiser M, Rothen-Rutishauser B, Kapp N, Schurch S, Kreyling W, Schulz H, Semmler M, Im Hof V, Heyder J & Gehr P (2005). Ultrafine particles cross cellular membranes by nonphagocytic mechanisms in lungs and in cultured cells. *Environ Health Perspect,* 113: 1555-60.

Geppert M, Hohnholt MC, Nurnberger S & Dringen R (2012). Ferritin up-regulation and transient ROS production in cultured brain astrocytes after loading with iron oxide nanoparticles. *Acta Biomater,* 8: 3832-9.

Geppert M, Hohnholt MC, Thiel K, Nurnberger S, Grunwald I, Rezwan K & Dringen R (2011). Uptake of dimercaptosuccinate-coated magnetic iron oxide nanoparticles by cultured brain astrocytes. *Nanotechnology,* 22: 145101.

Geppert M, Petters C, Thiel K & Dringen R (2013). The presence of serum alters the properties of iron oxide nanoparticles and lowers their accumulation by cultured brain astrocytes. *Journal of Nanoparticle Research,* 15: 1349.

Gordon J, Amini S & White MK (2013). General overview of neuronal cell culture. *Methods Mol Biol,* 1078: 1-8.

Gordon R, Hogan CE, Neal ML, Anantharam V, Kanthasamy AG & Kanthasamy A (2011). A simple magnetic separation method for high-yield isolation of pure primary microglia. *J Neurosci Methods,* 194: 287-96.

Gorshkov K, Aguisanda F, Thorne N & Zheng W (2018). Astrocytes as targets for drug discovery. *Drug Discov Today*.

Goswami P, Gupta S, Joshi N, Sharma S & Singh S (2015). Astrocyte activation and neurotoxicity: a study in different rat brain regions and in rat C6 astroglial cells. *Environ Toxicol Pharmacol,* 40: 122-39.

Grabrucker AM, Ruozi B, Belletti D, Pederzoli F, Forni F, Vandelli MA & Tosi G (2016). Nanoparticle transport across the blood brain barrier. *Tissue Barriers,* 4: e1153568.

Granger E, McNee G, Allan V & Woodman P (2014). The role of the cytoskeleton and molecular motors in endosomal dynamics. *Semin Cell Dev Biol,* 31: 20-9.

Grobben B, De Deyn PP & Slegers H (2002). Rat C6 glioma as experimental model system for the study of glioblastoma growth and invasion. *Cell Tissue Res,* 310: 257-70.

Gupta AK & Gupta M (2005). Synthesis and surface engineering of iron oxide nanoparticles for biomedical applications. *Biomaterials,* 26: 3995-4021.

Gupta AK & Wells S (2004). Surface-modified superparamagnetic nanoparticles for drug delivery: preparation, characterization, and cytotoxicity studies. *IEEE Trans Nanobioscience,* 3: 66-73.

Hamprecht B & Loffler F (1985). Primary glial cultures as a model for studying hormone action. *Methods Enzymol,* 109: 341-5.

Hare D, Ayton S, Bush A & Lei P (2013). A delicate balance: Iron metabolism and diseases of the brain. *Frontiers in Aging Neuroscience,* 5: 1-19.

Heiligtag FJ & Niederberger M (2013). The fascinating world of nanoparticle research. *Materials Today,* 16: 262-271.

Hirase H & Koizumi S (2018). Astrocytes as therapeutic targets in brain diseases. *Neurosci Res,* 126: 1-2.

Hohnholt MC, Geppert M, Luther EM, Petters C, Bulcke F & Dringen R (2013). Handling of iron oxide and silver nanoparticles by astrocytes. *Neurochem Res,* 38: 227-39.

Ivask A, Pilkington EH, Blin T, Kakinen A, Vija H, Visnapuu M, Quinn JF, Whittaker MR, Qiao R, Davis TP, Ke PC & Voelcker NH (2018). Uptake and transcytosis

of functionalized superparamagnetic iron oxide nanoparticles in an in vitro blood brain barrier model. *Biomater Sci,* 6: 314-323.

Iversen TG, Skotland T & Sandvig K (2011). Endocytosis and intracellular transport of nanoparticles: Present knowledge and need for future studies. *Nano Today,* 6: 176-185.

Jasmin, de Souza GT, Louzada RA, Rosado-de-Castro PH, Mendez-Otero R & Campos de Carvalho AC (2017). Tracking stem cells with superparamagnetic iron oxide nanoparticles: perspectives and considerations. *Int J Nanomedicine,* 12: 779-793.

Jenkins SI, Pickard MR, Granger N & Chari DM (2011). Magnetic nanoparticle-mediated gene transfer to oligodendrocyte precursor cell transplant populations is enhanced by magnetofection strategies. *ACS Nano,* 5: 6527-38.

Kaewsaneha C, Tangboriboonrat P, Polpanich D & Elaissari A (2015). Multifunctional fluorescent-magnetic polymeric colloidal particles: Preparations and bioanalytical applications. *ACS Appl Mater Interfaces,* 7: 23373-86.

Kariminia S, Shamsipur A & Shamsipur M (2016). Analytical characteristics and application of novel chitosan coated magnetic nanoparticles as an efficient drug delivery system for ciprofloxacin. Enhanced drug release kinetics by low-frequency ultrasounds. *J Pharm Biomed Anal,* 129: 450-457.

Kasten A, Gruttner C, Kuhn JP, Bader R, Pasold J & Frerich B (2014). Comparative in vitro study on magnetic iron oxide nanoparticles for MRI tracking of adipose tissue-derived progenitor cells. *PLoS One,* 9: e108055.

Kaur G & Dufour JM (2012). Cell lines: Valuable tools or useless artifacts. *Spermatogenesis,* 2: 1-5.

Khan I, Saeed I & Khan I (2017). Nanoparticles: Properties, applications and toxicities. *Arab J Chem*, in press

Koch M, May U, Kuhns S, Drechsler H, Adam N, Hattermann K, Wirtz S, Rose-John S & Scheller J (2007). Interleukin 27 induces differentiation of neural C6-precursor cells into astrocytes. *Biochem Biophys Res Commun,* 364: 483-7.

Kolosnjaj-Tabi J, Wilhelm C, Clement O & Gazeau F (2013). Cell labeling with magnetic nanoparticles: opportunity for magnetic cell imaging and cell manipulation. *J Nanobiotechnology,* 11: 7.

Krol S, Macrez R, Docagne F, Defer G, Laurent S, Rahman M, Hajipour MJ, Kehoe PG & Mahmoudi M (2013). Therapeutic benefits from nanoparticles: The potential significance of nanoscience in diseases with compromise to the blood brain barrier. *Chem Rev,* 113: 1877-903.

Ku S, Yan F, Wang Y, Sun Y, Yang N & Ye L (2010). The blood-brain barrier penetration and distribution of PEGylated fluorescein-doped magnetic silica nanoparticles in rat brain. *Biochem Biophys Res Commun,* 394: 871-6.

Kumar S, Holmes E, Scully S, Birren BW, Wilson RH & de Vellis J (1986). The hormonal regulation of gene expression of glial markers: glutamine synthetase and glycerol phosphate dehydrogenase in primary cultures of rat brain and in C6 cell line. *J Neurosci Res,* 16: 251-64.

Kumari S, Mg S & Mayor S (2010). Endocytosis unplugged: Multiple ways to enter the cell. *Cell Res,* 20: 256-75.

Kura AU, Fakurazi S, Hussein MZ & Arulselvan P (2014). Nanotechnology in drug delivery: The need for more cell culture based studies in screening. *Chem Cent J,* 8: 46.

Lai SK, Hida K, Man ST, Chen C, Machamer C, Schroer TA & Hanes J (2007). Privileged delivery of polymer nanoparticles to the perinuclear region of live cells via a non-clathrin, non-degradative pathway. *Biomaterials,* 28: 2876-84.

Lamaze C, Fujimoto LM, Yin HL & Schmid SL (1997). The actin cytoskeleton is required for receptor-mediated endocytosis in mammalian cells. *J Biol Chem,* 272: 20332-5.

Lamkowsky MC, Geppert M, Schmidt MM & Dringen R (2012). Magnetic field-induced acceleration of the accumulation of magnetic iron oxide nanoparticles by cultured brain astrocytes. *J Biomed Mater Res A,* 100: 323-34.

Lange SC, Bak LK, Waagepetersen HS, Schousboe A & Norenberg MD (2012). Primary cultures of astrocytes: Their value in understanding astrocytes in health and disease. *Neurochem Res,* 37: 2569-88.

Laurent S, Burtea C, Thirifays C, Rezaee F & Mahmoudi M (2013). Significance of cell "observer" and protein source in nanobiosciences. *J Colloid Interface Sci,* 392: 431-45.

Laurent S, Dutz S, Hafeli UO & Mahmoudi M (2011). Magnetic fluid hyperthermia: focus on superparamagnetic iron oxide nanoparticles. *Adv Colloid Interface Sci,* 166: 8-23.

Laurent S, Forge D, Port M, Roch A, Robic C, Vander Elst L & Muller RN (2008). Magnetic iron oxide nanoparticles: synthesis, stabilization, vectorization, physicochemical characterizations, and biological applications. *Chem Rev,* 108: 2064-110.

Lesniak A, Salvati A, Santos-Martinez MJ, Radomski MW, Dawson KA & Aberg C (2013). Nanoparticle adhesion to the cell membrane and its effect on nanoparticle uptake efficiency. *J Am Chem Soc,* 135: 1438-44.

Levy M, Lagarde F, Maraloiu VA, Blanchin MG, Gendron F, Wilhelm C & Gazeau F (2010). Degradability of superparamagnetic nanoparticles in a model of intracellular environment: Follow-up of magnetic, structural and chemical properties. *Nanotechnology,* 21: 395103.

Li L, Mak KY, Leung CW, Chan KY, Chan WK, Zhong W & Pong PWT (2013). Effect of synthesis conditions on the properties of citric-acid coated iron oxide nanoparticles. *Microelectron Eng,* 110: 329-334.

Lim JK, Majetich SA & Tilton RD (2009). Stabilization of superparamagnetic iron oxide core-gold shell nanoparticles in high ionic strength media. *Langmuir,* 25: 13384-93.

Liu H, Zhang J, Chen X, Du XS, Zhang JL, Liu G & Zhang WG (2016). Application of iron oxide nanoparticles in glioma imaging and therapy: From bench to bedside. *Nanoscale,* 8: 7808-26.

Lodhia J, Mandarano G, Ferris N, Eu P & Cowell S (2010). Development and use of iron oxide nanoparticles (Part 1): Synthesis of iron oxide nanoparticles for MRI. *Biomed Imaging Interv J,* 6: e12.

Luther EM, Petters C, Bulcke F, Kaltz A, Thiel K, Bickmeyer U & Dringen R (2013). Endocytotic uptake of iron oxide nanoparticles by cultured brain microglial cells. *Acta Biomater,* 9: 8454-65.

Mahmoudi M, Meng J, Xue X, Liang XJ, Rahman M, Pfeiffer C, Hartmann R, Gil PR, Pelaz B, Parak WJ, Del Pino P, Carregal-Romero S, Kanaras AG & Tamil Selvan S (2014). Interaction of stable colloidal nanoparticles with cellular membranes. *Biotechnol Adv,* 32: 679-92.

Maier-Hauff K, Ulrich F, Nestler D, Niehoff H, Wust P, Thiesen B, Orawa H, Budach V & Jordan A (2011). Efficacy and safety of intratumoral thermotherapy using magnetic iron-oxide nanoparticles combined with external beam radiotherapy on patients with recurrent glioblastoma multiforme. *J Neurooncol,* 103: 317-24.

Maity D & Agrawal DC (2007). Synthesis of iron oxide nanoparticles under oxidizing environment and their stabilization in aqueous and non-aqueous media. *J Magn Magn Mater,* 308: 46-55.

Mangoura D, Sakellaridis N, Jones J & Vernadakis A (1989). Early and late passage C-6 glial cell growth: similarities with primary glial cells in culture. *Neurochem Res,* 14: 941-7.

Massart R (1981). Preparation of aqueous magnetic liquids in alkaline and acidic media. *IEEE T Magn,* 17: 1247-1248.

Mazuel F, Espinosa A, Luciani N, Reffay M, Le Borgne R, Motte L, Desboeufs K, Michel A, Pellegrino T, Lalatonne Y & Wilhelm C (2016). Massive intracellular biodegradation of iron oxide nanoparticles evidenced magnetically at single-endosome and tissue levels. *ACS Nano,* 10: 7627-38.

McNamara K & Tofail SAM (2017). Nanoparticles in biomedical applications. *Adv Phys-X,* 2: 54-88.

Mejias R, Perez-Yague S, Roca AG, Perez N, Villanueva A, Canete M, Manes S, Ruiz-Cabello J, Benito M, Labarta A, Batlle X, Veintemillas-Verdaguer S, Morales MP, Barber DF & Serna CJ (2010). Liver and brain imaging through dimercaptosuccinic acid-coated iron oxide nanoparticles. *Nanomedicine (Lond),* 5: 397-408.

Michalski JP & Kothary R (2015). Oligodendrocytes in a nutshell. *Front Cell Neurosci,* 9: 340.

Mohammed L, Gomaa HG, Ragab D & Zhu J (2017). Magnetic nanoparticles for environmental and biomedical applications: A review. *Particuology,* 30: 1-14.

Mooren OL, Galletta BJ & Cooper JA (2012). Roles for actin assembly in endocytosis. *Annu Rev Biochem,* 81: 661-86.

Morris G, Berk M, Carvalho AF, Maes M, Walker AJ & Puri BK (2018). Why should neuroscientists worry about iron? The emerging role of ferroptosis in the pathophysiology of neuroprogressive diseases. *Behav Brain Res,* 341: 154-175.

Mu Q, Jiang G, Chen L, Zhou H, Fourches D, Tropsha A & Yan B (2014). Chemical basis of interactions between engineered nanoparticles and biological systems. *Chem Rev,* 114: 7740-81.

Murgoci AN, Cizkova D, Majerova P, Petrovova E, Medvecky L, Fournier I & Salzet M (2018). Brain cortex microglia derived exosomes: Novel nanoparticles for glioma therapy. *Chemphyschem*, in press

Nayak D, Roth TL & McGavern DB (2014). Microglia development and function. *Annu Rev Immunol,* 32: 367-402.

Nazarenus M, Zhang Q, Soliman MG, Del Pino P, Pelaz B, Carregal-Romero S, Rejman J, Rothen-Rutishauser B, Clift MJ, Zellner R, Nienhaus GU, Delehanty JB, Medintz IL & Parak WJ (2014). In vitro interaction of colloidal nanoparticles with mammalian cells: What have we learned thus far? *Beilstein J Nanotechnol,* 5: 1477-90.

Nel AE, Madler L, Velegol D, Xia T, Hoek EM, Somasundaran P, Klaessig F, Castranova V & Thompson M (2009). Understanding biophysicochemical interactions at the nano-bio interface. *Nat Mater,* 8: 543-57.

Oh N & Park JH (2014). Endocytosis and exocytosis of nanoparticles in mammalian cells. *Int J Nanomedicine,* 9: 51-63.

Patel MM, Chillrud SN, Deepti KC, Ross JM & Kinney PL (2013). Traffic-related air pollutants and exhaled markers of airway inflammation and oxidative stress in New York City adolescents. *Environl Res,* 121: 71-78.

Pelaz B, Charron G, Pfeiffer C, Zhao Y, de la Fuente JM, Liang XJ, Parak WJ & Del Pino P (2013). Interfacing engineered nanoparticles with biological systems: anticipating adverse nano-bio interactions. *Small,* 9: 1573-84.

Perillo E, Herve-Aubert K, Allard-Vannier E, Falanga A, Galdiero S & Chourpa I (2017). Synthesis and in vitro evaluation of fluorescent and magnetic nanoparticles functionalized with a cell penetrating peptide for cancer theranosis. *J Colloid Interface Sci,* 499: 209-217.

Peters DG & Connor JR (2014). Introduction to cells comprising the nervous system. *Adv Neurobiol,* 9: 33-45.

Petters C. (2015). *Uptake and metabolism of iron oxide nanoparticle in cultured brain cells.* Ph.D Thesis, Univeristy of Bremen.

Petters C, Bulcke F, Thiel K, Bickmeyer U & Dringen R (2014a). Uptake of fluorescent iron oxide nanoparticles by oligodendroglial OLN-93 cells. *Neurochem Res,* 39: 372-83.

Petters C & Dringen R (2014). Comparison of primary and secondary rat astrocyte cultures regarding glucose and glutathione metabolism and the accumulation of iron oxide nanoparticles. *Neurochem Res,* 39: 46-58.

Petters C & Dringen R (2015). Accumulation of iron oxide nanoparticles by cultured primary neurons. *Neurochem Int,* 81: 1-9.

Petters C, Irrsack E, Koch M & Dringen R (2014b). Uptake and metabolism of iron oxide nanoparticles in brain cells. *Neurochem Res,* 39: 1648-60.

Petters C, Thiel K & Dringen R (2016). Lysosomal iron liberation is responsible for the vulnerability of brain microglial cells to iron oxide nanoparticles: Comparison with neurons and astrocytes. *Nanotoxicology,* 10: 332-42.

Phogat N, Khan SA, Schankar S, Ansary AA & Uddin I (2016). Fate of inorganic nanoparticles in agriculture. *Adv Mater Lett,* 7: 3-12.

Piccinno F, Gottschalk F, Seeger S & Nowack B (2012). Industrial production quantities and uses of ten engineered nanomaterials in Europe and the world. *J Nanopart Res,* 14: 1109.

Pickard MR & Chari DM (2010). Robust uptake of magnetic nanoparticles (MNPs) by central nervous system (CNS) microglia: Implications for particle uptake in mixed neural cell populations. *Int J Mol Sci,* 11: 967-81.

Pieters N, Plusquin M, Cox B, Kicinski M, Vangronsveld J & Nawrot TS (2012). An epidemiological appraisal of the association between heart rate variability and particulate air pollution: A meta-analysis. *Heart,* 98: 1127-1135.

Pilakka-Kanthikeel S, Atluri VS, Sagar V, Saxena SK & Nair M (2013). Targeted brain derived neurotropic factors (BDNF) delivery across the blood-brain barrier for neuro-protection using magnetic nano carriers: An in-vitro study. *PLoS One,* 8: e62241.

Posadas I, Monteagudo S & Cena V (2016). Nanoparticles for brain-specific drug and genetic material delivery, imaging and diagnosis. *Nanomedicine (Lond),* 11: 833-49.

Qualmann B, Kessels MM & Kelly RB (2000). Molecular links between endocytosis and the actin cytoskeleton. *J Cell Biol,* 150: F111-6.

Rejman J, Oberle V, Zuhorn IS & Hoekstra D (2004). Size-dependent internalization of particles via the pathways of clathrin- and caveolae-mediated endocytosis. *Biochem J,* 377: 159-69.

Rivera-Gil P, Jimenez de Aberasturi D, Wulf V, Pelaz B, del Pino P, Zhao Y, de la Fuente JM, Ruiz de Larramendi I, Rojo T, Liang XJ & Parak WJ (2013). The challenge

to relate the physicochemical properties of colloidal nanoparticles to their cytotoxicity. *Acc Chem Res,* 46: 743-9.

Robertson S, Gray GA, Duffin R, McLean SG, Shaw CA, Hadoke PWF, Newby DE & Miller MR (2012). Diesel exhaust particulate induces pulmonary and systemic inflammation in rats without impairing endothelial function ex vivo or in vivo. *Part Fibre Toxicl,* 9.

Rooney JP (2007). The role of thiols, dithiols, nutritional factors and interacting ligands in the toxicology of mercury. *Toxicology,* 234: 145-56.

Rothen-Rutishauser BM, Schurch S, Haenni B, Kapp N & Gehr P (2006). Interaction of fine particles and nanoparticles with red blood cells visualized with advanced microscopic techniques. *Environ Sci Technol,* 40: 4353-4359.

Rouault TA (2013). Iron metabolism in the CNS: Implications for neurodegenerative diseases. *Nat Rev Neurosci,* 14: 551-564.

Ruiz A, Morais PC, de Azevedo RB, Lacava ZGM, Villanueva A & Morales MD (2014). Magnetic nanoparticles coated with dimercaptosuccinic acid: development, characterization, and application in biomedicine. *J Nanopart Res,* 16.

Sakulkhu U, Mahmoudi M, Maurizi L, Salaklang J & Hofmann H (2014). Protein corona composition of superparamagnetic iron oxide nanoparticles with various physico-chemical properties and coatings. *Sci Rep,* 4: 5020.

Santamaria A (2012). Historical overview of nanotechnology and nanotoxicology. *Methods Mol Biol,* 926: 1-12.

Sapsford KE, Algar WR, Berti L, Gemmill KB, Casey BJ, Oh E, Stewart MH & Medintz IL (2013). Functionalizing nanoparticles with biological molecules: Developing chemistries that facilitate nanotechnology. *Chem Rev,* 113: 1904-2074.

Saptarshi SR, Duschl A & Lopata AL (2013). Interaction of nanoparticles with proteins: relation to bio-reactivity of the nanoparticle. *J Nanobiotechnology,* 11: 26.

Saura J, Tusell JM & Serratosa J (2003). High-yield isolation of murine microglia by mild trypsinization. *Glia,* 44: 183-9.

Scalettar BA (2006). How neurosecretory vesicles release their cargo. *Neuroscientist,* 12: 164-176.

Scherer F, Anton M, Schillinger U, Henke J, Bergemann C, Kruger A, Gansbacher B & Plank C (2002). Magnetofection: Enhancing and targeting gene delivery by magnetic force in vitro and in vivo. *Gene Ther,* 9: 102-9.

Shevtsov MA, Nikolaev BP, Ryzhov VA, Yakovleva LY, Marchenko YY, Parr MA, Rolich VI, Mikhrina AL, Dobrodumov AV, Pitkin E & Multhoff G (2015). Ionizing radiation improves glioma-specific targeting of superparamagnetic iron oxide nanoparticles conjugated with cmHsp70.1 monoclonal antibodies (SPION-cmHsp70.1). *Nanoscale,* 7: 20652-64.

Shevtsov MA, Yakovleva LY, Nikolaev BP, Marchenko YY, Dobrodumov AV, Onokhin KV, Onokhina YS, Selkov SA, Mikhrina AL, Guzhova IV, Martynova MG, Bystrova OA, Ischenko AM & Margulis BA (2014). Tumor targeting using magnetic nanoparticle Hsp70 conjugate in a model of C6 glioma. *Neuro Oncol,* 16: 38-49.

Shi D, Mi G, Bhattacharya S, Nayar S & Webster TJ (2016). Optimizing superparamagnetic iron oxide nanoparticles as drug carriers using an in vitro blood-brain barrier model. *Int J Nanomedicine,* 11: 5371-5379.

Shi D, Sadat ME, Dunn AW & Mast DB (2015). Photo-fluorescent and magnetic properties of iron oxide nanoparticles for biomedical applications. *Nanoscale,* 7: 8209-32.

Shubayev VI, Pisanic TR, 2nd & Jin S (2009). Magnetic nanoparticles for theragnostics. *Adv Drug Deliv Rev,* 61: 467-77.

Skotland T, Sontum PC & Oulie I (2002). In vitro stability analyses as a model for metabolism of ferromagnetic particles (Clariscan), a contrast agent for magnetic resonance imaging. *J Pharm Biomed Anal,* 28: 323-9.

Soenen SJ, Himmelreich U, Nuytten N & De Cuyper M (2011). Cytotoxic effects of iron oxide nanoparticles and implications for safety in cell labelling. *Biomaterials,* 32: 195-205.

Sofroniew MV & Vinters HV (2010). Astrocytes: biology and pathology. *Acta Neuropathol,* 119: 7-35.

Soldati T & Schliwa M (2006). Powering membrane traffic in endocytosis and recycling. *Nat Rev Mol Cell Biol,* 7: 897-908.

Soler MA, Lima EC, Nunes ES, Silva FL, Oliveira AC, Azevedo RB & Morais PC (2011). Spectroscopic study of maghemite nanoparticles surface-grafted with DMSA. *J Phys Chem A,* 115: 1003-8.

Stapelfeldt K, Ehrke E, Steinmeier J, Rastedt W & Dringen R (2017). Menadione-mediated WST1 reduction assay for the determination of metabolic activity of cultured neural cells. *Anal Biochem,* 538: 42-52.

Suh WH, Suslick KS, Stucky GD & Suh YH (2009). Nanotechnology, nanotoxicology, and neuroscience. *Prog Neurobiol,* 87: 133-70.

Sun YK, Duan L, Guo ZR, Yun DM, Ma M, Xu L, Zhang Y & Gu N (2005). An improved way to prepare superparamagnetic magnetite-silica core-shell nanoparticles for possible biological application. *J Magn Magn Mat,* 285: 65-70.

Thiesen B & Jordan A (2008). Clinical applications of magnetic nanoparticles for hyperthermia. *Int J Hyperthermia,* 24: 467-74.

Thimiri Govinda Raj DB & Khan NA (2016). Designer nanoparticle: Nanobiotechnology tool for cell biology. *Nano Converg,* 3: 22.

Thomsen LB, Thomsen MS & Moos T (2015). Targeted drug delivery to the brain using magnetic nanoparticles. *Ther Deliv,* 6: 1145-55.

Tietze R, Zaloga J, Unterweger H, Lyer S, Friedrich RP, Janko C, Pottler M, Durr S & Alexiou C (2015). Magnetic nanoparticle-based drug delivery for cancer therapy. *Biochem Biophys Res Commun,* 468: 463-70.

Torrisi V, Graillot A, Vitorazi L, Crouzet Q, Marletta G, Loubat C & Berret JF (2014). Preventing corona effects: Multiphosphonic acid poly(ethylene glycol) copolymers for stable stealth iron oxide nanoparticles. *Biomacromolecules,* 15: 3171-9.

Tulpule K, Hohnholt MC, Hirrlinger J & Dringen R (2014). Primary cultures of astrocytes and neurons as model systems to study the metabolism and metabolite export from brain cells. *In:* Hirrlinger J & Waagepetersen HS (eds.) *Brain Energy Metabolism.* New York: Springer.

Turro NJ, Lakshminarasimhan PH, Jockusch S, O'Brien SP, Grancharov SG & Redl FX (2002). Spectroscopic probe of the surface of iron oxide nanocrystals. *Nano Lett,* 2: 325-328.

Valdiglesias V, Fernandez-Bertolez N, Kilic G, Costa C, Costa S, Fraga S, Bessa MJ, Pasaro E, Teixeira JP & Laffon B (2016). Are iron oxide nanoparticles safe? Current knowledge and future perspectives. *J Trace Elem Med Biol,* 38: 53-63.

Valdiglesias V, Kilic G, Costa C, Fernandez-Bertolez N, Pasaro E, Teixeira JP & Laffon B (2015). Effects of iron oxide nanoparticles: cytotoxicity, genotoxicity, developmental toxicity, and neurotoxicity. *Environ Mol Mutagen,* 56: 125-48.

Valois CR, Braz JM, Nunes ES, Vinolo MA, Lima EC, Curi R, Kuebler WM & Azevedo RB (2010). The effect of DMSA-functionalized magnetic nanoparticles on transendothelial migration of monocytes in the murine lung via a beta2 integrin-dependent pathway. *Biomaterials,* 31: 366-74.

van Landeghem FK, Maier-Hauff K, Jordan A, Hoffmann KT, Gneveckow U, Scholz R, Thiesen B, Bruck W & von Deimling A (2009). Post-mortem studies in glioblastoma patients treated with thermotherapy using magnetic nanoparticles. *Biomaterials,* 30: 52-7.

Veiseh O, Sun C, Gunn J, Kohler N, Gabikian P, Lee D, Bhattarai N, Ellenbogen R, Sze R, Hallahan A, Olson J & Zhang M (2005). Optical and MRI multifunctional nanoprobe for targeting gliomas. *Nano Lett,* 5: 1003-8.

Verma A & Stellacci F (2010). Effect of surface properties on nanoparticle-cell interactions. *Small,* 6: 12-21.

Villanueva A, Canete M, Roca AG, Calero M, Veintemillas-Verdaguer S, Serna CJ, Morales Mdel P & Miranda R (2009). The influence of surface functionalization on the enhanced internalization of magnetic nanoparticles in cancer cells. *Nanotechnology,* 20: 115103.

Vinzant N, Scholl JL, Wu CM, Kindle T, Koodali R & Forster GL (2017). Iron oxide nanoparticle delivery of peptides to the brain: Reversal of anxiety during drug withdrawal. *Front Neurosci,* 11: 608.

Walter P, Welcomme E, Hallegot P, Zaluzec NJ, Deeb C, Castaing J, Veyssiere P, Breniaux R, Leveque JL & Tsoucaris G (2006). Early use of PbS nanotechnology for an ancient hair dyeing formula. *Nano Lett,* 6: 2215-9.

Wang B, Feng WY, Wang M, Shi JW, Zhang F, Ouyang H, Zhao YL, Chai ZF, Huang YY, Xie YN, Wang HF & Wang J (2007). Transport of intranasally instilled fine Fe2O3 particles into the brain: micro-distribution, chemical states, and histopathological observation. *Biol Trace Elem Res,* 118: 233-43.

Wang TT, Bai J, Jiang X & Nienhaus GU (2012). Cellular ptake of nanoparticles by membrane penetration: A study combining confocal microscopy with FTIR spectroelectrochemistry. *ACS Nano,* 6: 1251-1259.

Wang YX (2015). Current status of superparamagnetic iron oxide contrast agents for liver magnetic resonance imaging. *World J Gastroenterol,* 21: 13400-2.

Weinstein JS, Varallyay CG, Dosa E, Gahramanov S, Hamilton B, Rooney WD, Muldoon LL & Neuwelt EA (2010). Superparamagnetic iron oxide nanoparticles: diagnostic magnetic resonance imaging and potential therapeutic applications in neurooncology and central nervous system inflammatory pathologies, a review. *J Cereb Blood Flow Metab,* 30: 15-35.

Weise G & Stoll G (2012). Magnetic resonance imaging of blood brain/nerve barrier dysfunction and leukocyte infiltration: Closely related or discordant? *Front Neurol,* 3: 178.

Wilhelm C, Billotey C, Roger J, Pons JN, Bacri JC & Gazeau F (2003). Intracellular uptake of anionic superparamagnetic nanoparticles as a function of their surface coating. *Biomaterials,* 24: 1001-11.

Wiogo HT, Lim M, Bulmus V, Yun J & Amal R (2011). Stabilization of magnetic iron oxide nanoparticles in biological media by fetal bovine serum (FBS). *Langmuir,* 27: 843-50.

Wu W, He Q & Jiang C (2008). Magnetic iron oxide nanoparticles: Synthesis and surface functionalization strategies. *Nanoscale Res Lett,* 3: 397-415.

Wu W, Wu Z, Yu T, Jiang C & Kim WS (2015). Recent progress on magnetic iron oxide nanoparticles: synthesis, surface functional strategies and biomedical applications. *Sci Technol Adv Mater,* 16: 023501.

Xu YY, Barregard L, Nielsen J, Gudmundsson A, Wierzbicka A, Axmon A, Jonsson BAG, Karedal M & Albin M (2013). Effects of diesel exposure on lung function and inflammation biomarkers from airway and peripheral blood of healthy volunteers in a chamber study. *Part Fibre Toxicol,* 10.

Yan F, Wang Y, He S, Ku S, Gu W & Ye L (2013). Transferrin-conjugated, fluorescein-loaded magnetic nanoparticles for targeted delivery across the blood-brain barrier. *J Mater Sci Mater Med,* 24: 2371-9.

Yang H (2010). Nanoparticle-mediated brain-specific drug delivery, imaging, and diagnosis. *Pharm Res,* 27: 1759-71.

Yarjanli Z, Ghaedi K, Esmaeili A, Rahgozar S & Zarrabi A (2017). Iron oxide nanoparticles may damage to the neural tissue through iron accumulation, oxidative stress, and protein aggregation. *BMC Neurosci,* 18: 51.

Zhang L & Liu Y (2017). Research of an iron oxide nanoparticles and potential application. *Toxicology Open Access,* 3: 3.

Zhang S, Gao H & Bao G (2015a). Physical principles of nanoparticle cellular endocytosis. *ACS Nano,* 9: 8655-71.

Zhang Y, Leu YR, Aitken RJ & Riediker M (2015b). Inventory of engineered nanoparticle-containing consumer products available in the Singapore retail market and likelihood of release into the aquatic environment. *Int J Environ Res Public Health,* 12: 8717-43.

Zou P, Yu Y, Wang YA, Zhong Y, Welton A, Galban C, Wang S & Sun D (2010). Superparamagnetic iron oxide nanotheranostics for targeted cancer cell imaging and pH-dependent intracellular drug release. *Mol Pharm,* 7: 1974-84.

2 Results

2 Results

2.1 Publication 1

Uptake of fluorescent iron oxide nanoparticles in C6 glioma cells

Wiebke Rastedt, Karsten Thiel, Ralf Dringen

Published in Biomed Phys Eng Express (2017) 3: 035007

Contribution of Wiebke Willmann (née Rastedt)

- Design of the study (50%)
- Performance of all experiments (except electron microscopy pictures and EDX)
- Preparation of the draft version of the manuscript

2.2 Publication 2 (Manuscript)

Monitoring of the cytoskeleton-dependent intracellular trafficking of fluorescent iron oxide nanoparticle by nanoparticles pulse-chase experiments in C6 glioma cells

Wiebke Willmann and Ralf Dringen

Submitted for publication

Contribution of Wiebke Willmann (née Rastedt)

- Design of the study (50%)
- Performance of all experiments
- Preparation of the first draft of the manuscript

Abstract

Iron oxide nanoparticles (IONPs) are used for various biomedical and therapeutic approaches. To investigate the uptake and the intracellular trafficking of IONPs in neural cells we have performed nanoparticle pulse-chase experiments to visualize the internalization and the fate of fluorescent IONPs in C6 glioma cells. Already a short exposure to IONPs for 10 min at 4°C (nanoparticle pulse) allowed binding of substantial amounts of nanoparticles to the cells, while internalization of IONPs into the cell was prevented. The uptake of bound IONPs and the intracellular trafficking was started by increasing the temperature to 37°C (chase period). While hardly any cellular fluorescence nor any iron staining was detectable directly after the nanoparticle pulse, dotted cellular fluorescence and iron patterns appeared already within a few minutes after start of the chase incubation and became intensified in the perinuclear region during further incubation for up to 90 min. Longer chase incubations resulted in separation of the fluorescent coat from the core of the internalized IONPs. Disruption of actin filaments strongly impaired the internalization of IONPs, whereas destabilization of microtubules traped IONP-containing vesicles to the plasma membrane. In conclusion, nanoparticle pulse-chase experiments allowed to synchronize the cellular uptake of fluorescent IONPs and to identify for C6 cells an actin-dependent early and a microtubules-dependent later process in the intracellular trafficking of fluorescent IONPs.

Keywords: actin; iron; microtubules; nanoparticles; pulse-chase; trafficking

1. Introduction

Superparamagnetic iron oxide nanoparticles (IONPs) are used for several neurobiomedical applications, for example for magnetic resonance imaging (MRI), for treatment of brain tumors by magnetic hyperthermia (Liu *et al.*, 2016) or as drug delivery tools for passing the blood-brain barrier (Vinzant *et al.*, 2017). Such applications make it essential to investigate the cytotoxic potential of IONPs (Shi *et al.*, 2016) and to understand the uptake and the intracellular metabolism of IONPs in brain cells. To increase the biocompatibility in physiological environments and to prevent agglomeration, IONPs are normally coated with organic materials (Ali *et al.*, 2016, Feliu *et al.*, 2016), which modify the physicochemical parameters of the nanoparticles such as size, charge and shape, and thereby, can modulate also the interactions between nanoparticles and cells as well as the endocytotic uptake of nanoparticles into cells (Nazarenus *et al.*, 2014, Oh and Park, 2014). Depending on the cell type investigated, different endocytotic pathway are involved in the uptake of nanoparticles, including macropinocytosis, pinocytosis, clathrin-dependent, clathrin-independent, degradative or non-degradative pathways (Lai *et al.*, 2007, Iversen *et al.*, 2011, Nazarenus *et al.*, 2014, Zhang *et al.*, 2015b). The cellular uptake of nanoparticles is a two-step process (Wilhelm *et al.*, 2003). First the nanoparticles bind to the cells and subsequently the nanoparticles are internalized by endocytosis (Wilhelm *et al.*, 2003). Both processes take place at physiological temperature. In contrast, at 4°C only the adsorption of nanoparticles to the cell membrane is observed, while the internalization of bound nanoparticles is prevented at this low temperature (Wilhelm *et al.*, 2003, Bertorelle *et al.*, 2006, Geppert *et al.*, 2011, Rastedt *et al.*, 2017).

Depending on the kind of exposure nanoparticles can reach the brain via various routes, such as inhalation, ingestion or the cutaneous route (Bencsik *et al.*, 2018). After crossing the first tissue barrier and entering the blood they may cross the blood-brain barrier from blood into brain. More direct ways of nanoparticles to reach the brain are after inhalation via the olfactory bulb that is directly accessible from the nasal fossae or by direct injection into the brain for tumor treatment (Petters *et al.*, 2014, Bencsik *et al.*, 2018). Several studies have shown that IONPs can be found in brain in various cell types, including neurons, astrocytes and microglia (van Landeghem *et al.*, 2009, Ku *et al.*, 2010, Yan *et al.*, 2013). As for peripheral cells, IONPs are also taken up in neural cells

via endocytotic pathways (Petters *et al.*, 2014). Cultured astrocytes and microglia take up protein-coated IONPs by macropinocytosis and clathrin-mediated endocytosis (Pickard *et al.*, 2011, Geppert *et al.*, 2013, Luther *et al.*, 2013), whereas cultured neurons internalize such IONPs by clathrin-mediated endocytosis (Petters and Dringen, 2015). Depending on the cell type investigated IONPs differ strongly in their cytotoxic potential (Petters *et al.*, 2014, Petters *et al.*, 2016). Whereas cultured astrocytes are not damaged even days after exposure to large amounts of IONPs (Geppert *et al.*, 2012), the viability of cultured microglia cells is strongly compromised already within hours after exposure to IONPs (Pickard and Chari, 2010, Luther *et al.*, 2013, Petters *et al.*, 2016).

C6 glioma cells are widely used as model to study glial cells (Mangoura *et al.*, 1989). Due to the expression of the glial fibrillary acidic protein (GFAP) and the glutamine synthetase C6 glioma cells are often considered as astrocyte model system (Kumar *et al.*, 1986, Mangoura *et al.*, 1989, Goswami *et al.*, 2015). The uptake of various types of nanoparticles have previously been investigated for C6 glioma cells (Mamani *et al.*, 2012, Shevtsov *et al.*, 2015, Joshi *et al.*, 2016). These cells accumulate IONPs in a time, concentration- and temperature dependent manner (Rastedt *et al.*, 2017) by processes that strongly depend on the composition of the particle coat and on the presence of serum (Mamani *et al.*, 2012, Shevtsov *et al.*, 2015, Rastedt *et al.*, 2017).

For peripheral cells it has been reported that the formation of endocytotic vesicle at the membrane appears to involve actin polymerization (Smythe and Ayscough, 2006, Mooren *et al.*, 2012, Granger *et al.*, 2014), while microtubules-based processes are involved in the further intracellular trafficking of nanoparticle-containing vesicles (Granger *et al.*, 2014, Yameen *et al.*, 2014). During the intracellular trafficking the nanoparticle-containing vesicles are thought to be passed to more acidic vesicular environments, which can lead to the degradation of the engineered surface coat and/or of the core of the nanoparticle (See *et al.*, 2009, Lunov *et al.*, 2010, Feliu *et al.*, 2016). In contrast to peripheral cells, only little is known on the intracellular trafficking and the metabolism of IONPs in brain cells (Petters *et al.*, 2014, Costa *et al.*, 2016) and the involvement of the cytoskeleton in the intracellular trafficking of IONPs in neural cells has to our knowledge not been reported so far.

Recently, we have synthesized dimercaptosuccinate (DMSA)-coated IONPs that contain the fluorescence dyes Oregon Green (OG) or tetramethylrhodamine (TMR) covalently bound to the coat and have demonstrated that the incorporation of the fluorescence dye into the coating material does not alter the physicochemical properties, the colloidal stability in different media, the biocompatibility or the cellular uptake in comparison to non-fluorescent DMSA-coated IONPs (Rastedt *et al.*, 2017). These fluorescent IONPs were now used as tools to study internalization and cytoskeleton-dependent intracellular trafficking of IONPs in C6 glioma cells in nanoparticle pulse-chase experiments with improved spatial resolution by epi-fluorescence microscopy.

2. Experimental Section

Materials

Fetal calf serum (FCS), trypsin solution and penicillin/streptomycin solution were obtained from Biochrom (Berlin, Germany). Dulbecco's modified Eagle's medium (DMEM) was from Gibco (Karlsruhe, Germany). Bovine serum albumin (BSA) and nicotinamide adenine dinucleotide (NADH) were purchased from Applichem (Darmstadt, Germany). Oregon Green®488 iodoacetamide (mixed isomers) and tetramethyl rhodamine-5-iodoacetamide dihydroiodide (single isomer) were obtained from Invitrogen (Darmstadt, Germany). Other chemicals of highest purity were purchased from Merck (Darmstadt, Germany), Sigma-Aldrich (Steinheim, Germany) or Fluka (Buchs, Switzerland). 24-well cell culture plates and 96-well microtiter plates were obtained from Sarstedt (Nümbrecht, Germany) and black 96-well plates were purchased from VWR (Darmstadt, Germany).

Synthesis and characterization of iron oxide nanoparticles

Fluorescent DMSA-coated IONPs containing the fluorophores Oregon Green (OG) or tetramethylrhodamine (TMR) in the coat were synthesized and intensively characterized as recently described in detail (Rastedt *et al.*, 2017). Transmission electron microscopy analysis revealed a particle size of 5-10 nm. In the incubation buffer (IB) that was also used for cell incubations in the present study the fluorescent IONPs had a hydrodynamic diameter of around 60 nm and a ζ-potential of -20 mV (Rastedt *et al.*, 2017). The concentrations of IONPs given for experiments and cell incubations represent the

concentration of total iron in the IONP-containing media and not the concentration of the nanoparticles.

Cell cultures

The C6 glioma cell line is widely used as cell model to study functions and properties of brain glial cells (Goswami *et al.*, 2015, Joshi *et al.*, 2016) and brain glioma (Grobben *et al.*, 2002). They express astrocyte marker proteins such as glial fibrillary acidic protein (Bissell *et al.*, 1975, Stapelfeldt *et al.*, 2017) and glutamine synthetase (Kumar *et al.*, 1986). C6 cells have been shown to efficiently bind and take up various types of nanoparticle (Huerta-Garcia *et al.*, 2015, Shevtsov *et al.*, 2015, Joshi *et al.*, 2016, Rastedt *et al.*, 2017). The C6 glioma cell line used for our study was kindly provided by Dr. Frank Dietz (University of Bremen). The C6 glioma cells were subcultured as recently described in detail (Joshi *et al.*, 2016). For experiments, harvested cells were seeded in 1 mL cell culture medium (90% DMEM containing 25 mM glucose, 10% fetal calf serum, 18 U/mL penicillin G, 18 µg/mL streptomycin sulfate and 1 mM sodium pyruvate) in a density of 100,000 cells per well into wells of a 24-well plate or on glas coverslips (12 mm in diameter, Roth, Karlsruhe) in wells of 24-well dishes. The cultures were used for experiments 24 h after seeding.

Basal experimental incubations

For basal particle uptake experiments, C6 glioma cells grown on coverslips or in wells of 24-well dishes were washed with 1 mL ice-cold (4°C) or pre-warmed (37°C) incubation buffer (IB; 20 mM HEPES, 145 mM NaCl, 5 mM D-glucose, 1.8 mM $CaCl_2$, 5.4 mM KCl, 1 mM $MgCl_2$, adjusted with NaOH to pH 7.4) and incubated in 200 µL IB containing 1 mM OG-IONPs or TMR-IONPs in the humidified atmosphere of an incubator at 37°C or on ice at 4°C for the time periods indicated in the legends of the figures.

Nanoparticle pulse-chase experiments

The pulse-chase strategy was originally developed to study the post-translational fate of proteins and to investigate the role of subcellular compartments in protein trafficking using radioactive labeling (Jamieson and Palade, 1967b, Jamieson and Palade, 1967a, Hou *et al.*, 2013). Recently, this strategy has also been adopted to study nanoparticle

endocytosis mechanisms and for subcellular compartment isolation (Thimiri Govinda Raj and Khan, 2016). Depending on the cell system, the nanoparticle applied and the question addressed, several protocols have been applied that differ substantially concerning the incubation conditions (Bertorelle *et al.*, 2006, Baltazar *et al.*, 2012, Iversen *et al.*, 2012, Sandin *et al.*, 2012). Here we describe a protocol optimized for C6 glioma cells that separates binding of fluorescent IONPs to the cells from uptake into the cells by alteration of the incubation temperature (Fig. 1).

For nanoparticle pulse-chase experiments (Fig.1A,C), the cultures were washed with ice-cold IB, incubated with 1 mM OG-IONPs for 10 min at 4°C (nanoparticle pulse), washed twice with 1 mL ice-cold IB and were then incubated in 200 µL pre-warmed (37°C) IB in the humidified atmosphere of an incubator at 37°C for the indicated time (chase period).

For sequential uptake studies, the nanoparticle pulse-chase experiment was modified to a double nanoparticle pulse-chase setting (Fig. 1B,C). After the first nanoparticle pulse with 1 mM OG-IONPs at 4°C and a first chase period of 30 min at 37°C, the second nanoparticle pulse was initiated by washing the cells with 1 mL ice-cold IB and incubating the cells with 1 mM TMR-IONPs for 10 min at 4°C (second nanoparticle pulse). Subsequently, the cells were washed twice with 1 mL ice-cold IB and then incubated in 200 µL pre-warmed (37°C) IB in the humidified atmosphere of an incubator at 37°C (second chase period).

To study the role of the cytoskeleton in the uptake of IONPs, cells were preincubated without or with 10 µg/mL cytochalasin D (cytoD) and/or 1.25 µM colchicine in IB for 60 min at 37°C before the cells were exposed to IONPs in nanoparticle pulse-chase experiments. The cytoskeleton-destabilizing compounds were also present during the chase periods of the experiments, but had to be omitted from the buffers used for the 4°C nanoparticle pulses and the 4°C washing steps to prevent artifacts caused by agglomeration of IONPs in the presence of colchicine or cytoD (data not shown).

After the given incubation periods the incubation media were harvested and used for the determination of extracellular lactate dehydrogenase activity (LDH) as indicator for potential cell damage, while the cells were washed with ice-cold (4°C) phosphate-buffered saline (PBS; 10 mM potassium phosphate buffer pH 7.4 containing 150 mM

NaCl) and lysed in 400 µL 50 mM NaOH. This lysate was used for the quantification of cellular iron, fluorescence and protein contents. For microscopical analysis of cellular fluorescence and cellular iron localization, the cells were washed with ice-cold PBS and treated as describe below.

Quantification of cellular iron, fluorescence and protein content

For the determination of the contents of cellular iron, fluorescence and protein, cells were lysed in 400 µL 50 mM NaOH for 30 min at room temperature (RT). The total iron content of cells was determined by a modification of the ferrozine-based colorimetric iron assay (Riemer *et al.*, 2004) as described previously in detail (Geppert *et al.*, 2009). Cellular fluorescence of the lysates was determined for 150 µL cell lysate that had been mixed with 150 µL 50 mM NaOH in wells of black microtiter plates. OG fluorescence was measured at an excitation wavelength of 485 nm and an emission wavelength of 520 nm and the TMR fluorescence at an excitation wavelength of 544 nm and an emission wavelength of 590 nm using the Fluoroskan Ascent Microtiterplate Fluorimeter (ThermoFisher, Darmstadt, Germany). The cellular protein content of the lysate was determined according to the Lowry method (Lowry *et al.*, 1951) using BSA as protein standard. The specific cellular iron contents and fluorescence signals were calculated by normalizing the total cellular iron content per well and the total fluorescence signal per well, respectively, to the cellular protein content determined for the respective well.

For the cytochemical visualization of cellular iron in cultured cells a modification of the histochemical Perls' staining (Moos and Mollgard, 1993, Bishop and Robinson, 2001) with a diaminobenzidine/nickel staining intensification was performed as described previously in detail (Geppert *et al.*, 2009). Subsequently the cells were washed three times with 1 mL 0.1 M potassium phosphate buffer pH 7.2 for 10 min and kept in this buffer overnight at 4°C to clear the iron staining. Finally, the nuclei were stained with 30 µL 1 µg/mL 4',6-diamidino-2-phenylindole dihydrochloride (DAPI) in PBS for 5 min at RT and the cells were washed three times with PBS prior to embedding the fixed cells in Mowiol mounting medium (2.4 g polyvinyl alcohol and 6 g glycerol dissolved in 18 mL 150 mM Tris/HCl buffer pH 8.5).

Determination of cell viability

Cell viability after a given treatment was investigated by measuring the extracellular presence of the cytosolic enzyme lactate dehydrogenase (LDH) which is an indicator for a loss in cell membrane integrity. The LDH activity in the incubation medium was determined using a microtiter plate assay as previously described in detail and was compared to the initial cellular LDH activity of untreated cells that had been lysed with 1% (w/v) Triton X-100 in IB (100% LDH release) (Dringen *et al.*, 1998, Tulpule *et al.*, 2014).

Presentation of data

The quantitative data are means ± standard deviation of values that had been obtained in at least three independent experiments on different passages of C6 cells. Microscopic images are derived from a representative experiment that had been reproduced at least twice with comparable results. Statistical analysis of data from multiple sets of quantitative data was carried out by ANOVA followed by the Bonferroni's *post hoc* test. Significance differences between two sets of data was analyzed by the Student's t-test. Values of $p>0.05$ were considered as not significant.

3. Results

3.1. Accumulation of fluorescent IONPs by C6 glioma cells

To investigate the temperature-dependence of the accumulation of OG-IONPs, C6 glioma cells were incubated with 1 mM OG-IONPs for up to 1 h at 37°C or at 4°C (Fig. 2). For both incubation temperatures the specific cellular iron content (Fig. 2A) and the cellular fluorescence (Fig. 2B) increased rapidly during the initial phase of the incubation. Already after 5 min of incubation, substantial amounts of cellular OG-IONPs were determined as demonstrated by specific cellular iron contents of 308 ± 27 nmol/mg protein (37°C) and 224 ± 33 nmol/mg protein (4°C) (Fig. 2A) and by cellular fluorescence values of 147 ± 28 a.u./mg protein (37°C) and 117 ± 16 a.u./mg protein (4°C) (Fig. 2B). For both temperatures, the increase in cellular iron content and fluorescence was slowed after the initial 10 min of incubation. After an incubation

period of 60 min, the OG-IONP-exposed cells contained specific iron contents of 936 ± 196 nmol/mg protein (37°C) and 612 ± 42 nmol/mg protein (4°C) and specific cellular fluorescence values of 409 ± 55 a.u./mg protein (37°C) and 263 ± 25 a.u./mg protein (4°C) (Fig. 2B). For each time point investigated, the values obtained for the 4°C incubations represented around 65-80% of the amounts determined for the respective 37°C experiments. None of the investigated incubation conditions compromised the cell viability as demonstrated by the absence of any increase in extracellular LDH activity (Fig. 2C). Comparison of the specific cellular iron contents with the respective specific cellular fluorescence values obtained for lysates of cells that had been exposed to OG-IONPs (Fig. 2A,B) revealed an excellent correlation of both values (Fig. 2D).

A direct comparison of data from a large number of independent experiments exposing cells with 1 mM OG-IONPs for 10 min or 60 min at 37°C revealed that cellular iron contents and cellular fluorescence were almost doubled after 60 min incubations compared with 10 min incubations (Fig. 3A,B). This difference was also found by fluorescence microscopy, showing for cells that had been incubated with OG-IONPs at 37°C for 10 min a dotted staining (Fig. 3E), which was found strongly intensified in cells that had been exposed to the nanoparticles for 60 min (Fig. 3F). Incubations of C6 cells with OG-IONPs at 4°C for 10 min or 60 min revealed specific cellular iron contents and specific cellular fluorescence values that were significantly lower by around 30 to 50% compared to the data determined for the respective 37°C incubations (Fig. 3A,B). However, hardly any fluorescence was detectable by fluorescence microscopy for cells that had been incubated with OG-IONPs at 4°C for 10 min or 60 min (Fig. 3C,D).

These data are consistent with the reported efficient binding of IONPs to cells at 4°C, while this low temperature prevented the internalization and packaging of the bound IONPs into intracellular vesicles (Geppert et al., 2011, Rastedt et al., 2017). The substantial cellular iron contents quantified already after 10 min incubations at 4°C with 1 mM fluorescent IONPs was considered as sufficient to further investigate the internalization and intracellular trafficking of the bound IONPs after an subsequent increase in the incubation temperature to 37°C in nanoparticle pulse-chase experiments (Fig. 1).

3.2. Nanoparticle pulse-chase experiments allow to synchronize cellular OG-IONPs uptake and trafficking

The internalization of IONPs that had bound to the cells during a 10 min exposure to OG-IONPs at 4°C was synchronized in nanoparticle pulse chase experiment (Fig. 1A) by applying 37°C prewarmed IB. The intracellular trafficking of the internalized OG-IONPs was monitored during the further chase incubation at 37°C for up to 240 min. During such incubations, the cell viability was not compromised as demonstrated by the absence of any increase in extracellular LDH activity during the chase incubation (Fig. 4A). Also the specific cellular iron content of the cells after the nanoparticle pulse was not significantly lowered during the chase incubation (Fig. 4B). In contrast, substantial changes were observed for the distribution of cellular OG fluorescence and the localization of cellular iron during the chase incubation following the nanoparticle pulse (Fig. 4C-V). Directly after the pulse, OG fluorescence (Fig. 4C) and iron staining (Fig. 4H) were not detectable, but already 5 min after the increase in incubation temperature to 37°C first dot-like fluorescence (Fig. 4D) and iron stainings (Fig. 4I) became visible in the cells. The intensities of these stainings increased substantially during longer incubations and became localized predominately in the perinuclear region of the cells (Fig. 4). Maximal fluorescence signals were observed after around 90 min chase incubation at 37°C (Fig. 4N), while during longer incubations the dot-like perinuclear fluorescence signals became weaker, the fluorescence signal became more blurry and a weak fluorescence signals was observed throughout the cells (Fig. 4O-Q). This finding of a transient increase in cellular OG fluorescence contrasted with results obtained for the cellular iron staining which remained very prominent in the perinuclear region even during long chase incubations of up to 240 min (Fig. 4T-V). Identical results to those recorded for OG-IONPs were also observed in nanoparticle pulse-chase experiments performed with 1 mM TMR-IONPs (data not shown). Simultaneous exposure of C6 cells with both OG-IONPs and TMR-IONPs during the pulse-phase revealed within minutes after onset of the chase incubation a rapid appearance of fluorescent structures that contained both types of fluorescent nanoparticles colocalized, while hardly any structures were observed that contained predominately OG or TMR fluorescence (data not shown).

3.3. Effects of cytoskeleton disruption on cellular uptake and intracellular trafficking of OG-IONPs

To investigate the involvement of the cytoskeleton in the internalization and trafficking of OG-IONPs in C6 glioma cells, the cells were incubated without or with cytochalasin D (cytoD), an inhibitor of the actin reorganization (Spector et al., 1999) and/or colchicine, a microtubules destabilizing agent (Banerjee et al., 2016) before nanoparticle pulse-chase experiments were performed with OG-IONPs. Immunocytochemical staining for tubulin and phalloidin staining for actin confirmed that colchicine and cytoD caused a disintegration of the microtuble network and of the actin filaments, respectively, under the conditions applied (data not shown).

Fig. 5 shows the results of a pulse-chase experiment with OG-IONPs on C6 glioma cells that had been preincubated without or with colchicine and/or cytoD. None of these conditions caused any signficant increase in extracellular LDH activity (Fig. 5A), nor any signficant loss in the cellular protein content (Fig. 5B) nor in the specific cellular iron content (Fig. 5C), suggesting that the cells were not damage by the conditions applied. In cells that had been exposed to colchicine to destabilize microtubules a rapid appearance of a dotted fluorescence pattern was observed (Fig. 5N-Q) as also found for control cells that had been treated in the absence of cytoskeleton destabilizing compounds (Fig. 5D-G). However, this punctated staining pattern for fluorescence and iron was distributed all over the cells and appeared to be membrane associated as trafficking of fluorescent and iron-containing structures to the perinuclear region of the cells was not observed (Fig. 5N-R). In contrast, for cultures that had been exposed to cytoD alone (Fig. 5I-M) to destabilize actin filaments or to the combination of cytoD plus colchicine (Fig. 5S-W) only few and weak fluorescent or iron-positive structures were detectable in cells during the chase incubation, the morphology of the cells was strongly affected as indicated by cell shrinking and the cell nuclei appeared to be condensed (Fig. 5).

3.4. Sequential uptake of fluorescent IONPs in double nanoparticle pulse-chase experiments

To further investigate the importance of the cytoskeleton for the internalization and the trafficking of fluorescent IONPs, double nanoparticle pulse-chase experiments were

performed to study the sequential uptake of OG-IONPs and TMR-IONPs (Fig. 1B,C). For this, C6 cells were preincubated without or with colchicine and/or cytoD and exposed in a first nanoparticle pulse to OG-IONPs. After a first chase period of 30 min at 37°C, TMR-IONPs were applied in a second nanoparticle pulse at 4°C before finally cellular fluorescence was monitored during the second chase incubation (Fig. 6). Double nanoparticle pulse-chase experiments in the absence or presence of cytoD or/and colchicine did not cause any significant change in the cellular protein content (Fig. 6A) nor any obvious increase in LDH release during the incubations (data not shown) or within the second chase period (Fig. 6C). As expected, exposure to the second nanoparticle pulse resulted in an almost doubling of the specific cellular iron content for all conditions applied (Fig. 6B) and this content was not significantly lowered during the second chase incubation within 60 min (Fig. 6B) or up to 240 min (data not shown).

Microscopical analysis of the cells at the onset of the second chase period directly after the second nanoparticle pulse revealed clearly the presence of punctured OG fluorescence in the cells (Fig. 6D), as expected for cells that had been incubated for a chase period of 30 min following an OG-IONP pulse (Fig. 4F; Fig. 5E), while no red TMR fluorescence was detectable for this time point (Fig. 6D). However, with increasing incubation time during the second chase period an additional dotted red staining pattern of TMR fluorescence appeared (Fig. 6E) and during further incubation substantial amounts of the OG (green dots) and TMR fluorescence (red dots) were detectable, mainly found colocalized in the perinuclear region of the cells (as indicated in yellow), although also individual dotted red and green structures remained visible in the cells (Fig. 6F-H).

In cells that had been exposed to cytoD (Fig. 6J) or cytoD plus colchicine (Fig. 6L), hardly any dotted fluorescence staining was observed for OG and TMR during the second chase period, while for colchicine-treated cells dotted fluorescent structures were observed in large numbers for both OG (green) and TMR (red) that were distributed all over the cells (Fig. 6K). Interestingly, the majority of these OG- and TMR-stainings remained separated from each other and only little colocalization of OG- and TMR-fluorescence was observed (Fig. 6K).

4. Scheme and figures

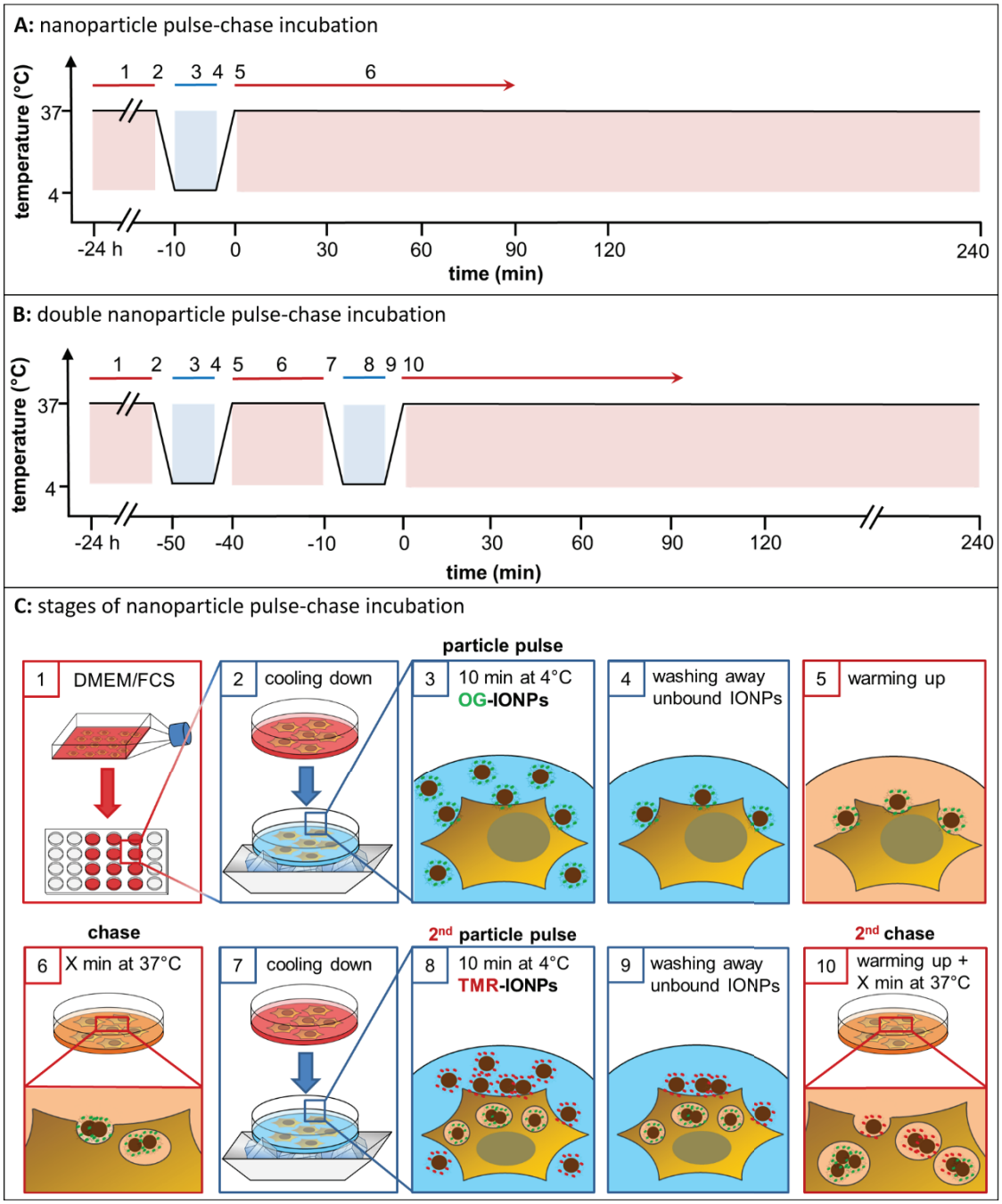

Fig. 1 Experimental protocols for nanoparticle pulse-chase experiments (A; steps 0-6 in C) and double nanoparticle pulse-chase experiments (B; steps 1-10 in C) with the individual incubations steps (C). **1:** Cells are seeded and cultured for 24 h in culture medium. **2:** The cells are cooled down to 4°C by washing the cells with ice-cold incubation buffer. **3:** The cells are incubated for 10 min at 4°C with OG-IONPs (nanoparticle pulse) to facilitate attachment of nanoparticles to the cell membrane while preventing internalization. **4:** Unbound nanoparticles are removed by washing the cells with ice-cold incubation buffer. **5:** The cells are warmed up

by application of prewarmed (37°C) incubation buffer to start uptake of the bound nanoparticles. **6:** The cells are further incubated at 37°C (chase period) for the given chase periods before the cells are analyzed. Alternatively, for double nanoparticle pulse-chase experiments the chase period is terminated after 30 min of incubation and steps 7-10 follow. **7:** The cells are cooled down to 4°C by washing the cells with ice-cold incubation buffer. **8:** The cells are incubated for 10 min at 4°C with TMR-IONPs (second nanoparticle pulse) to facilitate attachment of these nanoparticles to the cell membrane while preventing their internalization. **9:** Unbound nanoparticles are removed by washing the cells with ice-cold incubation buffer. **10:** The cells are warmed up by application of prewarmed (37°C) incubation buffer to start uptake of the nanoparticles bound to the cells during the second nanoparticle pulse and the cells are further incubated at 37°C for the given second chase periods to monitor the intracellular trafficking of both types of fluorescent nanoparticles.

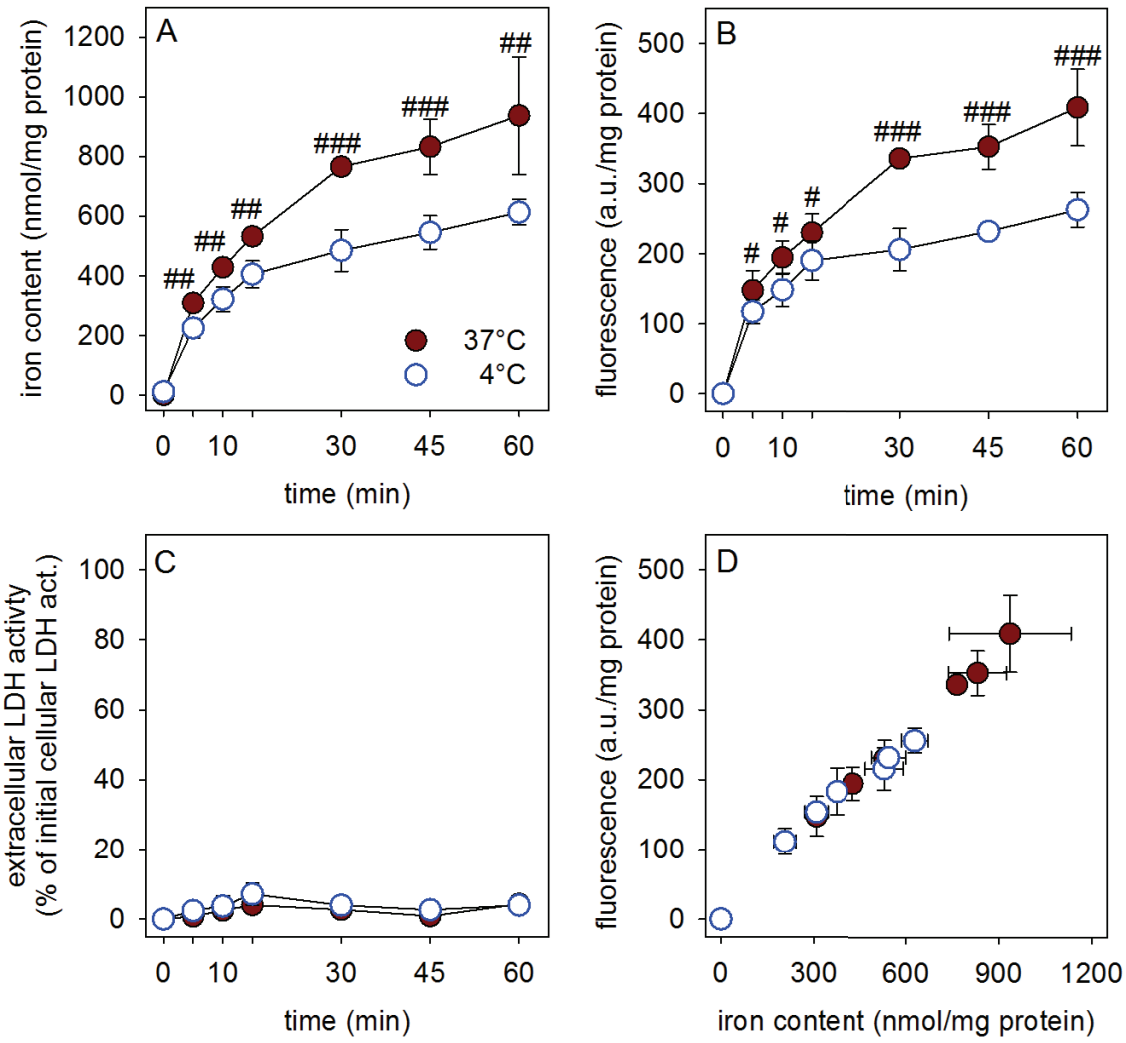

Fig. 2 Time- and temperature-dependent accumulation of OG-IONPs in C6 glioma cells. The cells were incubated with 1 mM OG-IONPs for up to 60 min at 37°C or at 4°C before the specific cellular iron content (A), the specific cellular OG fluorescence (B) and the extracellular LDH activity (C) were determined. Panel D shows the correlation between the specific cellular iron content and the specific cellular OG fluorescence for the cell lysates analyzed. The data shown represents means ± SD of values obtained in 3 (37°C conditions in panels a-d and 4°C condition in panel D) or 6 (4°C condition in panels A-C) independent experiments. The significance of differences between the values obtained for cells that had been incubated at 37°C and 4°C is indicated in panels a and b by $^{\#}p<0.05$; $^{\#\#}p<0.01$ and $^{\#\#\#}p<0.001$.

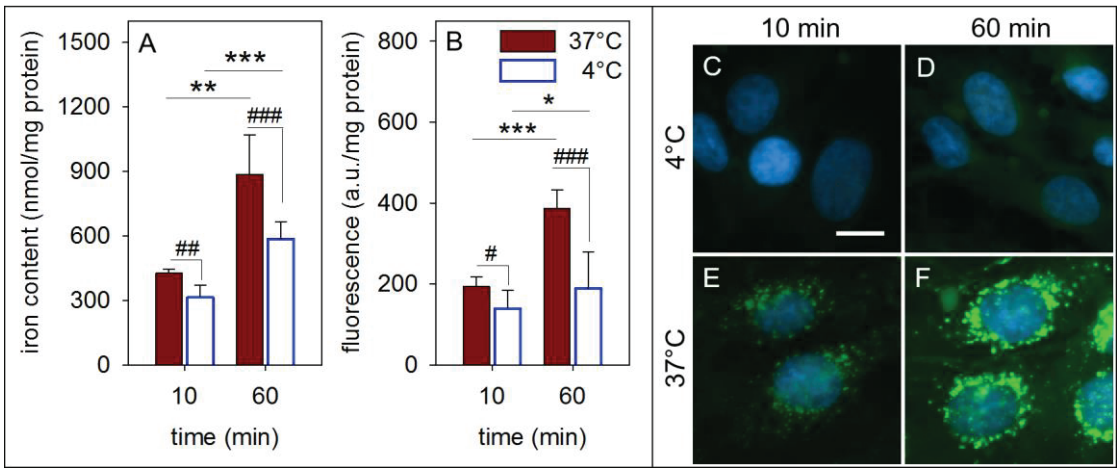

Fig. 3 Accumulation of OG-IONPs by C6 glioma cells. The cells were incubated with 1 mM OG-IONPs for 10 min or 60 min at 37°C or 4°C before the specific cellular iron content (A) and the specific cellular fluorescence (B) were determined or fluorescence images were recorded (C-F). The quantitative data shown (A,B) represent means ± SD of values obtained in 24 (10 min at 4°C) and 8 (10 min at 37°C; 60 min at 4°C; 60 min at 37°C) independent experiments. The significance of differences between the values obtained for cells that had been incubated at 37°C and 4°C ($^{\#}p<0.05$; $^{\#\#}p<0.01$; $^{\#\#\#}p<0.001$) or that had been incubated at a given temperature for 10 and 60 min (*p<0.05; **p<0.01; ***p<0.001) are indicated in panels A and B. The scale bar in panel C represents 10 µm and applies to panels C-F.

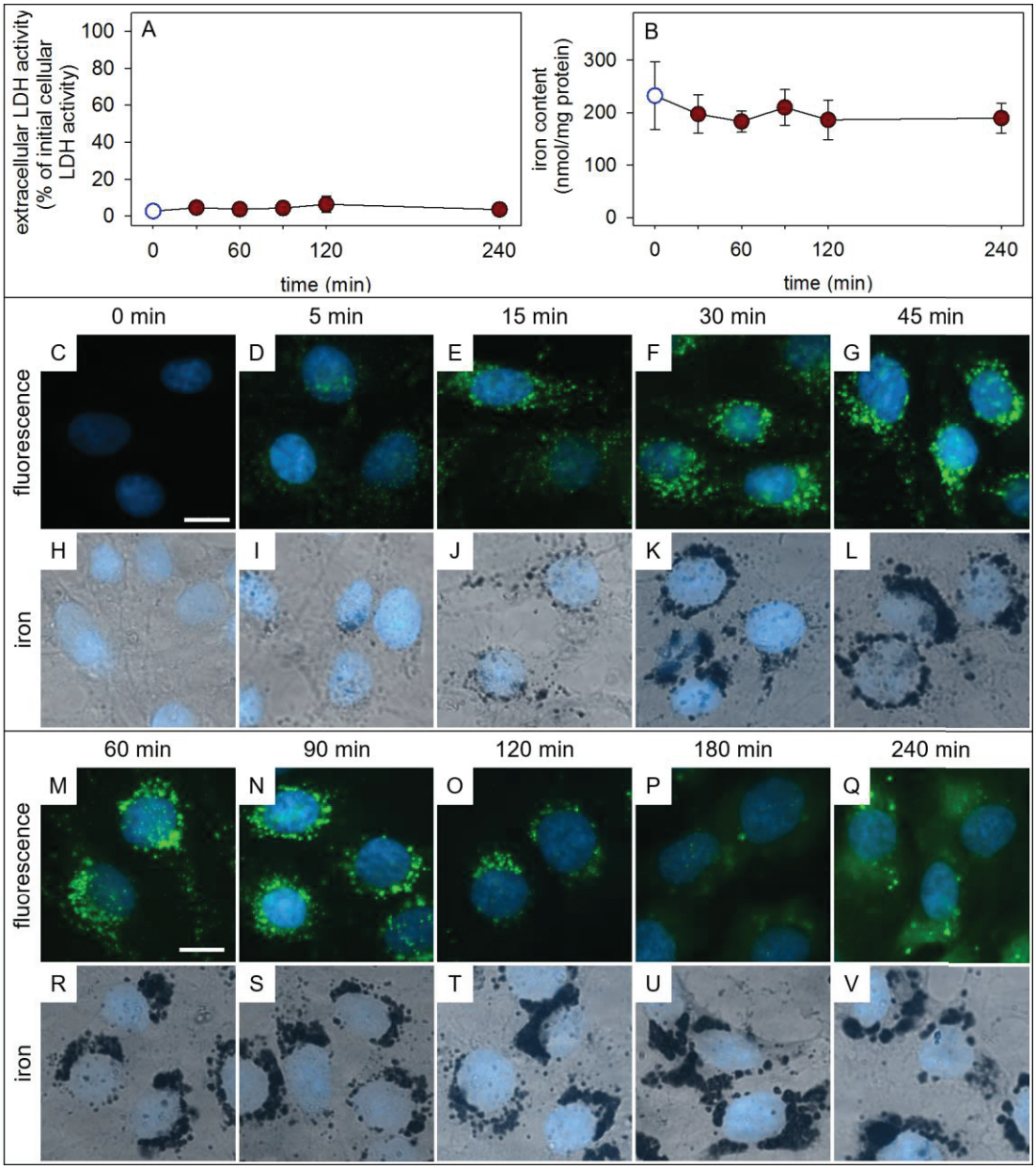

Fig. 4 Nanoparticle pulse-chase experiments with OG-IONPs on C6 glioma cells. The cells were incubated with 1 mM OG-IONPs for 10 min at 4°C to allow binding of OG-IONPs to the cells. Unbound IONPs were washed away and the cells were further incubated at 37°C for the indicated chase periods of up to 240 min. Extracellular LDH activity (A) and the specific cellular iron contents (B) were determined for the indicated time points. The quantitative data (A,B) represent means ± SD of values obtained in 4 independent experiments. No significant differences were found for the values obtained for chase periods of 0 min and longer time periods of up to 240 min ($p>0.05$). The cellular localization of OG was monitored by fluorescence microscopy (C-G, M-Q) and the localization of cellular iron was analyzed by the cytochemical iron staining (H-L, R-V). The cell nuclei were stained with DAPI (blue). The size

bars in panels c and m represents 10 μm and apply to the panels C-L and panels M-V, respectively.

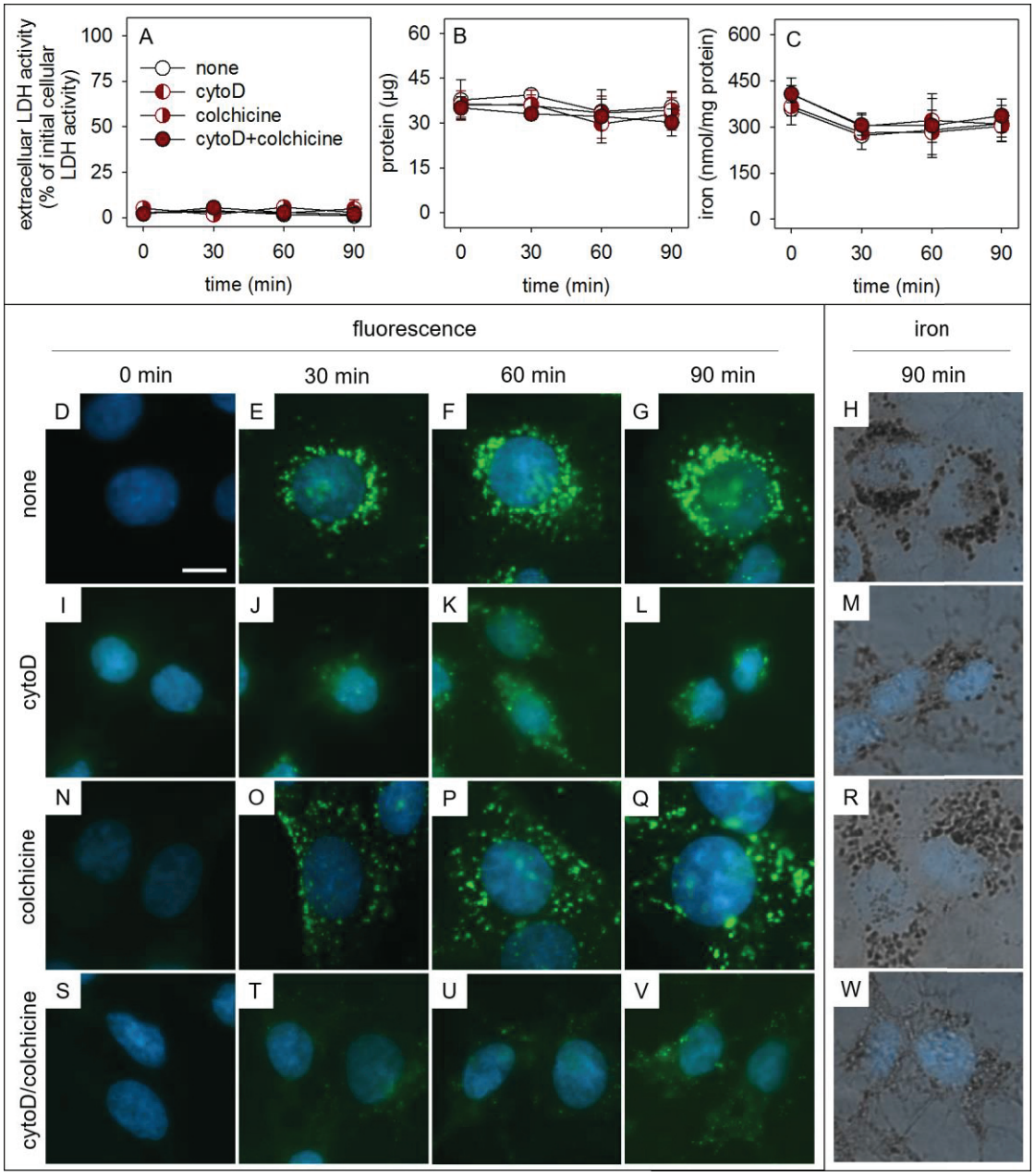

Fig. 5 Influence of disturbances of the cytoskeleton on the OG-IONPs trafficking in C6 glioma cells. Cells were pre-incubated in the absence or the presence of cytochalasin D (CytoD) and/or colchicine for 1 h at 37°C to disrupt actin filaments and/or to destabilize microtubules, before they were exposed to 1 mM OG-IONPs for 10 min at 4°C (nanoparticle pulse). Subsequently, the cells were washed and incubated at 37°C (chase period) for up to 90 min. Extracellular LDH activity (A), protein content (B) and specific iron content (C) were determined for the indicated chase periods. The quantiative data (A-C) represent means ± SD of values obtained in 3 independent experiments. No significant differences were observed between the data obtained for chase periods of 0 min and 90 min within one incubation condition nor for the values obtained for one chase period after the different treatments ($p>0.05$). For the indicated chase

periods images of cellular fluorescence and cytochemical iron staining were taken (D-W). The size bar in panel d represents 10 μm and applies to the panels D-W.

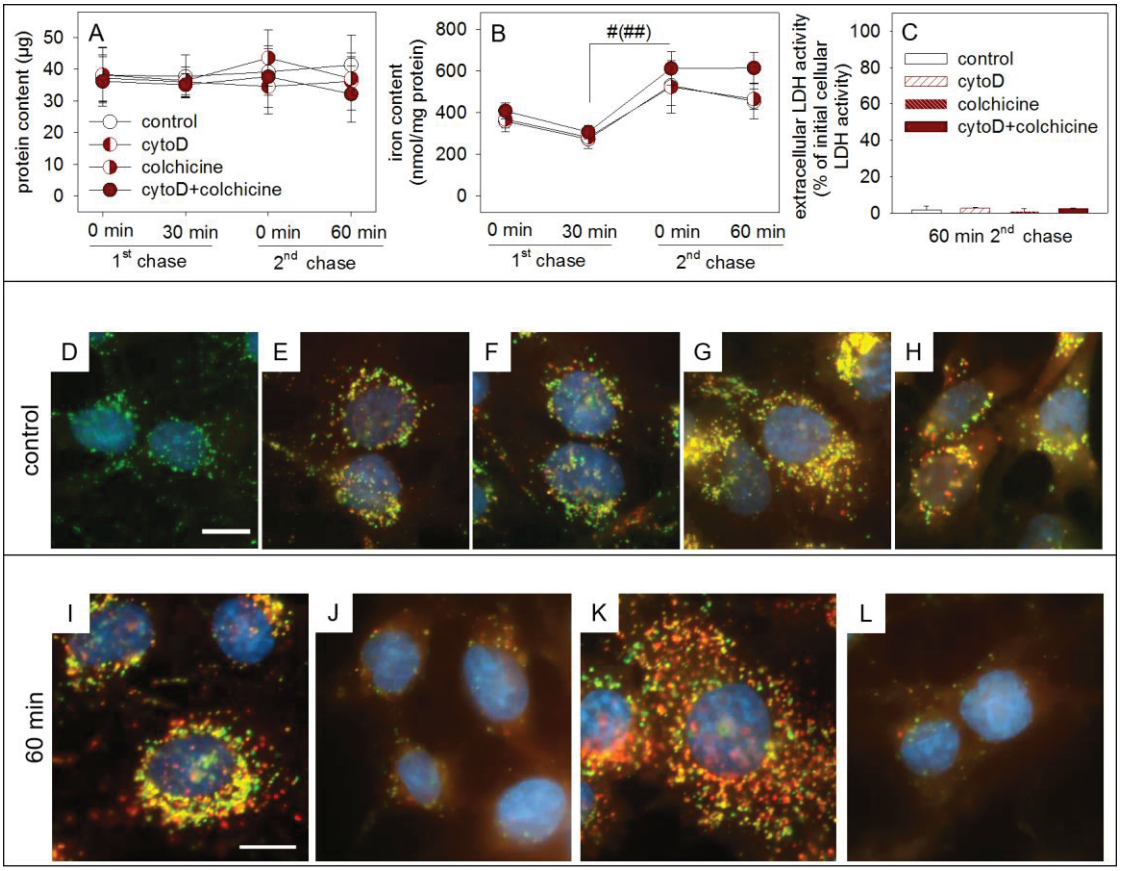

Fig. 6 Double nanoparticle pulse-chase experiments to study sequential uptake of fluorescence IONPs and the influence of cytoskeleton disruption on intracellular particle trafficking. C6 cells were pre-incubated in the absence or the presence of cytochalasin D (cytoD) and/or colchicine for 1 h at 37°C. Subsequently, a first nanoparticle pulse at 4°C with 1 mM OG-IONPs was applied. After 30 min chase incubation at 37°C in the absence or the presence of the inhibitors, a second nanoparticle pulse at 4°C was applied using 1 mM TMR-IONPs which was followed by the second chase incubation at 37°C for the indicated time periods. Protein content per well (A), specific cellular iron content (B) and extracellular LDH activity (C) were determined for the indicated time points. The quantiative data (A-C) represent means ± SD of values obtained in 3 independent experiments. In a and c, no significant differences were observed between the data obtained for cells treated without or with the test substances ($p>0.05$). The second pulse with TMR-IONP increased significantly the specific cellular iron content (B) of cells that had been exposed in the first pulse with OG-IONPs ($p<0.05$). Fluorescence images for OG and TMR (D-H) were taken at the indicated time points of the second chase period of control cells (preincubation without cytoD and colchicine). Panels (I-L) show fluorescence images taken 60 min after start of the second chase period for cells that had been preincubated without (I) or with cytoD and/or colchicine (I-L) before a double nanoparticle pulse-chase experiment was performed. The size bars in panels D and I represent 10 µm and apply for panels D-H and panels I-L, respectively.

5. Discussion

Fluorescent DMSA-coated IONPs have been shown as suitable tool to investigate basal mechanisms involved in the accumulation of IONPs by cultured neural cells (Petters *et al.*, 2014, Petters *et al.*, 2016, Rastedt *et al.*, 2017), but little is known on the intracellular trafficking of nanoparticles in such cells. C6 glioma cells are widely used as model to study glia cells (Mangoura *et al.*, 1989) and brain glioma (Grobben *et al.*, 2002). Recently we demonstrated that C6 glioma cells effiently accumulate DMSA-coated IONPs in a time- and concentration-dependent manner by a mechnism which is strongly affected by the temperature (Rastedt *et al.*, 2017). In the current study, we have established protocols for nanoparticle pulse-chase experiments to improve the temporal and spatial resolution in order to monitor uptake and intracellular trafficking of fluorescent IONPs and have used these experimental approaches to investigate the importance of the cellular cytoskeleton in nanoparticle trafficking in C6 glioma cells.

The cellular uptake of nanoparticles is a two-step process that includes binding of the nanoparticles to the cell and subsequent internalization into and trafficking within the cell (Wilhelm *et al.*, 2003, Lesniak *et al.*, 2013). As internalization of bound nanoparticles is prevented at 4°C (Geppert *et al.*, 2011, Lesniak *et al.*, 2013, Rastedt *et al.*, 2017), we separated in our pulse-chase settings the binding and internalization of IONPs by exposing the cells to fluorescent IONPs for a short 10 min nanoparticle pulse at 4°C that was followed, after washing away unbound nanoparticles, by the uptake of IONPs that was synchronized by an increase in the incubation temperature. The synchronized start of the nanoparticle internalization in such a pulse-chase experiment allowed to study with good spatial resolution the intracellular trafficking of only those particles during the chase phase that had been bound to cells during the pulse phase (Iversen *et al.*, 2012, Thimiri Govinda Raj and Khan, 2016).

Binding of IONPs to cells is a rapid process. Already during a 10 min pulse incubation at 4°C with OG-IONPs or TMR-IONPs large amounts of nanoparticles had bound to the membranes of the cells, representing around 70% of the values found for the respective 37°C incubations. These amounts of adsorbed fluorescent IONPs were sufficiently high to monitor alterations in the cellular localization of fluorescence and iron during chase incubations. Analysis of the extracellular LDH activity as indicator

for a potential impairment of the cell membrane, the cellular protein content, the cellular iron contents per well as well as the cell morphology revealed that none of the conditions applied (temperature shifts, presence of cytoskeleton-destabilizing compounds, long chase periods, double pulses) compromised the cell integrity and viability. Thus, the nanoparticle pulse-chase protocols applied are suitable to investigate uptake and intracellular trafficking of IONPs in viable C6 glioma cells.

The negative charges introduced to the IONPs by the DMSA coating results in a strong nonspecific binding of the IONPs to the cell membrane (Wilhelm *et al.*, 2003, Villanueva *et al.*, 2009, Rastedt *et al.*, 2017), which cannot be removed by more extensive washing procedures including even acidic or reducing conditions (data not shown). As during the chase incubation, the cellular iron contents of cells was maintained, a potential detachment of bound IONPs and/or release of IONPs or iron from the cells can be excluded for the incubation conditions applied.

Directly after the particle pulse at 4°C, which allowed binding of fluorescent IONPs to the cells, substantial amounts of cellular iron and cellular fluorescence were quantified in lysates but fluorescence microscopic images did not reveal specific fluorescence signals nor was positive iron staining observed by microscopic analysis for this condition. This initial lack of detectable staining patterns for fluorescence or iron confirms literature data (Geppert *et al.*, 2011, Rastedt *et al.*, 2017) and is most likely due to the very low local density of the fluorescence dyes and iron-containing nanoparticles at the cell membrane and the limitation of detection of the used widefield epifluorescence microscope. In contrast, already after a few minutes of incubation at the chase temperature of 37°C dotted fluorescence and iron stainings were detectable, suggesting that the internalization of the bound IONPs leads rapidly to the formation of intracellular vesicular structures which contain OG-IONPs in concentrations that are sufficiently high to allow detection and cellular localization of fluorescence and iron by the staining methods applied.

Maximal fluorescence in the perinuclear space of the cells were observed after around 60-90 min of chase incubation which was accompanied by maximal staining intensity for iron. During longer incubations the number and intensity of detectable fluorescent vesicles was lowered and a blurry fluorescence staining of the entire cells was observed.

In contrast, the perinuclear iron staining and its intensity was maintained during longer chase incubations for up to 240 min. These observations suggest an intracellular separation of the fluorescent DMSA coat from the iron oxide core of the internalized fluorescent IONPs during the chase incubation. The apparent high stability of the iron oxide core of the internalized fluorescent IONPs in the perinuclear area of the cells is consistent with results reported for cultured astrocytes that contained large amounts of agglomerated IONPs even days after exposure to IONPs (Geppert *et al.*, 2012).

The DMSA coat of the IONPs used contains only in low number thioether-attached fluorescent molecules (Rastedt *et al.*, 2017) and forms a disulfide cage around the iron oxide core (Fauconnier *et al.*, 1997, Valois *et al.*, 2010). Thus, processes that allow reduction of disulfide bridges can disintegrate the DMSA coat and are likely to be involved in the observed separation of the fluorescent coat from the iron oxide core. After endocytosis nanoparticle are passed to more and more acidic vesicles (Nazarenus *et al.*, 2014) and are likely to encounter the lysosomal thiol reductase that has been suggested to reduce DMSA disulfides in the coat and to release DMSA (Chen *et al.*, 2008, Zhang *et al.*, 2015a, Zhang and Liu, 2017). Additionally, DMSA may also be liberated during the trafficking process by ligand exchange processes with glutathione or other thiol-containing endogenous biomolecules (Hong *et al.*, 2006, See *et al.*, 2009). Further studies are now required to investigate in detail the molecular mechanisms responsible for the observed separation of coat and core of the intracellular fluorescent IONPs. Nanoparticle pulse-chase experiments can be a suitable experimental paradigm that will help to address such questions.

Double nanoparticle pulse-chase experiment were performed to study the sequential uptake and trafficking of two types of fluorescent IONPs. Only for the initial phase of the second chase period a clear separation of green OG-containing vesicles and red TMR-containing vesicles was observed in C6 glioma cells, while during longer incubation the fluorescence became colocalized as indicated by the yellow fluorescence overlay. These findings suggest that a sequential uptake and trafficking of two types of fluorescent IONPs can indeed be studied by the double nanoparticle pulse-chase setting, but that the intracellular trafficking of the internalized IONPs leads to a rapid colocalization of the fluorescent vesicles in the perinuclear space which may include fusion of green and red vesicles. However, an apparent colocalization could also be the

consequence of insufficient microscopical resolution in combination with high fluorescence signals which does not allow to discriminate between a real colocalisation of both types of fluorescence signals in one vesicle and a close proximity of vesicle that contain separate fluorescent dyes (Iversen *et al.*, 2011).

Uptake of IONPs in cells is mediated mainly by endocytotic processes (Luther *et al.*, 2013, Zhang *et al.*, 2015b, Chen *et al.*, 2017). For example, macropinocytosis and clathrin-mediated endocytosis have been reported to be involved in the uptake of protein-coated IONPs in cultured glial cells (Geppert *et al.*, 2013, Luther *et al.*, 2013). As actin polymerization appears to play an important role in several endocytotic process in mammalian cells (Smythe and Ayscough, 2006, Mooren *et al.*, 2012, Granger *et al.*, 2014), we investigated whether cytochalasin D, a compound that prevents polymerization of actin filaments and leads to the disassembly of the actin network (Spector *et al.*, 1999), affects IONP internalization and trafficking in nanoparticle pulse-chase experiments. Exposure of C6 glioma cells to cytochalasin D did not affect the binding of OG-IONPs to the cells during the particle pulse, but almost completely prevented the formation of fluorescent dots which are likely to represent intracellular vesicles that contain large amounts of internalized OG-IONPs, suggesting that actin polymerization is crucial for the endocytotic uptake and the packaging of OG-IONPs into intracellular vesicles. This actin-dependent internalization is consistent with results from previous studies on the uptake of carboxylated polystrene particles, silica nanoparticles or quantum dots in several cell lines, although the degree of the effects observed depended strongly ion the type of nanoparticle and the cell line investigated (dos Santos *et al.*, 2011, Iversen *et al.*, 2012, Nowak *et al.*, 2014, Prietl *et al.*, 2014). After endocytotic vesicle formation, the vesicles are transported away from the plasma membrane and a switch from actin-based movement to microtubules-based movement takes place (Granger *et al.*, 2014). After successful disruption of microtubules by colchicine exposure in a nanoparticle pulse-chase experiment, extensive formation of IONP-containing vesicles was observed all over the cells. However, the florescent IONP-containing vesicles appeared to be trapped near the plasma membrane and trafficking of the vesicles to the perinuclear space was not observed. This observation is consistent with results obtained for the transport of fluorescent microspheres in murine melanoma cells and has been interpreted as evidence for a discruption of the microtuble-dependent trafficking from the early to the late endosome (Rejman *et al.*,

2004). Also the sequential double nanoparticle pulse-chase experiments on colchicine-treated C6 cells revealed that both the green vesicles derived from the OG-IONP pulse and the red vesicles derived from the TMR-IONP pulse remained separately trapped at the cell membrane showing hardly any colocalization of the fluorescence signals, thereby demonstrating that the intracellular trafficking of internalized IONPs to the perinuclear region and the fusion of different types of nanoparticle-containing vesicles depends on intact microtubules.

In conclusion, nanoparticle pulse-chase protocols were established that make use of the efficient adsorption, but not internalization, of IONPs to cells at 4°C while an increase in temperature to 37°C synchronizes uptake and intracellular trafficking of the bound nanoparticles. The conditions applied did not affect cell viability and allowed a robust and reproducible analysis of IONP trafficking in cultured C6 glioma cells. In addition, the importance of the cytoskeleton for IONP uptake and trafficking was demonstrated by the dependence of nanoparticle internalization on actin polymerization and by the inhibition of intracellular trafficking by disintegration of microtubules. Furthermore, the synchronization of nanoparticle uptake and trafficking by the pulse-chase approach allowed to detect a separation of the fluorescent DMSA coat from the iron oxide core of the internalized IONPs during the chase incubations. Further studies are now required to elucidate in more detail the actin-dependent endocytotic pathways that are involved in the internalization of IONPs in the absence or the presence of protein by glial cells, the types of endosomal compartments involved in the trafficking of IONP-containing vesicles from the plasma membrane to the perinuclear regions of the cells, the mechanisms involved in the removal of the DMSA coat from the internalized IONPs, and the cellular fate of coat components that are removed from the particles during the trafficking. Nanoparticle pulse-chase experiments are well suited to address such questions already with simple epifluorescence microscopy with good spacial and temporal resolution, which could be further improved by using confocal microscopy to study the intracellular localization and the fate of internalized IONPs.

Acknowledgements

The authors thank Dr Frank Dietz (University of Bremen) for providing us with C6 glioma cellss

5. References

Ali A, Zafar H, Zia M, Ul Haq I, Phull AR, Ali JS & Hussain A (2016). Synthesis, characterization, applications, and challenges of iron oxide nanoparticles. *Nanotechnol Sci Appl,* 9: 49-67.

Baltazar GC, Guha S, Lu W, Lim J, Boesze-Battaglia K, Laties AM, Tyagi P, Kompella UB & Mitchell CH (2012). Acidic nanoparticles are trafficked to lysosomes and restore an acidic lysosomal pH and degradative function to compromised ARPE-19 cells. *PLoS One,* 7: e49635.

Banerjee S, Hwang DJ, Li W & Miller DD (2016). Current advances of tubulin inhibitors in nanoparticle drug delivery and vascular disruption/angiogenesis. *Molecules,* 21.

Bencsik A, Lestaevel P & Guseva Canu I (2018). Nano- and neurotoxicology: An emerging discipline. *Prog Neurobiol,* 160: 45-63.

Bertorelle F, Wilhelm C, Roger J, Gazeau F, Menager C & Cabuil V (2006). Fluorescence-modified superparamagnetic nanoparticles: Intracellular uptake and use in cellular imaging. *Langmuir,* 22: 5385-91.

Bishop GM & Robinson SR (2001). Quantitative analysis of cell death and ferritin expression in response to cortical iron: Implications for hypoxia-ischemia and stroke. *Brain Res,* 907: 175-87.

Bissell MG, Eng LF, Herman MM, Bensch KG & Miles LE (1975). Quantitative increase of neuroglia-specific GFA protein in rat C-6 glioma cells in vitro. *Nature,* 255: 633-4.

Chen D, Monteiro-Riviere NA & Zhang LW (2017). Intracellular imaging of quantum dots, gold, and iron oxide nanoparticles with associated endocytic pathways. *Wiley Interdiscip Rev Nanomed Nanobiotechnol,* 9.

Chen ZP, Zhang Y, Zhang S, Xia JG, Liu JW, Xu K & Gu N (2008). Preparation and characterization of water-soluble monodisperse magnetic iron oxide nanoparticles via surface double-exchange with DMSA. *Colloid Surface A,* 316: 210-216.

Costa C, Brandao F, Bessa MJ, Costa S, Valdiglesias V, Kilic G, Fernandez-Bertolez N, Quaresma P, Pereira E, Pasaro E, Laffon B & Teixeira JP (2016). In vitro cytotoxicity of superparamagnetic iron oxide nanoparticles on neuronal and glial cells. Evaluation of nanoparticle interference with viability tests. *J Appl Toxicol,* 36: 361-72.

dos Santos T, Varela J, Lynch I, Salvati A & Dawson KA (2011). Effects of transport inhibitors on the cellular uptake of carboxylated polystyrene nanoparticles in different cell lines. *PLoS One,* 6: e24438.

Dringen R, Kussmaul L & Hamprecht B (1998). Detoxification of exogenous hydrogen peroxide and organic hydroperoxides by cultured astroglial cells assessed by microtiter plate assay. *Brain Res Brain Res Protoc,* 2: 223-8.

Fauconnier N, Pons JN, Roger J & Bee A (1997). Thiolation of maghemite nanoparticles by dimercaptosuccinic acid. *J Colloid Interface Sci,* 194: 427-33.

Feliu N, Docter D, Heine M, Del Pino P, Ashraf S, Kolosnjaj-Tabi J, Macchiarini P, Nielsen P, Alloyeau D, Gazeau F, Stauber RH & Parak WJ (2016). In vivo degeneration and the fate of inorganic nanoparticles. *Chem Soc Rev,* 45: 2440-57.

Geppert M, Hohnholt M, Gaetjen L, Grunwald I, Baumer M & Dringen R (2009). Accumulation of iron oxide nanoparticles by cultured brain astrocytes. *J Biomed Nanotechnol,* 5: 285-93.

Geppert M, Hohnholt MC, Nurnberger S & Dringen R (2012). Ferritin up-regulation and transient ROS production in cultured brain astrocytes after loading with iron oxide nanoparticles. *Acta Biomater,* 8: 3832-9.

Geppert M, Hohnholt MC, Thiel K, Nurnberger S, Grunwald I, Rezwan K & Dringen R (2011). Uptake of dimercaptosuccinate-coated magnetic iron oxide nanoparticles by cultured brain astrocytes. *Nanotechnology,* 22: 145101.

Geppert M, Petters C, Thiel K & Dringen R (2013). The presence of serum alters the properties of iron oxide nanoparticles and lowers their accumulation by cultured brain astrocytes. *J Nanopart Res,* 15: 1349.

Goswami P, Gupta S, Joshi N, Sharma S & Singh S (2015). Astrocyte activation and neurotoxicity: a study in different rat brain regions and in rat C6 astroglial cells. *Environ Toxicol Pharmacol,* 40: 122-39.

Granger E, McNee G, Allan V & Woodman P (2014). The role of the cytoskeleton and molecular motors in endosomal dynamics. *Semin Cell Dev Biol,* 31: 20-9.

Grobben B, De Deyn PP & Slegers H (2002). Rat C6 glioma as experimental model system for the study of glioblastoma growth and invasion. *Cell Tissue Res,* 310: 257-70.

Hong R, Han G, Fernandez JM, Kim BJ, Forbes NS & Rotello VM (2006). Glutathione-mediated delivery and release using monolayer protected nanoparticle carriers. *J Am Chem Soc,* 128: 1078-9.

Hou T, Rinderknecht CH, Hadjinicolaou AV, Busch R & Mellins E (2013). Pulse-chase analysis for studies of MHC class II biosynthesis, maturation, and peptide loading. *Methods Mol Biol,* 960: 411-432.

Huerta-Garcia E, Marquez-Ramirez SG, Ramos-Godinez Mdel P, Lopez-Saavedra A, Herrera LA, Parra A, Alfaro-Moreno E, Gomez EO & Lopez-Marure R (2015). Internalization of titanium dioxide nanoparticles by glial cells is given at short times and is mainly mediated by actin reorganization-dependent endocytosis. *Neurotoxicology,* 51: 27-37.

Iversen TG, Frerker N & Sandvig K (2012). Uptake of ricinB-quantum dot nanoparticles by a macropinocytosis-like mechanism. *J Nanobiotechnology,* 10: 33.

Iversen TG, Skotland T & Sandvig K (2011). Endocytosis and intracellular transport of nanoparticles: Present knowledge and need for future studies. *Nano Today,* 6: 176-185.

Jamieson JD & Palade GE (1967a). Intracellular transport of secretory proteins in the pancreatic exocrine cell. I. Role of the peripheral elements of the Golgi complex. *J Cell Biol,* 34: 577-96.

Jamieson JD & Palade GE (1967b). Intracellular transport of secretory proteins in the pancreatic exocrine cell. II. Transport to condensing vacuoles and zymogen granules. *J Cell Biol,* 34: 597-615.

Joshi A, Rastedt W, Faber K, Schultz AG, Bulcke F & Dringen R (2016). Uptake and toxicity of copper oxide nanoparticles in C6 glioma cells. *Neurochem Res,* 41: 3004-3019.

Ku S, Yan F, Wang Y, Sun Y, Yang N & Ye L (2010). The blood-brain barrier penetration and distribution of PEGylated fluorescein-doped magnetic silica nanoparticles in rat brain. *Biochem Biophys Res Commun,* 394: 871-6.

Kumar S, Holmes E, Scully S, Birren BW, Wilson RH & de Vellis J (1986). The hormonal regulation of gene expression of glial markers: Glutamine synthetase and glycerol phosphate dehydrogenase in primary cultures of rat brain and in C6 cell line. *J Neurosci Res,* 16: 251-64.

Lai SK, Hida K, Man ST, Chen C, Machamer C, Schroer TA & Hanes J (2007). Privileged delivery of polymer nanoparticles to the perinuclear region of live cells via a non-clathrin, non-degradative pathway. *Biomaterials,* 28: 2876-84.

Lesniak A, Salvati A, Santos-Martinez MJ, Radomski MW, Dawson KA & Aberg C (2013). Nanoparticle adhesion to the cell membrane and its effect on nanoparticle uptake efficiency. *J Am Chem Soc,* 135: 1438-44.

Liu H, Zhang J, Chen X, Du XS, Zhang JL, Liu G & Zhang WG (2016). Application of iron oxide nanoparticles in glioma imaging and therapy: From bench to bedside. *Nanoscale,* 8: 7808-26.

Lowry OH, Rosebrough NJ, Farr AL & Randall RJ (1951). Protein measurement with the Folin phenol reagent. *J Biol Chem,* 193: 265-75.

Lunov O, Syrovets T, Rocker C, Tron K, Nienhaus GU, Rasche V, Mailander V, Landfester K & Simmet T (2010). Lysosomal degradation of the carboxydextran shell of coated superparamagnetic iron oxide nanoparticles and the fate of professional phagocytes. *Biomaterials,* 31: 9015-22.

Luther EM, Petters C, Bulcke F, Kaltz A, Thiel K, Bickmeyer U & Dringen R (2013). Endocytotic uptake of iron oxide nanoparticles by cultured brain microglial cells. *Acta Biomater,* 9: 8454-65.

Mamani JB, Pavon LF, Miyaki LA, Sibov TT, Rossan F, Silveira PH, Cardenas WH, Amaro Junior E & Gamarra LF (2012). Intracellular labeling and quantification process by magnetic resonance imaging using iron oxide magnetic nanoparticles in rat C6 glioma cell line. *Einstein (Sao Paulo),* 10: 216-21.

Mangoura D, Sakellaridis N, Jones J & Vernadakis A (1989). Early and late passage C-6 glial cell growth: similarities with primary glial cells in culture. *Neurochem Res,* 14: 941-7.

Mooren OL, Galletta BJ & Cooper JA (2012). Roles for actin assembly in endocytosis. *Annu Rev Biochem,* 81: 661-86.

Moos T & Mollgard K (1993). A sensitive post-DAB enhancement technique for demonstration of iron in the central nervous system. *Histochemistry,* 99: 471-5.

Nazarenus M, Zhang Q, Soliman MG, Del Pino P, Pelaz B, Carregal-Romero S, Rejman J, Rothen-Rutishauser B, Clift MJ, Zellner R, Nienhaus GU, Delehanty JB, Medintz IL & Parak WJ (2014). In vitro interaction of colloidal nanoparticles with mammalian cells: What have we learned thus far? *Beilstein J Nanotechnol,* 5: 1477-90.

Nowak JS, Mehn D, Nativo P, Garcia CP, Gioria S, Ojea-Jimenez I, Gilliland D & Rossi F (2014). Silica nanoparticle uptake induces survival mechanism in A549 cells by the activation of autophagy but not apoptosis. *Toxicol Lett,* 224: 84-92.

Oh N & Park JH (2014). Endocytosis and exocytosis of nanoparticles in mammalian cells. *Int J Nanomedicine,* 9: 51-63.

Petters C & Dringen R (2015). Accumulation of iron oxide nanoparticles by cultured primary neurons. *Neurochem Int,* 81: 1-9.

Petters C, Irrsack E, Koch M & Dringen R (2014). Uptake and metabolism of iron oxide nanoparticles in brain cells. *Neurochem Res,* 39: 1648-60.

Petters C, Thiel K & Dringen R (2016). Lysosomal iron liberation is responsible for the vulnerability of brain microglial cells to iron oxide nanoparticles: Comparison with neurons and astrocytes. *Nanotoxicology,* 10: 332-42.

Pickard MR & Chari DM (2010). Robust uptake of magnetic nanoparticles (MNPs) by central nervous system (CNS) microglia: Implications for particle uptake in mixed neural cell populations. *Int J Mol Sci,* 11: 967-81.

Pickard MR, Jenkins SI, Koller CJ, Furness DN & Chari DM (2011). Magnetic nanoparticle labeling of astrocytes derived for neural transplantation. *Tissue Eng Part C Methods,* 17: 89-99.

Prietl B, Meindl C, Roblegg E, Pieber TR, Lanzer G & Frohlich E (2014). Nano-sized and micro-sized polystyrene particles affect phagocyte function. *Cell Biol Toxicol,* 30: 1-16.

Rastedt W, Thiel K & Dringen R (2017). Uptake of fluorescent iron oxide nanoparticles in C6 glioma cells. *BiomPhys Eng Expr* 3: 035007.

Rejman J, Oberle V, Zuhorn IS & Hoekstra D (2004). Size-dependent internalization of particles via the pathways of clathrin- and caveolae-mediated endocytosis. *Biochem J,* 377: 159-69.

Riemer J, Hoepken HH, Czerwinska H, Robinson SR & Dringen R (2004). Colorimetric ferrozine-based assay for the quantitation of iron in cultured cells. *Anal Biochem,* 331: 370-5.

Sandin P, Fitzpatrick LW, Simpson JC & Dawson KA (2012). High-speed imaging of Rab family small GTPases reveals rare events in nanoparticle trafficking in living cells. *ACS Nano,* 6: 1513-21.

See V, Free P, Cesbron Y, Nativo P, Shaheen U, Rigden DJ, Spiller DG, Fernig DG, White MR, Prior IA, Brust M, Lounis B & Levy R (2009). Cathepsin L digestion of nanobioconjugates upon endocytosis. *ACS Nano,* 3: 2461-8.

Shevtsov MA, Nikolaev BP, Ryzhov VA, Yakovleva LY, Marchenko YY, Parr MA, Rolich VI, Mikhrina AL, Dobrodumov AV, Pitkin E & Multhoff G (2015). Ionizing radiation improves glioma-specific targeting of superparamagnetic iron oxide nanoparticles conjugated with cmHsp70.1 monoclonal antibodies (SPION-cmHsp70.1). *Nanoscale,* 7: 20652-64.

Shi D, Mi G, Bhattacharya S, Nayar S & Webster TJ (2016). Optimizing superparamagnetic iron oxide nanoparticles as drug carriers using an in vitro blood-brain barrier model. *Int J Nanomedicine,* 11: 5371-5379.

Smythe E & Ayscough KR (2006). Actin regulation in endocytosis. *J Cell Sci,* 119: 4589-98.

Spector I, Braet F, Shochet NR & Bubb MR (1999). New anti-actin drugs in the study of the organization and function of the actin cytoskeleton. *Microsc Res Tech,* 47: 18-37.

Stapelfeldt K, Ehrke E, Steinmeier J, Rastedt W & Dringen R (2017). Menadione-mediated WST1 reduction assay for the determination of metabolic activity of cultured neural cells. *Anal Biochem,* 538: 42-52.

Thimiri Govinda Raj DB & Khan NA (2016). Designer nanoparticle: nanobiotechnology tool for cell biology. *Nano Converg,* 3: 22.

Tulpule K, Hohnholt MC, Hirrlinger J & Dringen R (2014). Primary cultures of astrocytes and neurons as model systems to study the metabolism and metabolite export from brain cells. *In:* Hirrlinger J & Waagepetersen HS (eds.) *Brain Energy Metabolism.* New York: Springer.

Valois CR, Braz JM, Nunes ES, Vinolo MA, Lima EC, Curi R, Kuebler WM & Azevedo RB (2010). The effect of DMSA-functionalized magnetic nanoparticles on transendothelial migration of monocytes in the murine lung via a beta2 integrin-dependent pathway. *Biomaterials,* 31: 366-74.

van Landeghem FK, Maier-Hauff K, Jordan A, Hoffmann KT, Gneveckow U, Scholz R, Thiesen B, Bruck W & von Deimling A (2009). Post-mortem studies in glioblastoma patients treated with thermotherapy using magnetic nanoparticles. *Biomaterials,* 30: 52-7.

Villanueva A, Canete M, Roca AG, Calero M, Veintemillas-Verdaguer S, Serna CJ, Morales Mdel P & Miranda R (2009). The influence of surface functionalization on the enhanced internalization of magnetic nanoparticles in cancer cells. *Nanotechnology,* 20: 115103.

Vinzant N, Scholl JL, Wu CM, Kindle T, Koodali R & Forster GL (2017). Iron oxide nanoparticle delivery of peptides to the brain: Reversal of anxiety during drug withdrawal. *Front Neurosci,* 11: 608.

Wilhelm C, Billotey C, Roger J, Pons JN, Bacri JC & Gazeau F (2003). Intracellular uptake of anionic superparamagnetic nanoparticles as a function of their surface coating. *Biomaterials,* 24: 1001-11.

Yameen B, Choi WI, Vilos C, Swami A, Shi J & Farokhzad OC (2014). Insight into nanoparticle cellular uptake and intracellular targeting. *J Control Release,* 190: 485-99.

Yan F, Wang Y, He S, Ku S, Gu W & Ye L (2013). Transferrin-conjugated, fluorescein-loaded magnetic nanoparticles for targeted delivery across the blood-brain barrier. *J Mater Sci Mater Med,* 24: 2371-9.

Zhang L & Liu Y (2017). Research of an iron oxide nanoparticles and potential application. *Toxicology Open Access,* 3: 3.

Zhang L, Wang X, Zou J, Liu Y & Wang J (2015a). DMSA-coated iron oxide nanoparticles greatly affect the expression of genes coding cysteine-rich proteins by their DMSA coating. *Chem Res Toxicol,* 28: 1961-74.

Zhang S, Gao H & Bao G (2015b). Physical principles of nanoparticle cellular endocytosis. *ACS Nano,* 9: 8655-71.

2.3 Publication 3 (Manuscript)

How to study the consequences of an exposure of cultured neural cells to nanoparticles: The Dos and Don't forgets.

Wiebke Willmann and Ralf Dringen

Submitted for publication

Contribution of Wiebke Willmann (née Rastedt)

- Design of the study (50%)
- Performance of all experiments
- Preparation of the draft version of the manuscript

Abstract

Due to their exciting properties, engineered nanoparticles have obtained substantial attention over the last two decades. As many types of nanoparticles are already used for technical and biomedical applications, the chances that cells in the brain will encounter nanoparticles has strongly increased. To test for potential consequences of an exposure of brain cells to engineered nanoparticles, cell culture models for different types of neural cells are frequently used. In this review article we will discuss experimental strategies and important controls that should be used to investigate the physicochemical properties of nanoparticles for the cell incubation conditions applied as well as for studies on the biocompatibility and the cellular uptake of nanoparticles in neural cells. The main focus of this article will be the interaction of cultured neural cells with iron oxide nanoparticles, but similar considerations are important for studying the consequences of an exposure of other types of nanoparticles with other types of cultured cells. Our article aims to improve the understanding of the special challenges of working with nanoparticles on cultured neural cells, to identify potential artifacts and to prevent misinterpretation of data on the potential adverse or beneficial consequences of a treatment of cultured cells with nanoparticles.

Keywords: adsorption; biocompatibility; cell cultures; endocytosis; experimental strategies; iron oxide nanoparticles

1. Introduction

Nanoparticles (NPs) have obtained increasing attention over the last two decades as the use of engineered NPs for various technical approaches, industrial and commercial purposes as well as for biomedical applications has severely increased (Patil *et al.*, 2015, Mohammed *et al.*, 2017). NPs are defined as particles that have a size less than 100 nm in at least two dimension (Auffan *et al.*, 2009). Due to their small size and the resulting high surface to volume ratio, NPs differ in some of their chemical and physical properties from non-nanoscale particles or the bulk material of the same composition (Auffan *et al.*, 2009, Bobo *et al.*, 2016). NPs can be composed of inorganic and/or organic materials, including carbon, metals, metal oxides, silica, liposomes and polymers (Algar *et al.*, 2011, Colombo *et al.*, 2012, De la Fuente and Grazu, 2012). The basic NP material, the core, defines functional physical features of NPs such as plasmonic, superparamagnetic or fluorescent properties (Feliu *et al.*, 2016).

In biological environments, most NPs are not colloidally stable and tend to agglomerate or even precipitate (Akbarzadeh *et al.*, 2012, Feliu *et al.*, 2016). A common approach to prevent agglomeration of NPs and to increase the biocompatible of NPs in physiological environments is the encapsulation of the NP core with a coat that consists of organic coating materials such as lipids, proteins, or synthetic polymers (Gupta and Gupta, 2005, Valdiglesias *et al.*, 2015, Ali *et al.*, 2016, Mohammed *et al.*, 2017). Such a coating of NPs provides additional opportunities to further functionalize the NPs, for example with fluorescent dyes, drugs, antibodies and other compounds which enable better monitoring of the NPs and improve their use for specific applications (Sperling and Parak, 2010, Akbarzadeh *et al.*, 2012, Ali *et al.*, 2016, Mohammed *et al.*, 2017). Due to the high variability in core and coat, NPs have become exciting tools for many biomedical applications including drug delivery and bioimaging (Oh and Park, 2014, McNamara and Tofail, 2017).

The increased usage of NPs and the intended or unintended release of NPs in the environment (Rivera-Gil *et al.*, 2013, Nazarenus *et al.*, 2014, Patil *et al.*, 2015) makes it essential to study potential adverse and toxic consequences of NPs on mammalian cells. A large number of studies deals with the interaction between NPs and peripheral mammalian cells (Nazarenus *et al.*, 2014, Oh and Park, 2014), but less is known on the

consequences of a NP exposure of brain cells (Petters *et al.*, 2014b, Costa *et al.*, 2016). As frequently stated it is difficult to compare results described in different articles (Calero *et al.*, 2014, Kura *et al.*, 2014, Patil *et al.*, 2015, Soenen *et al.*, 2015, Valdiglesias *et al.*, 2016, Meindl *et al.*, 2017), as experimental conditions differ strongly between reported studies. In addition, each component of the test system applied (media components, buffer, temperature, incubation time, inhibitors, coatings etc.) may severely affect the interaction between NPs and cultured cells by modulating either the physicochemical properties of the NPs (such as shape, size and surface charge), the properties of the cell cultures investigated or both NP properties and cell behavior. The list of potential modulators of NP-cell interaction is long and, accordingly, standardizes protocols to enable a reliable comparison of different studies and to allow a valid risk assessment of NP have been requested (Worle-Knirsch *et al.*, 2006, Bregoli *et al.*, 2013, Rivera-Gil *et al.*, 2013, Meindl *et al.*, 2017).

Among the different types of engineered NPs, IONPs have gained a huge interest due to their use for several biomedical and clinical applications. IONPs possess superparamagnetic properties at room temperature (therefore they are also abbreviated as SPIONs), have a high surface-to-volume ratio and are non-toxic to most cell systems (Akbarzadeh *et al.*, 2012, Petters *et al.*, 2014b, Ali *et al.*, 2016, Mohammed *et al.*, 2017). These properties make IONPs useful for a number of biomedical applications (Mohammed *et al.*, 2017), e.g. as contrast agent for magnetic resonance imaging (Weinstein *et al.*, 2010, Wang, 2015), for cancer treatment by induced hyperthermia (Baetke *et al.*, 2015, Shi *et al.*, 2015), and as therapeutic agents for targeted drug delivery (Akbarzadeh *et al.*, 2012, Tietze *et al.*, 2015, El-Boubbou, 2018) across the blood-brain barrier (Yang, 2010, Ivask *et al.*, 2018). The combination of magnetic and fluorescent properties in fluorescently labeled IONPs has even further increased the potential of IONPs for biomedical applications (Kaewsaneha *et al.*, 2015, Shi *et al.*, 2015).

The promising use of IONPs for diagnostic and therapeutic applications with the potential of such IONPs to enter the brain, makes it mandatory to study the consequences of an exposure of brain cells to IONPs (Shi *et al.*, 2016). In particular, the uptake, intracellular trafficking and the fate of intracellular IONPs should be investigated as a potential release of large amounts of redox active iron in brain cells may cause oxidative stress and should

be considered in the context of the reported disturbances of brain iron homeostasis for neurodegenerative diseases (Hare *et al.*, 2013, Rouault, 2013, Morris *et al.*, 2018).

In this review article we will discuss basic problems and challenges of an exposure of cultured neural cells with NPs. Our main focus will be on the interactions of cultured neural cells with dimercaptosuccinate (DMSA)-coated IONPs (DMSA-IONPs). We would like to draw attention to problems and limitations which we have encountered during our studies and which we recommend to consider for designing and performing experiments in order to gain reliable, conclusive and reproducible results and to prevent misinterpretation of the cell data obtained after exposure of neural cells to NPs. Such aspects are also important to consider for studies on the interactions of other type of NPs with other types of cultured cells.

2. Testing for physicochemical properties of nanoparticles for incubation conditions

Cell binding and uptake of NPs depends on various factors, including the size, the charge and the shape of the NPs (Rivera-Gil *et al.*, 2013, Mahmoudi *et al.*, 2014, Nazarenus *et al.*, 2014, Mohammed *et al.*, 2017). For example, small NPs appear to be internalized quicker than large NPs (Nazarenus *et al.*, 2014, Shang *et al.*, 2014). Also the colloidal stability of NPs depends on the size, charge and surface chemistry of the NPs (Akbarzadeh *et al.*, 2012, Nazarenus *et al.*, 2014, Ali *et al.*, 2016) and is strongly affected by media composition and experimental conditions such as pH, salt concentrations and protein availability (Petri-Fink *et al.*, 2008, Rivera-Gil *et al.*, 2013, Nazarenus *et al.*, 2014, Feliu *et al.*, 2016). Thus, physiochemical characterization of NPs for the conditions applied is crucial to understand and interpret the results that will be obtained in cell culture studies.

Many groups have the knowledge to synthesize and characterize the NPs of interest and many companies offer NPs with special features which make them interesting for cell based studies. Nevertheless, for each type of NPs, for each new compound added to the medium, for each cell culture type, and for each other alteration of incubation conditions it should be investigated whether the new condition may affect the physicochemical

properties and the colloidal stability of the NPs. Several techniques are frequently used to characterizes IONPs (Ali *et al.*, 2016) and other types of NPs (Bhatia, 2016, Kumar and Dixit, 2017). Although the determination of each recommended parameter may be difficult due to unavailability of the required equipment, insufficient experience or high costs, a certain knowledge on physicochemical properties and confirmation of the colloidal stability of NPs for the incubation conditions used is essential to avoid artifacts and to prevent misinterpretations.

As it cannot be excluded that minor amounts of contaminants may still be present from the synthesis procedure in the NP preparation provided by the supplier or that components of the NPs may have been released from the NPs during storage or handling (for example iron ions from IONPs), it is strongly recommended to test for potentials presence and potential side effects of such contaminants. This can for example be done by removing the NPs from the dispersion by filtration or high speed centrifugation (Kowalczyk *et al.*, 2011, Wang *et al.*, 2011) and by subsequent testing of appropriate amounts of the NP-free filtrate or supernatant in the biological test system used for NP experiments.

Uncoated IONPs are frequently not stable as colloidal dispersion in physiological media due to strong magnetic attraction between the particles, van der Waals forces and their high energy surface (Lodhia *et al.*, 2010, Ali *et al.*, 2016). Therefore, IONPs are normally coated for applications in physiological conditions. In addition, substantial differences exists in physiochemical properties and the stability of available IONPs due to variations in the synthesis procedure, the selection of an appropriate coat and the large number of additional functionalization of the IONPs (Ali *et al.*, 2016, Mohammed *et al.*, 2017). As physicochemical properties and colloidal stability of NPs may strongly differ between dispersions in different solvents and incubation media, the determination of such parameters is essential for NP dispersed in the physiological medium that will be used for cell incubations. Table 1 shows the summary of the physicochemical characterization of DMSA-IONPs in a physiological incubation buffer (IB) that we have frequently used to study uptake of IONPs into cultured neural cells.

2.1 Test for size, elemental composition and successful coating of NPs

The nanoscale size of NPs can be best determined by electron microscopy. Here the elemental composition of the NP core is important as the electron density of the core material determines the intensity of the signals obtained (Westsson and Koper, 2014). Especially transmission electron microscopy (TEM) is the method of choice for size and shape determination of NPs that contain metals or metal oxides (Laurent *et al.*, 2008, Lodhia *et al.*, 2010, Lim *et al.*, 2013, Ali *et al.*, 2016). Regarding the size distribution, NPs preparations can be monodisperse (uniform; composed of NPs of the same size, shape and mass) or polydisperse (non-uniform) depending on the synthesis and the coating used (Laurent *et al.*, 2008, Stepto, 2009, Lim *et al.*, 2013). The polydispersity index (PDI; dispersity) gives a number on the heterogeneity of the NP population in a given NP dispersion (Lim *et al.*, 2013, Stetefeld *et al.*, 2016, Kumar and Dixit, 2017). Information on the dispersity can be obtained by dynamic light scattering (DLS), which gives information about the size, the colloidal stability and the size distribution of NPs dispersed in a given solvent (Xu, 2008, Lodhia *et al.*, 2010, Ali *et al.*, 2016). An important parameter of dispersed NPs is also the surface charge that is frequently analyzed by determination of the ζ-potential (Tantra *et al.*, 2010, Clogston and Patri, 2011). Valuable information on the elemental composition of the NP core and coat can also be obtained from TEM analysis, if the equipment used allows elemental analysis by energy-dispersive X-ray spectroscopy (EDX) (Rades *et al.*, 2014, Slater *et al.*, 2016, Kumar and Dixit, 2017).

Successful coating of NPs will modify physicochemical properties of NPs. For example the change of the surface charge (Tantra *et al.*, 2010, Clogston and Patri, 2011) or the colloidal stability in physiological medium are a good first indication for a successful coating. Further evidence for the presence of a coat around NPs can be obtained by identification of elements from the coat by EDX (Luther *et al.*, 2013, Petters *et al.*, 2014a, Rades *et al.*, 2014), by the demonstration of functional groups of the coat by infrared spectroscopy or by the presence of fluorophores as demonstrated by fluorescence spectroscopy (Bertorelle *et al.*, 2006, Luther *et al.*, 2013, Herrmann *et al.*, 2014, Lopez-Lorente and Mizaikoff, 2016, Rastedt *et al.*, 2017).

For DMSA-IONPs, TEM analysis revealed a polydispersed size distribution of 5-20 nm (Table 1, Fig. 1). Dispersed in physiological incubation buffer (IB) these IONPs had an average hydrodynamic diameter of around 60 nm (Fig. 1, Table 1), suggesting that some agglomeration of the primary particles had occurred. A polydispersity index of 0.257 demonstrated polydisperse size distribution in IB. The magnetic properties of the IONPs were used for magnetic separation during the synthesis process and were confirmed by recording a magnetization curve in a vibrating sample magnetometer (Petters *et al.*, 2014b). The negative ζ-potential due to the carboxylate groups in the DMSA coat as well as the identification of sulfur by EDX (Geppert *et al.*, 2011, Petters *et al.*, 2014a, Rastedt *et al.*, 2017) confirmed the successful coating of IONPs with DMSA (Table 1). For fluorescent DMSA-IONPs the presence of the introduced fluorophores in the obtained IONPs also confirmed successful coating of IONPs with fluorescent DMSA (Luther *et al.*, 2013, Rastedt *et al.*, 2017).

2.2 Quantify the NP content of a NP dispersion

For metal-containing NP such as IONPs, CuONPs or AgNPs the metal content of the dispersions can be determined for example by atomic absorption spectroscopy (AAS) or inductively coupled plasma mass spectrometry (ICP-MS) (Lodhia *et al.*, 2010, Patil *et al.*, 2015). The iron content of IONP dispersions can also be determined reliably and sensitive by a ferrozine-based colometric assay (Geppert *et al.*, 2013, Petters *et al.*, 2016, Rastedt *et al.*, 2017). However, for reliable quantification of metal contents of a NP dispersion the complete liberation of the metal from the NPs is required that will include the application of concentrated acids and may involve some ashing procedures (Geppert *et al.*, 2009, Luther *et al.*, 2011, Bulcke *et al.*, 2014, Joshi *et al.*, 2016).

If the NP possess fluorescent properties these fluorescent properties can be used to quantify the NPs in dispersion and in cells by fluorescence spectroscopy, flow cytometry or fluorescence imaging techniques (Drasler *et al.*, 2017). A drawback in the fluorescent quantification is the possible bleaching or quenching of the fluorescent signal, which could result in an incorrect quantification (Corr *et al.*, 2008, Waters, 2009, Drasler *et al.*, 2017). In addition, the type of fluorescence labeling can affect the fluorescent properties of the NPs. Fluorophores can either be encapsulated within the NPs or immobilized to

the polymer coat of the NPs (Ruedas-Rama *et al.*, 2012, Kaewsaneha *et al.*, 2015, Wolfbeis, 2015). The distance between fluorophore and core can lead to quenching or alteration of the fluorescent signal (Kaewsaneha *et al.*, 2015). Here it is important to compare the fluorescence spectra of the fluorescent NPs with those of the free fluorescent dyes (Bertorelle *et al.*, 2006, Luther *et al.*, 2013, Rastedt *et al.*, 2017).

2.3 Modulation of NP properties by variation of the coating materials

The coating of the NPs provides opportunities to further functionalize the particles for example with fluorescence dyes (Ruedas-Rama *et al.*, 2012, Petters *et al.*, 2014a, Kaewsaneha *et al.*, 2015, Rastedt *et al.*, 2017), with drugs, antibodies or other compounds (Shevtsov *et al.*, 2014, Shevtsov *et al.*, 2015, Galli *et al.*, 2017) that may modify physicochemical properties and colloidal stability of the NPs and thereby the interaction with cultured cells. Thus, for each type of coating the NPs should be carefully characterized. For example, the use of different coating materials during the synthesis of IONPs caused strong differences in the hydrodynamic diameter of the NPs ranging from 20 to 200 nm (Shi *et al.*, 2014, Shi *et al.*, 2016). Such alterations in particle size but also size distribution, shape and surface charge are likely to affect binding to and uptake of NPs into cells.

Uncoated IONPs have a strongly positive zeta potential of around +40 mV and are colloidal stable in water, but they precipitate rapidly in salt-containing physiological media such as basal incubation buffer (Geppert *et al.*, 2011). Such IONPs can be stabilized by coating with citrate (Geppert *et al.*, 2009) or DMSA (Geppert *et al.*, 2011). DMSA-coating does not significantly increase the diameter of the IONPs, but generates in water a negative zeta potential (-60 mV) which maintains the coated IONPs in dispersion (Table 2). Modification of the DMSA coat by low amounts of fluorescent dyes (around 1% of thiol groups present in DMSA used for coating) did not alter the physicochemical properties of the IONPs nor their binding or internalization into cultured neural cells (Luther *et al.*, 2013, Petters *et al.*, 2014a, Rastedt *et al.*, 2017), thereby defining such fluorescent IONPs as suitable tool to trace by fluorescence microscopy the internalization and the intracellular trafficking of DMSA-IONPs in cultured brain cells (Luther *et al.*, 2013, Petters *et al.*, 2014a, Rastedt *et al.*, 2017).

2.4 Modulation of NP properties by the components added to the incubation media

In complex biological environments a variety of the molecules are present including lipids, sugars and proteins that may adsorb onto the surface of the NPs (Rivera-Gil *et al.*, 2013, Nazarenus *et al.*, 2014, Feliu *et al.*, 2016), but even simple physiological buffers contain ions and other compounds that may affect the properties of dispersed NPs. In fact, as it is difficult to predict which compounds may severely affect the stability and the properties of NPs, analysis of such parameters is recommended for each incubation medium used for cell exposure to NPs.

Table 2 shows the consequences of the presence of various compounds in a given incubation media on the size (hydrodynamic diameter) and the surface charge (ζ-potential) of dispersed DMSA-IONPs. Compared to water as dispersant, the use of a physiological HEPES-buffered incubation buffer (Table 2) does not alter the average hydrodynamic diameter of the IONPs but increases the ζ-potential from -60 mV to -16 mV. The size of the NPs is moderately increased in the presence of proteins such as bovine serum albumin (BSA) or fetal calf serum (FCS), while the ζ-potential is further increased in the presence of proteins to around -10 mV (Table 2). In contrast, already the presence of 0.8 mM phosphate, a component that is frequently present in physiological buffers used for metabolic studies on cultured brain cells (Tulpule *et al.*, 2014), causes rapid agglomeration and precipitation of the IONPs as demonstrated by the micromolar diameter of the particle agglomerates. Similarly, also dispersion of IONPs in DMEM culture medium that contains 0.9 mM phosphate are not stable and rapid agglomeration was observed which was prevented by the presence of 10% FCS, but not by BSA application (Table 2). Thus, the presence of proteins or protein mixtures can prevent agglomeration of IONPs, most likely by forming a protein coat around the DMSA-IONPs that affects NP properties and stability as well as their interactions with the cell surface (Doak *et al.*, 2009, Nel *et al.*, 2009, Feliu *et al.*, 2016).

To study the mechanisms of cellular uptake of NPs and to identify the endocytotic pathways involved in the internalization of NPs, a battery of more or less specific inhibitors for given endocytotic pathways are available and have been used (Iversen *et al.*, 2011). This strategy has already been critically discussed due to the lack of specificity

and severe side effects of some inhibitors (Iversen *et al.*, 2011, Dutta and Donaldson, 2012, Kuhn *et al.*, 2014, Guo *et al.*, 2015). In addition, a further disadvantage of some endocytosis inhibitors is their effect on the stability of NPs. Examples for such effects are shown in Table 2. Dynasore (Macia *et al.*, 2006, Kirchhausen *et al.*, 2008) and chlorpromazine (Dutta and Donaldson, 2012) are frequently applied to test for an involvement of clathrin-mediated endocytosis in the cellular uptake of NPs. However, the presence of dynasore leads to agglomeration and precipitation of IONPs, whereas the presence of chlorpromazine does not affect particle size and colloidal stability (Table 2). Furthermore, the agglomeration of IONPs by dynasore is almost completely prevented in the additional presence of 10 % FCS (Table 2). These results underline the importance to investigate the potential effects of each compound that will be added to the given incubation medium to study the accumulation of NPs by cells, as modulation of the physiochemical properties and the stability of the IONPs may strongly affect the interaction between particles and cells as well as the biocompatibility or cytotoxicity of NPs (Frohlich, 2012, Kroll *et al.*, 2012, Yang *et al.*, 2013).

2.5 Alteration of NP properties by cell-derived components

Last but not least, it has also to be considered that during the incubation of cells with NPs physicochemical properties and the colloidal stability of NPs could be changed by compounds that are released from the exposed cells during the incubation. For example, substances that are released from viable cultured astrocytes and are present in conditioned media lead to an agglomeration of IONPs and can therefore alter the binding to or the internalization of the IONPs into the cells (Geppert *et al.*, 2011, Geppert *et al.*, 2012, Lamkowsky *et al.*, 2012, Geppert *et al.*, 2013). Such effects may be even more dramatic, if NPs have some toxic potential. As soon as the first cells have died and have released their content, the surface of the applied NPs can be covered by cellular biomolecules and cell debris that is likely to alter the interaction between NPs and cells. Therefore, it should be considered to characterize the extracellular NPs also during or after a given incubation of cells to learn whether cell-derived material has modulated the properties of the NPs during the incubation.

3. Using an appropriate cell culture test system for NP studies

3.1 Cell lines and primary cultures

In addition to the properties of NPs, also cellular parameters and the type of cell culture models chosen for NP interactions studies are important. Here, biomechanical properties of the cell membrane including membrane tension and bending modulus, composition and thickness of the phospholipid bilayer, cell size, proliferation rate, growth pattern as well the environmental factors like cell-cell-interaction play an important role in the NP adhesion and uptake (Iversen *et al.*, 2011, Mahmoudi *et al.*, 2014, Zhang *et al.*, 2015, Meindl *et al.*, 2017). As the mechanisms of NP uptake depend on the cell type and the culture model investigated, it is important to select an appropriate test system for studying the consequences of an exposure of neural brain cells to NPs. Here, the characterization of the cell culture model system chosen is very important, as such models differ strongly in cell density, media requirements and sensitivity to given incubation conditions that are required for incubations with NPs.

For first screening tests on the biocompatibility or toxicity of a given type of NP, immortalized cell lines of neural origin are frequently used. Such cell lines are easy to handle, can be sub-cultured, batch-to-batch variability is considered to be low and the costs of such studies are reasonable (Bregoli *et al.*, 2013). However, as cell lines are mostly transformed, have a disturbed proliferation control mechanisms, and possess when compared to the genuine brain cells genetic and chromosomal aberrations that may even increase with passage number (Bregoli *et al.*, 2013), an interpretation of data obtained on cell lines for potential consequences of a respective NP incubation of genuine brain cells is problematic. In addition, due to the long handling of immortalized cell lines evolution of cells over the passaging procedure, potential contamination with mycoplasma as well as potential cross-contamination with other cell lines should be considered and/or excluded (Freedman *et al.*, 2015, Drexler *et al.*, 2017). Thus, cell lines used for NP studies should be characterized concerning their properties and authenticity, for example by testing for expression of the cell type specific markers and/or by genetic testing to confirm the cell line origin (Freedman *et al.*, 2015).

Primary cultures of brain cells, for example, primary cultures of astrocytes or neurons, have frequently been used to study properties and functions of the respective brain cell types *in vitro* (Sunol *et al.*, 2008, Lange *et al.*, 2012, Gordon *et al.*, 2013, Petters *et al.*, 2014b, Tulpule *et al.*, 2014). Compared to cell lines, such cultures have a limited life span, show substantial variability between different culture preparations, require the access to living animals as cell donors and are more expensive. Nevertheless, primary cultures of brain cells are likely to reflect properties of the respective cell type *in vivo* more strongly than immortalized cell lines (Kaur and Dufour, 2012, Bregoli *et al.*, 2013, Gordon *et al.*, 2013). Thus, for studies to investigate the basic mechanisms of NP uptake, intracellular trafficking or the fate of internalized NPs in brain cells, primary cultures of brain cells, which are strongly enriched for one type of brain cells, appear to be a better model than cell lines of neural origin. If using primary cultures of brain cells, the cultures obtained should be characterized for the cell types present by immunocytochemical staining for cell type specific markers (Petters and Dringen, 2014, Tulpule *et al.*, 2014) in order to learn about the enrichment of the desired cell type in these cultures but also about contaminations with other types of brain cells.

3.2 Potential problems with cell density and proliferation state

Depending on the cell cultures and the culturing conditions selected, the density of cells in cell cultures can substantially vary. Primary cultures of astrocytes as well as cell lines of neural origin can be investigated during the proliferation period and different cell densities can be established by variation of the number of cells seeded per dish. Primary astrocyte cultures will reach after a given culture time confluency, while cultures of neurons will not become confluent due to the post mitotic status of these cells (Tulpule *et al.*, 2014).

Differences in cell density, cell-cell contacts, membrane tension and cell cycle phases have been described to strongly affect NP uptake (Snijder *et al.*, 2009, Kim *et al.*, 2011, Wang *et al.*, 2016). An example for the effects of cell density on the cellular uptake of fluorescent Oregon Green (OG)-DMSA-IONPs is shown for C6 glioma cells (Fig. 2). With increasing seeding density, the protein content of the cultures increases almost linearly within a 24 h incubation period (Fig. 2A). Also the amount of iron and

fluorescence accumulated by the cultured cells during a 1 h exposure to IONPs increased almost linearly, but only for low cell densities, while hardly any differences in accumulated iron or fluorescence was observed for cultures generated by seeding the cells at densities of 200,000 or 400,000 cells per well (Fig. 2B,C).

During the cell cycle the ratio of cholesterol and phospholipid, the expression of membrane proteins, surface antigens and receptors can vary (Boucrot and Kirchhausen, 2007, Mahmoudi *et al.*, 2014, Tang *et al.*, 2015), thereby influencing the interaction of cells with NPs and subsequently the uptake of NPs (Tang *et al.*, 2015). Accordingly, in synchronized cells the uptake of NPs can vary depending on the cell cycle phases (Kim *et al.*, 2011, Patel *et al.*, 2016). As most cultured cells used for NP uptake studies are not synchronized for their cell cycle, it should be considered that the data obtained on such cultures represent average values derived from cells in different phases of the cell cycle (Kim *et al.*, 2011).

3.3 Potential problem due to unspecific binding to NPs to the culture plates

To improve binding of cells to cell culture plates, manufacturers use frequently chemical and/or physical surface modifications to alter the polystyrene surface of the culture plates (Curtis *et al.*, 1983, Roder *et al.*, 2015). In addition, some cell types require special dish coatings to ensure cell attachment or to facilitate cell differentiation. For example, coating of cell culture dishes with collagen or poly-D-lysine is frequently used for primary neurons, hepatocytes or stem cells (Aday *et al.*, 2011, Gordon *et al.*, 2013, Tulpule *et al.*, 2014, Salzig *et al.*, 2016). As such coatings of plastic surfaces have the potential to bind NPs, a potential cell-independent adsorption of NPs to the surface of the culture dishes has to be considered. Data for such a cell-independent binding of NPs to coated dishes are shown in Table 3. While uncoated dishes hardly contain any detectable iron or fluorescence after incubation with fluorescent OG-DMSA-IONPs, substantial amounts of iron and OG fluorescence were determined for culture plates that had been preincubated (coated) with DMEM containing proteins or with a poly-D-lysine solution (Table 3). Such unspecific interactions between the NPs and the treated culture materials may strongly contribute to quantitative data obtained for the potential uptake of IONPs in cultures of low cell density.

4. Test for the consequences of an exposure of cultured neural cells to NPs

4.1 Test for biocompatibility or toxic potential of NPs

To study the cellular uptake mechanisms of NPs into neural cells, the potential cytotoxic potential of the chosen incubation conditions must be investigated in order to confirm that indeed the uptake and internalization of NP is monitored for viable cells. The size, shape, agglomeration state and surface coating play an important role in the cytotoxicity of NPs (Frohlich, 2012, Kroll *et al.*, 2012, Yang *et al.*, 2013), because these factors highly influence the binding to the cells and their internalization. In this context it is important to considered that already partial cell toxicity will lead to substantial release of biomolecules from damaged cells which in turn can bind to the NPs, and thereby alter their physicochemical properties.

For IONPs, the cytotoxic potential is controversially discussed (Patil *et al.*, 2015, Valdiglesias *et al.*, 2015, Costa *et al.*, 2016). Several studies state that IONPs have a low toxic potential (Dunning *et al.*, 2004, Villanueva *et al.*, 2009, Kunzmann *et al.*, 2011, Calero *et al.*, 2014, Feng *et al.*, 2018), whereas other studies observed a cytotoxic potential of IONPs depending on cell type and surface coating of the NPs (Chen *et al.*, 2008, Sun *et al.*, 2013, Petters *et al.*, 2016, Feng *et al.*, 2018). Smaller NPs have an increased reactive surface in relation to their volume and are usually faster internalized that may contribute to their higher cytotoxic potential (Rivera-Gil *et al.*, 2013). Likely reasons for the controversial observations may be the use of different coating materials and different physicochemical properties of the IONPs applied that will affect binding to the cells and subsequent uptake (Warheit, 2008, Hong *et al.*, 2011) as shown for differently coated IONPs on cultured primary neurons (Rivet *et al.*, 2012). In addition, also cell-type differences strongly affect the toxic potential of IONPs. For example, DMSA-IONPs were not toxic for cultured astrocytes or neurons even in millimolar concentrations, but showed strong toxic potential to cultured microglial cells (Petters *et al.*, 2016).

To investigate the biocompatibility or the toxicity of a given treatment, a large number of viability assays is available and frequently used that address mostly either membrane integrity or metabolic functions (Kroll *et al.*, 2009, Kroll *et al.*, 2012, Hohnholt *et al.*,

2015). For studies of potential toxicity of NPs it is recommended to apply at least two different viability assays that have independent underlying principles, in order to become aware of potential disturbances by NPs on the viability assay systems used.

4.2 Test for potential interferences of NPs with the assay systems used to determine cell viability or toxicity

The determination of cellular viability during or after an exposure of cells to NPs is important but not always easy as NPs may interfere with the viability assay applied. Similarly, also the quantification of cellular NPs or of cellular parameters and functions can be disturbed in the presence of NPs as their unique physicochemical properties, their high reactivity and their high adsorptive capacity may interfere with components of the test system applied (Doak *et al.*, 2009, Stone *et al.*, 2009, Galdiero *et al.*, 2015, Costa *et al.*, 2016). This can result in artifacts and a false-positive or false-negative misinterpretation of the data obtained.

A large number of viability or toxicity assays are based on colorimetic and fluorimetric dyes and depend on the light absorption and/or emission at a specific wavelength. It is obvious that the use of fluorescence labeled IONPs limits the applicable number of these assay regarding interference of absorption and emission spectra. For example, measuring the generation of reactive oxygen species using Rhodamine123 (Almeida *et al.*, 2002) would not be suitable after exposure of cells to OG-DMSA-IONPs due to the overlap of the excitation and emission spectra of these both dyes. But besides this obvious problems, nanomaterials have widely been shown to interfere with assays by altering the optical properties of dyes leading to under- or overestimation of the NP toxicity (Bregoli *et al.*, 2013, Patil *et al.*, 2015). For example, determination of the release of cellular LDH is considered as a good indicator for a loss in membrane integrity of cultured cells (Tulpule *et al.*, 2014). However, this assay should not be used for analysis of cellular consequences of CuONPs, as such NPs inactivate LDH (Bulcke *et al.*, 2014). Thereby, a quantification of released LDH is prevented which will lead to false negative results suggesting absence of any cell toxicity of CuONPs.

To identify potential artifacts by NPs on the assay systems applied, several controls are recommended such as (1) exposing cells with NPs but without assay reagents (Hoskins *et al.*, 2012), (2) applying a cell free control incubation (Doak *et al.*, 2009), (3) removing or lowering the amount of NPs present in samples by centrifugation (Stone *et al.*, 2009) and (4) intensive washing after the cell incubation before applying the assay system (Hoskins *et al.*, 2012). But even all these precautions cannot fully exclude interference in the results due to membrane adhesion and internalization of NPs by cells (Hoskins *et al.*, 2012, Costa *et al.*, 2016). Therefore, it is strongly recommended to run always additional controls including the addition of a standard concentration of NPs to cell samples that were obtained of viable cells and a toxic control condition.

4.3 Test for adsorption of NP to the cells and/or uptake of NPs into cells

The cellular uptake of NPs is a two-step process (Wilhelm *et al.*, 2002, Wilhelm *et al.*, 2003). First the NPs adsorb to the cell membrane and then the internalization by endocytosis takes place (Wilhelm *et al.*, 2003, Lamkowsky *et al.*, 2012, Lesniak *et al.*, 2013). The surface properties are the crucial factor in cell-nanoparticle interaction as the engineered surface is first recognized by a cell (Pelaz *et al.*, 2013, Mahmoudi *et al.*, 2014). This will mediate the binding of NPs to the cells before internalization of the NPs can take place. Uptake of NPs in cultured brain cells can be verified depending on the type of NP investigated by electron, fluorescence or light microscopy.

The successful uptake of NPs into cells and the intracellular localization of NPs can be visualized by TEM. Concerning IONPs in cultured brain cells, a vesicular localization of electron dense material was reported for IONP-treated cultured primary astrocytes (Geppert *et al.*, 2009, Geppert *et al.*, 2011, Geppert *et al.*, 2012). For such staining even elemental analysis of the cellular NPs can be done and the material taken up into the cells can be confirmed. Fluorescence microscopy of neural cells that had been exposed to fluorescent IONPs allows also a qualitative view on the internalization of such NPs (Luther *et al.*, 2013, Petters *et al.*, 2014a, Petters and Dringen, 2015, Petters *et al.*, 2016, Rastedt *et al.*, 2017). Finally cytochemical staining of the exposed cells for iron allows a qualitative view on the cellular presence of IONPs in cultured neural cells (Geppert *et al.*, 2009, Geppert *et al.*, 2011, Hohnholt *et al.*, 2011, Luther *et al.*, 2013, Petters *et al.*,

2014a, Calero *et al.*, 2015). For cytochemical or fluorescence analysis of the uptake of IONPs into cells it is important to consider that the signals obtained in light or fluorescence microscopic images do not represent the signals derived from individual fluorescent NPs but that rather a given amount of NPs has to be packed into vesicular structures in order to generate sufficient local density of NPs to allow detection.

Various methods can be applied to quantify cellular contents of NP as long as the assay of choice is sufficiently sensitive for quantifying the low amounts of material that has been internalized into the cells by NP uptake. For NPs containing copper or silver, we have used highly sensitive AAS methods (Geppert *et al.*, 2009, Luther *et al.*, 2011, Bulcke *et al.*, 2014, Joshi *et al.*, 2016), and for IONPs a sensitive ferrozine-based colorimetric assay in microtiter plates (Geppert *et al.*, 2009, Geppert *et al.*, 2011, Geppert *et al.*, 2013, Petters *et al.*, 2016, Rastedt *et al.*, 2017). However, for reliable quantification of metal contents of cellular NP the complete liberation of the metal from the NPs is required which will include the application of concentrated acids and involves some ashing procedures. Concerning the NP quantification, it should be kept in mind, that the NP amount determined reflects the total amount of NPs in a well that consists of the amount of internalized NPs plus the amount of NPs bound extracellularly to cells plus the amount of NPs bound to the plastic of the dish in a cell-independent process.

In order to quantify the amount of internalized NP it is important to discriminate between NPs that are adsorbed to the cells (and/or the culture plate) and the NPs that had been taken up by cellular endocytosis. This can be achieved by performing control adsorption experiments at 4°C. This low temperature prevents the energy-dependent NP internalization, but does hardly affect adsorption and desorption processes (Wilhelm *et al.*, 2002, Wilhelm *et al.*, 2003, Bertorelle *et al.*, 2006, Lamkowsky *et al.*, 2012). Thus, after a 4°C incubation only the extracellularly adsorbed NPs are quantified as NP uptake is prevented, while the values obtained for a respective incubation at 37°C represents the sum of adsorbed plus internalized NPs. The temperature dependence of IONP uptake in order to discriminate between adsorbed and internalized IONPs has been performed for several types of neural cell cultures and revealed that the amounts of adsorbed NPs after exposure of the cells to DMSA-IONPs represents between 50% and 70% of the total amount of IONPs (Hohnholt *et al.*, 2013, Petters *et al.*, 2014a, Petters and Dringen, 2014,

Petters and Dringen, 2015, Rastedt *et al.*, 2017). Similar results were found for non-neural cells (Wilhelm *et al.*, 2002, dos Santos *et al.*, 2011).

Most of this extracellular adsorption of IONPs to neural cells may be caused by unspecific electrostatic interactions between the coat of the NPs and cell surface molecules which cannot be simply removed by additional washing steps. However, the binding of NPs to cells can also be made more specific by introducing cell receptor specific ligands, signal peptides or antibodies (Ahrens *et al.*, 2003, Pilakka-Kanthikeel *et al.*, 2013, Galli *et al.*, 2017, Lachowicz *et al.*, 2017). In some cases, the presence of protein can reduce the adsorption of NPs to the cell membrane (Wilhelm *et al.*, 2003, Lesniak *et al.*, 2013, Rastedt *et al.*, 2017) and thereby also dramatically lower the cellular uptake.

After internalization into cells, NPs are encountering changes in their environment that can affect the stability and the cellular metabolism of the intracellular NPs. Uptake by endocytosis delivers NPs into endosomal compartments that is characterized by a slightly acidic pH (Rejman *et al.*, 2016). This may lead to degradation of the core and/or the coat of the NPs that may affect cellular parameters, cell viability but also the interpretation of the results obtained. Therefore, it is important to verify whether the internalized NPs are still intact and/or whether the coat is still colocalized with the core of the NPs (Nazarenus *et al.*, 2014, Feliu *et al.*, 2016). If the NPs are disintegrated or the coat is separated from the core of the NP it has to be considered that components of core or coat are liberated from the NPs that can affect properties and functions of cells (Rejman *et al.*, 2016). For example, IONP uptake causes severe toxicity of cultured microglia due to iron-mediated oxidative stress caused by lysosomal liberation of iron ions from the internalized IONPs (Luther *et al.*, 2013, Petters *et al.*, 2016, Zhang *et al.*, 2016).

4.4 An example how to analyse the uptake of fluorescent DMSA- IONPs in cultured neural cells

Fig. 3 shows experimental data that were obtained for an exposure of C6 glioma cells with OG-DMSA-IONPs. The fluorescent IONPs have been carefully characterized for their physicochemical properties and their colloidal stability in the incubation buffer (IB) used for the incubations (Rastedt *et al.*, 2017). Compared to the non-fluorescent DMSA-IONPs (Table 1), the presence of the low amounts of the fluorescent dye OG in the coat of the IONPs does not affect the physicochemical properties of the IONPs nor their interaction with cells (Rastedt *et al.*, 2017). For the cell experiments 100,000 C6-glioma cells were seeded per well of a 24-well plate in 1 mL of DMEM with 10% FCS. After 24 h incubation the cells were washed twice with IB and subsequently incubated for 1 h with given concentrations of OG-DMSA-IONPs in 200 µL IB at 4°C or at 37°C. The concentrations given for the IONPs represent the concentration of iron present in the IONPs applied and not the particle concentration.

Analysis of cell morphology did not reveal any obvious alteration after exposure to the IONPs (data not shown) and also the quantification of extracellular LDH activity after the 1 h exposure time did not show any increase in extracellular LDH (Fig. 3A). The lack of any influence of the NPs applied on the LDH assay performed was investigated by applying IONPs to lysates generated from cultured C6 cells before measuring LDH activity for the lysates. Even in final concentrations of up to 3 mM iron as IONPs, the presence of IONPs did not affect the measurement of LDH activity in cell lysates (Fig. 3D), thereby excluding that a potential toxicity (LDH release) of the treatment could have been masked by inactivation of liberated LDH by IONPs. Analysis of the unspecific binding of IONPs to protein-coated cell culture plates (24 h preincubation with DMEM + 10% FCS) revealed by quantification of iron and fluorescence that the cell-independent binding of IONPs was low and even substantially lower that the adsorption of IONPs to the cells at 4°C (Fig. 3E,F).

Analysis of the cellular fluorescence and cellular iron contents in cell lysates obtained from cells after exposure to OG-IONPs at 4°C and 37°C allows to discriminate between adsorbed IONPs and internalized IONPs (Fig. 3B,C). For incubations with 1 mM and 3 mM IONPs, the specific iron contents and the specific cellular fluorescence determined

after 4°C incubations represented around 65% of the values observed for the respective 37°C incubations, demonstrating that after a 37°C incubation only around 35% of the cellular IONPs had been taken up into the cells (Fig. 3B,C). Despite of the substantial amounts of iron and fluorescence determined in lysates generated from cells after exposure to OG-IONPs at 4°C, hardly any cellular fluorescence or iron signals were observed for this treatment (Fig. 3M-P), due to insufficient local density of the extracellularly adsorbed fluorescent IONPs to allow detection of iron or fluorescence (Waters, 2009, Nazarenus *et al.*, 2014, Drasler *et al.*, 2017). In contrast, after the respective incubations at 37°C, strong fluorescence signals and a strong cellular iron staining were detectable (Fig. 3H-K), indicating cellular uptake and intracellular packaging of the fluorescent IONPs to local concentrations that are sufficiently high to allow detection of the internalization of OD-DMSA-IONPs by iron staining and florescence microscopy.

5. Conclusion

To test and screen for potential consequences of an exposure of brain cells to NPs, cultures of neural cells are good and easy to use model systems. However, due to their unique properties NPs will strongly interact with components of physiological media, with biomolecules and with cells. This can affect the physicochemical properties of the NPs but also the properties and the viability of cells. Therefore, it is important to analyze in detail the physicochemical properties of the NPs in the physiological media used for cell experiments, the potential effect of cell components on the NPs as well as the consequences of an NPs exposure to the cells. A number of special control experiments are recommended to avoid artifacts and misinterpretations of data on the consequences of an exposure of brain cells to NPs. These dos and don´t forgets will help to appropriately address the special challenges connected with studying the interactions between NPs and cultured cells and will help to avoid unnecessary artifacts in order to deliver robust and reproducible data and reliable and correct interpretations of the data obtained on the potential toxicity, uptake and intracellular fate of NPs in neural cells.

6. Acknowledgments

The authors thank Dr. Karsten Thiel (Fraunhofer IFAM, Bremen) for kindly providing the TEM picture of the DMSA-IONPs.

7. Table and figures

Table 1. Characterization of DMSA-IONPs

Parameter	Method	Values
Shape	Transmission electron microscopy	spherical
Size	Transmission electron microscopy	5-20 nm
Size distribution	Transmission electron microscopy Dynamic light scattering	polydisperse
Hydrodynamic diameter	Dynamic light scattering	61 ± 5 nm
Surface charge (ζ-potential)	Electrophoretic light scattering	-20 ± 5 mV
Element content	Energy dispersive X-ray spectrometry	iron, oxygen, sulfur
Magnetism	Vibrating sample magnetometer	superparamagnetic
Coating present	Energy dispersive X-ray spectrometry	presence of sulfur peak
	Electrophoretic light scattering	negative surface charge in water

The data shown in this table have been taken from the articles (Geppert *et al.*, 2011, Petters *et al.*, 2014a, Petters *et al.*, 2014b, Rastedt *et al.*, 2017).

Table 2. Modulation of physicochemical parameters of DMSA-IONPs by media components

Solvent	Test compound	Hydrodynamic diameter (nm)	ζ-potential (mV)
H_2O		54 ± 11	-61 ± 13
IB		60 ± 8	-16 ± 4
IB	phosphate (0.8 mM)	>1000 ***	n.d.
IB	BSA (0.5 mg/mL)	75 ± 4 *	-9 ± 2 *
IB	FCS (10%)	95 ± 14 *	-9 ± 2 *
IB	chlorpromazine (20 µM)	72 ± 11	-18 ± 7
IB	dynasore (100 µM)	>1000 ***	n.d.
IB	FCS (10%) + dynasore (100 µM)	111 ± 5 **	-9 ± 1 *
DMEM		>1000	n.d.
DMEM	BSA (0.5 mg/mL)	>1000	n.d.
DMEM	FCS (10%)	148 ± 22 **	-10 ± 1

DMSA-IONPs were dispersed in a final concentration of 1 mM iron in the indicated solvents (water, or incubation buffer (IB; 20 mM HEPES, 145 mM NaCL, 5 mM D-glucose, 1.8 mM $CaCl_2$, 5.4 mM KCl, 1 mM $MgCl_2$, adjusted with NaOH to pH 7.4) or Dulbecco's modified Eagle´s medium (DMEM; containing 20 U/mL penicillin G, 20 µg/mL streptomycin sulfate, 25 mM glucose and 1 mM sodium pyruvate) in the absence or the presence of the indicated test compounds before the average hydrodynamic diameter and the ζ-potential were determined. The data represent mean values ± SD of data obtained in 3 experiments performed on independently prepared batches of DMSA-IONPs. The significance of differences between the values obtained for the IONP-containing medium without or with the indicated test compounds is indicated by *$p<0.05$; **$p<0.01$ and ***$p<0.001$. BSA: bovine serum albumin, FCS: fetal calf serum, n.d.: not detectable.

Table 3. Binding of fluorescence OG-DMSA-IONPs to cell culture plates

Preincubation medium	Iron content (nmol/well)	Fluorescence (a.u./well)
none	0.3 ± 0.1	1.6 ± 0.2
DMEM	2.3 ± 0.4**	3.3 ± 2.5
DMEM + BSA (0.5 mg/mL)	7.4 ± 1.8**	16.8 ± 7.1**
DMEM + FCS (10%)	6.0 ± 1.5**	13.6 ± 0.3***
Poly-D-lysine (15 µg/mL in H_2O)	22.0 ± 6.1**	23.0 ± 1.7***

24-well cell culture plates were preincubated for 24 h with 1 mL of the indicated solutions in a humidified atmosphere of an incubator at 37°C for 24 h. Subsequently, the wells were washed twice with IB, incubated with 200 µL of 1 mM Oregon Green (OG)-DMSA-IONPs (200 nmol iron per well and 262 ± 26 a.u. fluorescence per well) in IB at 37°C for 1 h, were washed twice with 1 mL phosphate-buffered saline and were treated with 400 µL 50 mM NaOH to solubilize bound IONPs that were subsequently quantified by determining the contents of iron and OG fluorescence (Geppert *et al.*, 2009, Rastedt *et al.*, 2017). The data represent mean values ± SD of data obtained in 3 experiments performed on independently prepared batche s of OG-DMSA-IONPs. The significance of differences between the data obtained for uncoated (none) and preincubated wells is indicated by **$p<0.01$ and ***$p<0.001$. DMEM, Dulbecco's modified Eagle´s medium; BSA, bovine serum albumin; FCS, fetal calf serum

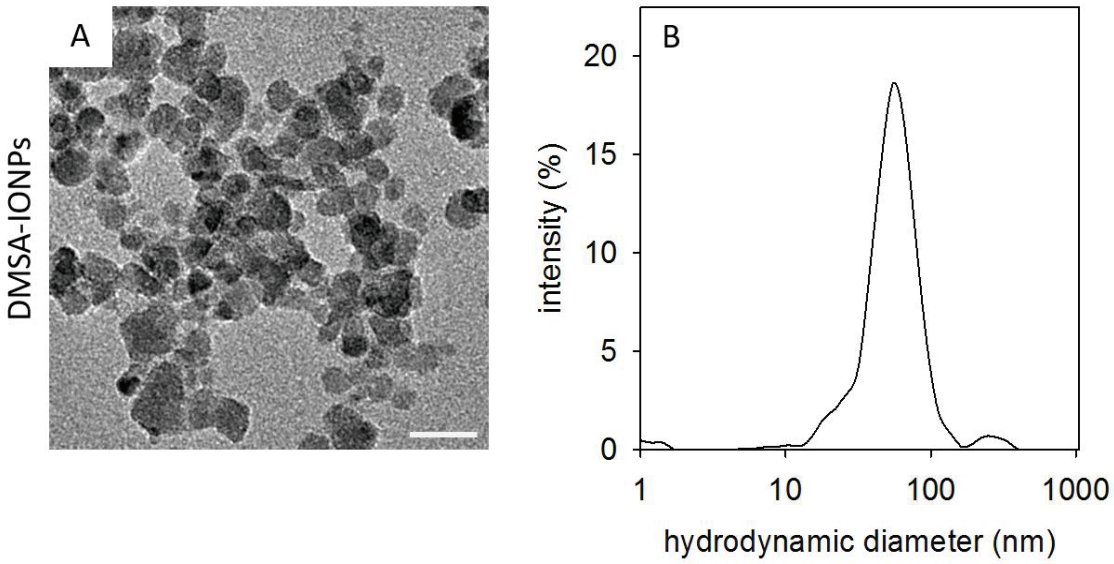

Fig. 1 DMSA-IONPs. The panels show a transmission electron microscopic (TEM) image (A) and the hydrodynamic diameter distribution curve (B) for 1 mM IONPs dissolved in physiological incubation buffer (IB) that were obtained as previously descibed (Tulpule *et al.*, 2014, Rastedt *et al.*, 2017). The *scale bar* in the TEM image represent 20 nm. The TEM image (A) was kindly provided by Dr. Karsten Thiel (Fraunhofer IFAM, Bremen).

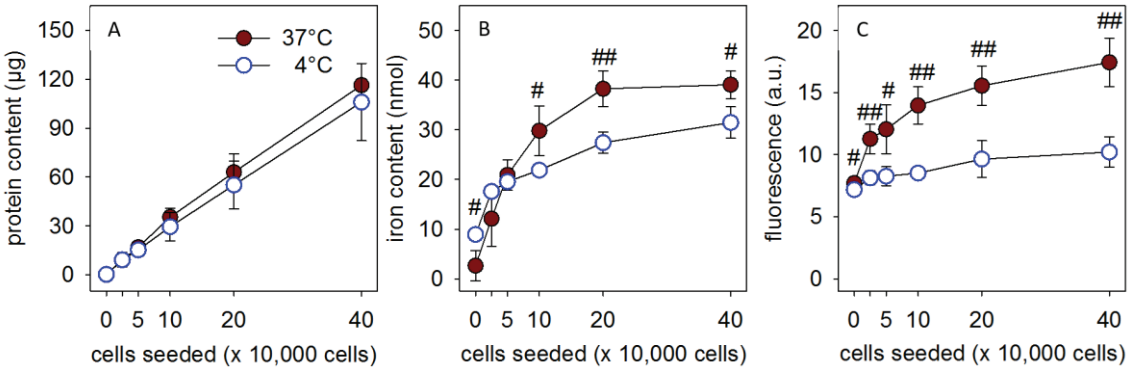

Fig. 2 Cell density-dependent accumulation of OG-DMSA-IONPs in C6 glioma cells. The cells were seeded in different densities and grown for 24 h before an 1 h incubation in IB with 1 mM fluorescent OG-DMSA-IONPs (Rastedt *et al.*, 2017) was performed at 37°C or 4°C. The OG-DMSA-IONP incubation was terminated by washing the cells twice with ice-cold phosphate-buffered saline. The cells were lysed in 400 µL 50 mM NaOH and the lysates were used to determine the protein content (A), the cellular iron content (B) and the cellular OG fluorescence (C) using established assays as described before (Lowry *et al.*, 1951, Geppert *et al.*, 2009, Rastedt *et al.*, 2017). The data shown represents means ± SD of values obtained in 4 independent experiments. The significance of differences between the values obtained for cells that had been incubated at 37°C and 4°C is indicated by $^{\#}p<0.05$; $^{\#\#}p<0.01$ and $^{\#\#\#}p<0.001$.

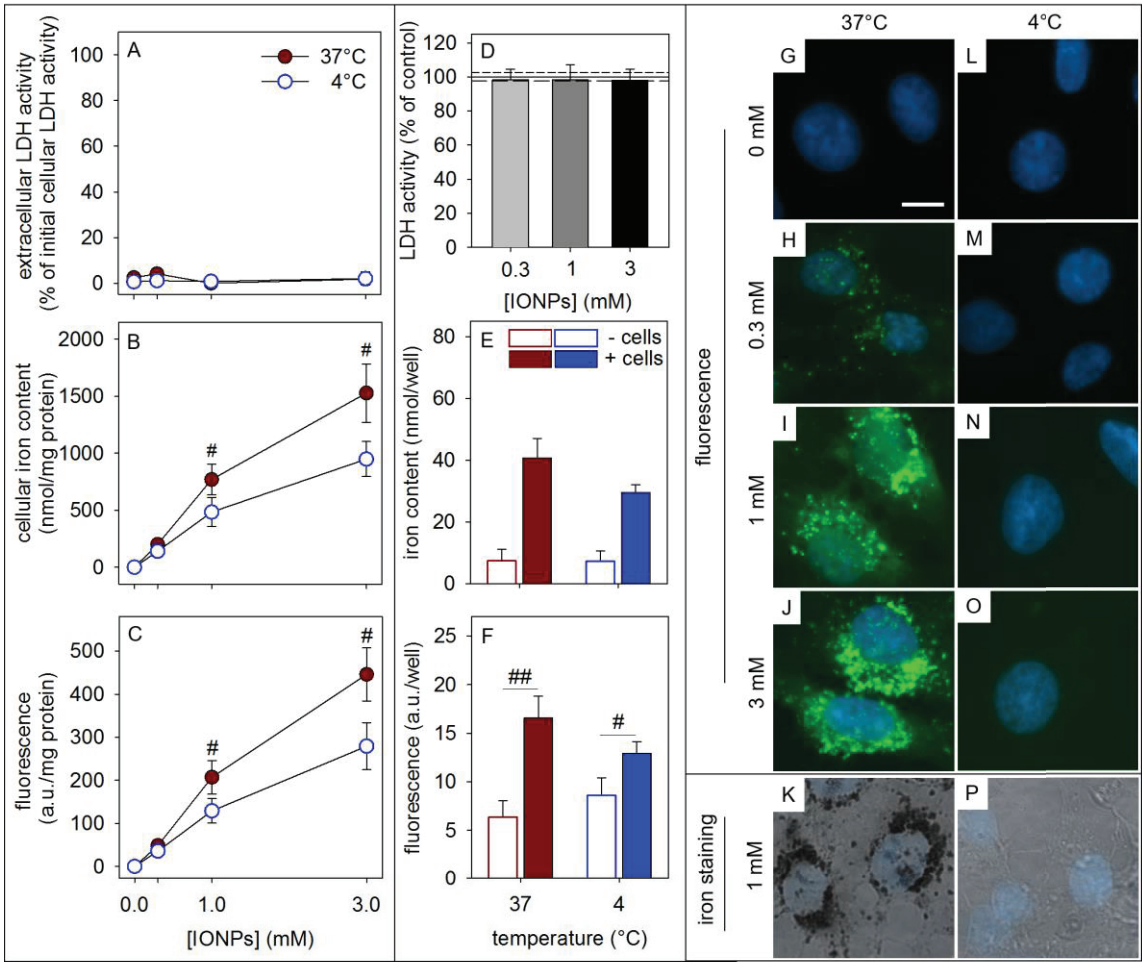

Fig. 3 Concentration-dependent accumulation of OG-DMSA-IONPs in C6 glioma cells. Per well, 100,000 cells were seeded and grown for 24 h before the cells were incubated for 1 h with the indicated concentrations of OG-DMSA-IONPs at 37°C or 4°C. The cell viability was investigated by testing for impaired membrane integrity by measuring the release of the cytosolic enzyme LDH (A) as previously described (Dringen *et al.*, 1998, Tulpule *et al.*, 2014). The cellular iron content (B) and the cellular OG fluorescence (C) were determined from NaOH lysates (400 µL 50 mM) as recently described (Geppert *et al.*, 2009, Rastedt *et al.*, 2017). Potential disturbances by IONPs on the LDH assay used were excluded by determining LDH activity in 1% Triton X-100 cell lysate in the presence of the given final concentrations of IONPs (D). The extend of cell-independent binding of OG-DMSA-IONPs to protein-coated wells (wells exposed to culture medium containing 10% FCS for 24 h) was determined in parallel to cell incubations (1 h at 37°C or 4°C with 1 mM IONPs) by measuring iron content (E) and fluorescence (F). The data shown represents means ± SD of values obtained in 3 independent experiments. The significance of differences between values obtained for incubations at 37°C and 4°C or for incubations in the presence or absence of cells is indicated by $^{\#}p<0.05$; $^{\#\#}p<0.01$ and $^{\#\#\#}p<0.001$. Fluorescence microscopy was used to localize cellular OG fluorescence after 1 h incubation of cells with the indicated concentrations of OG-DMSA-IONPs at 37°C (G.I) or 4°C (L-O) and the cellular iron

was localized by cytochemical Perls staining (K,P) as previously described (Geppert *et al.*, 2009, Rastedt *et al.*, 2017). The cell nuclei were stained with DAPI (blue) (G-P). The size bar in panel g represents 10 µm and applies for the panels (G-P).

8. References

Aday S, Hasirci N & Gurhan I (2011). A cost-effective and simple culture method for primary hepatocytes. *Animal Cells and Systems,* 15: 19-27.

Ahrens ET, Feili-Hariri M, Xu H, Genove G & Morel PA (2003). Receptor-mediated endocytosis of iron-oxide particles provides efficient labeling of dendritic cells for in vivo MR imaging. *Magn Reson Med,* 49: 1006-13.

Akbarzadeh A, Samiei M & Davaran S (2012). Magnetic nanoparticles: Preparation, physical properties, and applications in biomedicine. *Nanoscale Res Lett,* 7: 144.

Algar WR, Prasuhn DE, Stewart MH, Jennings TL, Blanco-Canosa JB, Dawson PE & Medintz IL (2011). The controlled display of biomolecules on nanoparticles: A challenge suited to bioorthogonal chemistry. *Bioconjug Chem,* 22: 825-58.

Ali A, Zafar H, Zia M, Ul Haq I, Phull AR, Ali JS & Hussain A (2016). Synthesis, characterization, applications, and challenges of iron oxide nanoparticles. *Nanotechnol Sci Appl,* 9: 49-67.

Almeida A, Delgado-Esteban M, Bolanos JP & Medina JM (2002). Oxygen and glucose deprivation induces mitochondrial dysfunction and oxidative stress in neurones but not in astrocytes in primary culture. *J Neurochem,* 81: 207-17.

Auffan M, Rose J, Bottero JY, Lowry GV, Jolivet JP & Wiesner MR (2009). Towards a definition of inorganic nanoparticles from an environmental, health and safety perspective. *Nat Nanotechnol,* 4: 634-41.

Baetke SC, Lammers T & Kiessling F (2015). Applications of nanoparticles for diagnosis and therapy of cancer. *Br J Radiol,* 88: 1054.

Bertorelle F, Wilhelm C, Roger J, Gazeau F, Menager C & Cabuil V (2006). Fluorescence-modified superparamagnetic nanoparticles: Intracellular uptake and use in cellular imaging. *Langmuir,* 22: 5385-91.

Bhatia S 2016. Nanoparticles types, classification, characterization, fabrication methods and drug dilvery. *In:* Bhatia S (ed.) Natural polymer drug delivery systems: Nanoparticle, plats, and algae. 1 ed. Switzerland: Springer.

Bobo D, Robinson KJ, Islam J, Thurecht KJ & Corrie SR (2016). Nanoparticle-based medicines: a review of FDA-approved materials and clinical trials to date. *Pharm Res,* 33: 2373-87.

Boucrot E & Kirchhausen T (2007). Endosomal recycling controls plasma membrane area during mitosis. *Proc Natl Acad Sci,* 104: 7939-44.

Bregoli L, Benetti F, Venturini M & Sabbioni E (2013). ECSIN's methodological approach for hazard evaluation of engineered nanomaterials. *J Phys Conf Ser,* 429: 012017.

Bulcke F, Thiel K & Dringen R (2014). Uptake and toxicity of copper oxide nanoparticles in cultured primary brain astrocytes. *Nanotoxicology,* 8: 775-85.

Calero M, Chiappi M, Lazaro-Carrillo A, Rodriguez MJ, Chichon FJ, Crosbie-Staunton K, Prina-Mello A, Volkov Y, Villanueva A & Carrascosa JL (2015). Characterization of interaction of magnetic nanoparticles with breast cancer cells. *J Nanobiotechnology,* 13: 16.

Calero M, Gutierrez L, Salas G, Luengo Y, Lazaro A, Acedo P, Morales MP, Miranda R & Villanueva A (2014). Efficient and safe internalization of magnetic iron oxide nanoparticles: two fundamental requirements for biomedical applications. *Nanomedicine (Lond),* 10: 733-43.

Chen J, Zhu JM, Cho HH, Cui KM, Li FH, Zhou XB, Rogers JT, Wong STC & Huang XD (2008). Differential cytotoxicity of metal oxide nanoparticles. *J Exp Nanosci,* 3: 321-328.

Clogston JD & Patri AK (2011). Zeta potential measurement. *Methods Mol Biol,* 697: 63-70.

Colombo M, Carregal-Romero S, Casula MF, Gutierrez L, Morales MP, Bohm IB, Heverhagen JT, Prosperi D & Parak WJ (2012). Biological applications of magnetic nanoparticles. *Chem Soc Rev,* 41: 4306-34.

Corr SA, Rakovich YP & Gun'ko YK (2008). Multifunctional magnetic-fluorescent nanocomposites for biomedical applications. *Nanoscale Res Lett,* 3: 87-104.

Costa C, Brandao F, Bessa MJ, Costa S, Valdiglesias V, Kilic G, Fernandez-Bertolez N, Quaresma P, Pereira E, Pasaro E, Laffon B & Teixeira JP (2016). In vitro cytotoxicity of superparamagnetic iron oxide nanoparticles on neuronal and glial cells. Evaluation of nanoparticle interference with viability tests. *J Appl Toxicol,* 36: 361-72.

Curtis AS, Forrester JV, McInnes C & Lawrie F (1983). Adhesion of cells to polystyrene surfaces. *J Cell Biol,* 97: 1500-6.

De la Fuente JM & Grazu V (2012). Nanobiotechnology: Inorganic Nanoparticles vs organic nanoparticles. United Kingdom, Elsevier.

Doak SH, Griffiths SM, Manshian B, Singh N, Williams PM, Brown AP & Jenkins GJS (2009). Confounding experimental considerations in nanogenotoxicology. *Mutagenesis,* 24: 285-293.

dos Santos T, Varela J, Lynch I, Salvati A & Dawson KA (2011). Effects of transport inhibitors on the cellular uptake of carboxylated polystyrene nanoparticles in different cell lines. *PLoS One,* 6: e24438.

Drasler B, Vanhecke D, Rodriguez-Lorenzo L, Petri-Fink A & Rothen-Rutishauser B (2017). Quantifying nanoparticle cellular uptake: Which method is best? *Nanomedicine (Lond),* 12: 1095-1099.

Drexler HG, Dirks WG, MacLeod RA & Uphoff CC (2017). False and mycoplasma-contaminated leukemia-lymphoma cell lines: Time for a reappraisal. *Int J Cancer,* 140: 1209-1214.

Dringen R, Kussmaul L & Hamprecht B (1998). Detoxification of exogenous hydrogen peroxide and organic hydroperoxides by cultured astroglial cells assessed by microtiter plate assay. *Brain Res Brain Res Protoc,* 2: 223-8.

Dunning MD, Lakatos A, Loizou L, Kettunen M, ffrench-Constant C, Brindle KM & Franklin RJ (2004). Superparamagnetic iron oxide-labeled Schwann cells and olfactory ensheathing cells can be traced in vivo by magnetic resonance imaging and retain functional properties after transplantation into the CNS. *J Neurosci,* 24: 9799-810.

Dutta D & Donaldson JG (2012). Search for inhibitors of endocytosis: Intended specificity and unintended consequences. *Cell Logist,* 2: 203-208.

El-Boubbou K (2018). Magnetic iron oxide nanoparticles as drug carriers: Clinical relevance. *Nanomedicine (Lond),* in press.

Feliu N, Docter D, Heine M, Del Pino P, Ashraf S, Kolosnjaj-Tabi J, Macchiarini P, Nielsen P, Alloyeau D, Gazeau F, Stauber RH & Parak WJ (2016). In vivo degeneration and the fate of inorganic nanoparticles. *Chem Soc Rev,* 45: 2440-57.

Feng Q, Liu Y, Huang J, Chen K, Huang J & Xiao K (2018). Uptake, distribution, clearance, and toxicity of iron oxide nanoparticles with different sizes and coatings. *Sci Rep,* 8: 2082.

Freedman LP, Gibson MC, Ethier SP, Soule HR, Neve RM & Reid YA (2015). Reproducibility: Changing the policies and culture of cell line authentication. *Nat Methods,* 12: 493-7.

Frohlich E (2012). The role of surface charge in cellular uptake and cytotoxicity of medical nanoparticles. *Int J Nanomedicine,* 7: 5577-91.

Galdiero S, Falanga A, Morelli G & Galdiero M (2015). gH625: A milestone in understanding the many roles of membranotropic peptides. *Biochim Biophys Acta,* 1848: 16-25.

Galli M, Guerrini A, Cauteruccio S, Thakare P, Dova D, Orsini F, Arosio P, Carrara C, Sangregorio C, Lascialfari A, Maggioni D & Licandro E (2017). Superparamagnetic iron oxide nanoparticles functionalized by peptide nucleic acids. *Rsc Advances,* 7: 15500-15512.

Geppert M, Hohnholt M, Gaetjen L, Grunwald I, Baumer M & Dringen R (2009). Accumulation of iron oxide nanoparticles by cultured brain astrocytes. *J Biomed Nanotechnol,* 5: 285-93.

Geppert M, Hohnholt MC, Nurnberger S & Dringen R (2012). Ferritin up-regulation and transient ROS production in cultured brain astrocytes after loading with iron oxide nanoparticles. *Acta Biomater,* 8: 3832-9.

Geppert M, Hohnholt MC, Thiel K, Nurnberger S, Grunwald I, Rezwan K & Dringen R (2011). Uptake of dimercaptosuccinate-coated magnetic iron oxide nanoparticles by cultured brain astrocytes. *Nanotechnology,* 22: 145101.

Geppert M, Petters C, Thiel K & Dringen R (2013). The presence of serum alters the properties of iron oxide nanoparticles and lowers their accumulation by cultured brain astrocytes. *J Nanopart Res,* 15: 1349.

Gordon J, Amini S & White MK (2013). General overview of neuronal cell culture. *Methods Mol Biol,* 1078: 1-8.

Guo S, Zhang X, Zheng M, Zhang X, Min C, Wang Z, Cheon SH, Oak MH, Nah SY & Kim KM (2015). Selectivity of commonly used inhibitors of clathrin-mediated and caveolae-dependent endocytosis of G protein-coupled receptors. *Biochim Biophys Acta,* 1848: 2101-10.

Gupta AK & Gupta M (2005). Synthesis and surface engineering of iron oxide nanoparticles for biomedical applications. *Biomaterials,* 26: 3995-4021.

Hare D, Ayton S, Bush A & Lei P (2013). A delicate balance: Iron metabolism and diseases of the brain. *Front Aging Neurosci,* 5: 1-19.

Herrmann R, Rennhak M & Reller A (2014). Synthesis and characterization of fluorescence-labelled silica core-shell and noble metal-decorated ceria nanoparticles. *Beilstein J Nanotechnol,* 5: 2413-2423.

Hohnholt MC, Blumrich EM & Dringen R (2015). Multiassay analysis of the toxic potential of hydrogen peroxide on cultured neurons. *J Neurosci Res,* 93: 1127-37.

Hohnholt MC, Geppert M & Dringen R (2011). Treatment with iron oxide nanoparticles induces ferritin synthesis but not oxidative stress in oligodendroglial cells. *Acta Biomater,* 7: 3946-54.

Hohnholt MC, Geppert M, Luther EM, Petters C, Bulcke F & Dringen R (2013). Handling of iron oxide and silver nanoparticles by astrocytes. *Neurochem Res,* 38: 227-39.

Hong SC, Lee JH, Lee J, Kim HY, Park JY, Cho J, Lee J & Han DW (2011). Subtle cytotoxicity and genotoxicity differences in superparamagnetic iron oxide nanoparticles coated with various functional groups. *Int J Nanomedicine,* 6: 3219-31.

Hoskins C, Wang LJ, Cheng WP & Cuschieri A (2012). Dilemmas in the reliable estimation of the in-vitro cell viability in magnetic nanoparticle engineering: which tests and what protocols? *Nanoscale Res Lett,* 7: 1-12.

Ivask A, Pilkington EH, Blin T, Kakinen A, Vija H, Visnapuu M, Quinn JF, Whittaker MR, Qiao R, Davis TP, Ke PC & Voelcker NH (2018). Uptake and transcytosis of functionalized superparamagnetic iron oxide nanoparticles in an in vitro blood brain barrier model. *Biomater Sci,* 6: 314-323.

Iversen TG, Skotland T & Sandvig K (2011). Endocytosis and intracellular transport of nanoparticles: Present knowledge and need for future studies. *Nano Today,* 6: 176-185.

Joshi A, Rastedt W, Faber K, Schultz AG, Bulcke F & Dringen R (2016). Uptake and toxicity of copper oxide nanoparticles in C6 glioma cells. *Neurochem Res,* 41: 3004-3019.

Kaewsaneha C, Tangboriboonrat P, Polpanich D & Elaissari A (2015). Multifunctional fluorescent-magnetic polymeric colloidal particles: Preparations and bioanalytical applications. *ACS Appl Mater Interfaces,* 7: 23373-86.

Kaur G & Dufour JM (2012). Cell lines: Valuable tools or useless artifacts. *Spermatogenesis,* 2: 1-5.

Kim JA, Aberg C, Salvati A & Dawson KA (2011). Role of cell cycle on the cellular uptake and dilution of nanoparticles in a cell population. *Nat Nanotechnol,* 7: 62-8.

Kirchhausen T, Macia E & Pelish HE (2008). Use of dynasore, the small molecule inhibitor of dynamin, in the regulation of endocytosis. *Methods Enzymol,* 438: 77-93.

Kowalczyk B, Lagzi I & Grzybowski BA (2011). Nanoseparations: Strategies for size and/or shape-selective purification of nanoparticles. *Curr Opin Colloid In,* 16: 135-148.

Kroll A, Pillukat MH, Hahn D & Schnekenburger J (2009). Current in vitro methods in nanoparticle risk assessment: Limitations and challenges. *Eur J Pharm Biopharm,* 72: 370-377.

Kroll A, Pillukat MH, Hahn D & Schnekenburger J (2012). Interference of engineered nanoparticles with in vitro toxicity assays. *Arch Toxicol,* 86: 1123-36.

Kuhn DA, Vanhecke D, Michen B, Blank F, Gehr P, Petri-Fink A & Rothen-Rutishauser B (2014). Different endocytotic uptake mechanisms for nanoparticles in epithelial cells and macrophages. *Beilstein J Nanotechnol,* 5: 1625-36.

Kumar A & Dixit CK (2017). Methods for characterization of nanoparticles. *In:* Nimesh S, Ramesh C & Gupta N (eds.) Advances in Nanomedicine for the Delivery of Therapeutic Nucleic Acids. United Kingdom: Woodhead Publishing.

Kunzmann A, Andersson B, Thurnherr T, Krug H, Scheynius A & Fadeel B (2011). Toxicology of engineered nanomaterials: Focus on biocompatibility, biodistribution and biodegradation. *Biochim Biophys Acta,* 1810: 361-73.

Kura AU, Fakurazi S, Hussein MZ & Arulselvan P (2014). Nanotechnology in drug delivery: The need for more cell culture based studies in screening. *Chem Cent J,* 8: 46.

Lachowicz D, Szpak A, Malek-Zietek KE, Kepczynski M, Muller RN, Laurent S, Nowakowska M & Zapotoczny S (2017). Biocompatible and fluorescent superparamagnetic iron oxide nanoparticles with superior magnetic properties coated with charged polysaccharide derivatives. *Colloids Surf B Biointerfaces,* 150: 402-407.

Lamkowsky MC, Geppert M, Schmidt MM & Dringen R (2012). Magnetic field-induced acceleration of the accumulation of magnetic iron oxide nanoparticles by cultured brain astrocytes. *J Biomed Mater Res A,* 100: 323-34.

Lange SC, Bak LK, Waagepetersen HS, Schousboe A & Norenberg MD (2012). Primary cultures of astrocytes: Their value in understanding astrocytes in health and disease. *Neurochem Res,* 37: 2569-88.

Laurent S, Forge D, Port M, Roch A, Robic C, Vander Elst L & Muller RN (2008). Magnetic iron oxide nanoparticles: Synthesis, stabilization, vectorization, physicochemical characterizations, and biological applications. *Chem Rev,* 108: 2064-110.

Lesniak A, Salvati A, Santos-Martinez MJ, Radomski MW, Dawson KA & Aberg C (2013). Nanoparticle adhesion to the cell membrane and its effect on nanoparticle uptake efficiency. *J Am Chem Soc,* 135: 1438-44.

Lim J, Yeap SP, Che HX & Low SC (2013). Characterization of magnetic nanoparticle by dynamic light scattering. *Nanoscale Res Lett,* 8: 381-394.

Lodhia J, Mandarano G, Ferris N, Eu P & Cowell S (2010). Development and use of iron oxide nanoparticles (Part 1): Synthesis of iron oxide nanoparticles for MRI. *Biomed Imaging Interv J,* 6: e12.

Lopez-Lorente AI & Mizaikoff B (2016). Recent advances on the characterization of nanoparticles using infrared spectroscopy. *Trends Anal Chem,* 84: 97-106.

Lowry OH, Rosebrough NJ, Farr AL & Randall RJ (1951). Protein measurement with the Folin phenol reagent. *J Biol Chem,* 193: 265-75.

Luther EM, Koehler Y, Diendorf J, Epple M & Dringen R (2011). Accumulation of silver nanoparticles by cultured primary brain astrocytes. *Nanotechnology,* 22: 375101.

Luther EM, Petters C, Bulcke F, Kaltz A, Thiel K, Bickmeyer U & Dringen R (2013). Endocytotic uptake of iron oxide nanoparticles by cultured brain microglial cells. *Acta Biomater,* 9: 8454-65.

Macia E, Ehrlich M, Massol R, Boucrot E, Brunner C & Kirchhausen T (2006). Dynasore, a cell-permeable inhibitor of dynamin. *Dev Cell,* 10: 839-50.

Mahmoudi M, Meng J, Xue X, Liang XJ, Rahman M, Pfeiffer C, Hartmann R, Gil PR, Pelaz B, Parak WJ, Del Pino P, Carregal-Romero S, Kanaras AG & Tamil Selvan S (2014). Interaction of stable colloidal nanoparticles with cellular membranes. *Biotechnol Adv,* 32: 679-92.

McNamara K & Tofail SAM (2017). Nanoparticles in biomedical applications. *Advances in Physics-X,* 2: 54-88.

Meindl C, Oehlinger K, Ober J, Roblegg E & Froehlich E (2017). Comparison of fluorescence-based methods to determine nanoparticle uptake by phagocytes and non-phagocytic cells in vitro. *Toxicology,* 378: 25-36.

Mohammed L, Gomaa HG, Ragab D & Zhu J (2017). Magnetic nanoparticles for environmental and biomedical applications: A review. *Particuology,* 30: 1-14.

Morris G, Berk M, Carvalho AF, Maes M, Walker AJ & Puri BK (2018). Why should neuroscientists worry about iron? The emerging role of ferroptosis in the pathophysiology of neuroprogressive diseases. *Behav Brain Res,* 341: 154-175.

Nazarenus M, Zhang Q, Soliman MG, Del Pino P, Pelaz B, Carregal-Romero S, Rejman J, Rothen-Rutishauser B, Clift MJ, Zellner R, Nienhaus GU, Delehanty JB, Medintz IL & Parak WJ (2014). In vitro interaction of colloidal nanoparticles with mammalian cells: What have we learned thus far? *Beilstein J Nanotechnol,* 5: 1477-90.

Nel AE, Madler L, Velegol D, Xia T, Hoek EM, Somasundaran P, Klaessig F, Castranova V & Thompson M (2009). Understanding biophysicochemical interactions at the nano-bio interface. *Nat Mater,* 8: 543-57.

Oh N & Park JH (2014). Endocytosis and exocytosis of nanoparticles in mammalian cells. *Int J Nanomedicine,* 9: 51-63.

Patel P, Kansara K, Senapati VA, Shanker R, Dhawan A & Kumar A (2016). Cell cycle dependent cellular uptake of zinc oxide nanoparticles in human epidermal cells. *Mutagenesis,* 31: 481-90.

Patil US, Adireddy S, Jaiswal A, Mandava S, Lee BR & Chrisey DB (2015). In vitro/in vivo toxicity evaluation and quantification of iron oxide nanoparticles. *Int J Mol Sci,* 16: 24417-50.

Pelaz B, Charron G, Pfeiffer C, Zhao Y, de la Fuente JM, Liang XJ, Parak WJ & Del Pino P (2013). Interfacing engineered nanoparticles with biological systems: anticipating adverse nano-bio interactions. *Small,* 9: 1573-84.

Petri-Fink A, Steitz B, Finka A, Salaklang J & Hofmann H (2008). Effect of cell media on polymer coated superparamagnetic iron oxide nanoparticles (SPIONs): colloidal stability, cytotoxicity, and cellular uptake studies. *Eur J Pharm Biopharm,* 68: 129-37.

Petters C, Bulcke F, Thiel K, Bickmeyer U & Dringen R (2014a). Uptake of fluorescent iron oxide nanoparticles by oligodendroglial OLN-93 cells. *Neurochem Res,* 39: 372-83.

Petters C & Dringen R (2014). Comparison of primary and secondary rat astrocyte cultures regarding glucose and glutathione metabolism and the accumulation of iron oxide nanoparticles. *Neurochem Res,* 39: 46-58.

Petters C & Dringen R (2015). Accumulation of iron oxide nanoparticles by cultured primary neurons. *Neurochem Int,* 81: 1-9.

Petters C, Irrsack E, Koch M & Dringen R (2014b). Uptake and metabolism of iron oxide nanoparticles in brain cells. *Neurochem Res,* 39: 1648-60.

Petters C, Thiel K & Dringen R (2016). Lysosomal iron liberation is responsible for the vulnerability of brain microglial cells to iron oxide nanoparticles: Comparison with neurons and astrocytes. *Nanotoxicology,* 10: 332-42.

Pilakka-Kanthikeel S, Atluri VS, Sagar V, Saxena SK & Nair M (2013). Targeted brain derived neurotropic factors (BDNF) delivery across the blood-brain barrier for neuro-protection using magnetic nano carriers: An in-vitro study. *PLoS One,* 8: e62241.

Rades S, Hodoroaba VD, Salge T, Wirth T, Lobera MP, Labrador RH, Natte K, Behnke T, Gross T & Unger WES (2014). High-resolution imaging with SEM/T-SEM, EDX and SAM as a combined methodical approach for morphological and elemental analyses of single engineered nanoparticles. *Rsc Advances,* 4: 49577-49587.

Rastedt W, Thiel K & Dringen R (2017). Uptake of fluorescent iron oxide nanoparticles in C6 glioma cells. *Biomed Phys Eng Expr,* 3: 035007.

Rejman J, Nazarenus M, de Aberasturi DJ, Said AH, Feliu N & Parak WJ (2016). Some thoughts about the intracellular location of nanoparticles and the resulting consequences. *J Colloid Interf Sci,* 482: 260-266.

Rivera-Gil P, Jimenez de Aberasturi D, Wulf V, Pelaz B, del Pino P, Zhao Y, de la Fuente JM, Ruiz de Larramendi I, Rojo T, Liang XJ & Parak WJ (2013). The challenge to relate the physicochemical properties of colloidal nanoparticles to their cytotoxicity. *Acc Chem Res,* 46: 743-9.

Rivet CJ, Yuan Y, Borca-Tasciuc DA & Gilbert RJ (2012). Altering iron oxide nanoparticle surface properties induce cortical neuron cytotoxicity. *Chem Res Toxicol,* 25: 153-61.

Roder A, Garcia-Gareta E, Theodoropoulos C, Ristovski N, Blackwood KA & Woodruff MA (2015). An assessment of cell culture plate surface chemistry for in vitro studies of tissue engineering scaffolds. *J Funct Biomater,* 6: 1054-63.

Rouault TA (2013). Iron metabolism in the CNS: Implications for neurodegenerative diseases. *Nature Reviews Neuroscience,* 14: 551-564.

Ruedas-Rama MJ, Walters JD, Orte A & Hall EA (2012). Fluorescent nanoparticles for intracellular sensing: A review. *Anal Chim Acta,* 751: 1-23.

Salzig D, Leber J, Merkewitz K, Lange MC, Koster N & Czermak P (2016). Attachment, growth, and detachment of human mesenchymal stem cells in a chemically defined medium. *Stem Cells Int,* 2016: 5246584.

Shang L, Nienhaus K & Nienhaus GU (2014). Engineered nanoparticles interacting with cells: Size matters. *J Nanobiotechnology,* 12: 1-11.

Shevtsov MA, Nikolaev BP, Ryzhov VA, Yakovleva LY, Marchenko YY, Parr MA, Rolich VI, Mikhrina AL, Dobrodumov AV, Pitkin E & Multhoff G (2015). Ionizing radiation improves glioma-specific targeting of superparamagnetic iron oxide nanoparticles conjugated with cmHsp70.1 monoclonal antibodies (SPION-cmHsp70.1). *Nanoscale,* 7: 20652-64.

Shevtsov MA, Yakovleva LY, Nikolaev BP, Marchenko YY, Dobrodumov AV, Onokhin KV, Onokhina YS, Selkov SA, Mikhrina AL, Guzhova IV, Martynova MG, Bystrova OA, Ischenko AM & Margulis BA (2014). Tumor targeting using magnetic nanoparticle Hsp70 conjugate in a model of C6 glioma. *Neuro Oncol,* 16: 38-49.

Shi D, Mi G, Bhattacharya S, Nayar S & Webster TJ (2016). Optimizing superparamagnetic iron oxide nanoparticles as drug carriers using an in vitro blood-brain barrier model. *Int J Nanomedicine,* 11: 5371-5379.

Shi D, Sadat ME, Dunn AW & Mast DB (2015). Photo-fluorescent and magnetic properties of iron oxide nanoparticles for biomedical applications. *Nanoscale,* 7: 8209-32.

Shi D, Sun L, Mi G, Sheikh L, Bhattacharya S, Nayar S & Webster TJ (2014). Controlling ferrofluid permeability across the blood-brain barrier model. *Nanotechnology,* 25: 075101.

Slater TJA, Janssen A, Camargo PHC, Burke MG, Zaluzec NJ & Haigh SJ (2016). STEM-EDX tomography of bimetallic nanoparticles: A methodological investigation. *Ultramicroscopy,* 162: 61-73.

Snijder B, Sacher R, Ramo P, Damm EM, Liberali P & Pelkmans L (2009). Population context determines cell-to-cell variability in endocytosis and virus infection. *Nature,* 461: 520-3.

Soenen SJ, Parak WJ, Rejman J & Manshian B (2015). (Intra)cellular stability of inorganic nanoparticles: effects on cytotoxicity, particle functionality, and biomedical applications. *Chem Rev,* 115: 2109-35.

Sperling RA & Parak WJ (2010). Surface modification, functionalization and bioconjugation of colloidal inorganic nanoparticles. *Philos Trans A Math Phys Eng Sci,* 368: 1333-83.

Stepto RFT (2009). Dispersity in polymer science. *Pure Appl Chem,* 81: 351-353.

Stetefeld J, McKenna SA & Patel TR (2016). Dynamic light scattering: a practical guide and applications in biomedical sciences. *Biophys Rev,* 8: 409-427.

Stone V, Johnston H & Schins RPF (2009). Development of in vitro systems for nanotoxicology: methodological considerations. *Critical Reviews in Toxicology,* 39: 613-626.

Sun Z, Yathindranath V, Worden M, Thliveris JA, Chu S, Parkinson FE, Hegmann T & Miller DW (2013). Characterization of cellular uptake and toxicity of aminosilane-coated iron oxide nanoparticles with different charges in central nervous system-relevant cell culture models. *Int J Nanomedicine,* 8: 961-70.

Sunol C, Babot Z, Fonfria E, Galofre M, Garcia D, Herrera N, Iraola S & Vendrell I (2008). Studies with neuronal cells: From basic studies of mechanisms of neurotoxicity to the prediction of chemical toxicity. *Toxicol In Vitro,* 22: 1350-5.

Tang J, Liu Z, Ji F, Li Y, Liu J, Song J, Li J & Zhou J (2015). The role of the cell cycle in the cellular uptake of folate-modified poly(L-amino acid) micelles in a cell population. *Nanoscale,* 7: 20397-404.

Tantra R, Schulze P & Quincey P (2010). Effect of nanoparticle concentration on zeta-potential measurement results and reproducibility. *Particuology,* 8: 279-285.

Tietze R, Zaloga J, Unterweger H, Lyer S, Friedrich RP, Janko C, Pottler M, Durr S & Alexiou C (2015). Magnetic nanoparticle-based drug delivery for cancer therapy. *Biochem Biophys Res Commun,* 468: 463-70.

Tulpule K, Hohnholt MC, Hirrlinger J & Dringen R (2014). Primary cultures of astrocytes and neurons as model systems to study the metabolism and metabolite export from brain cells. *In:* Hirrlinger J & Waagepetersen HS (eds.) Brain Energy Metabolism. New York: Springer.

Valdiglesias V, Fernandez-Bertolez N, Kilic G, Costa C, Costa S, Fraga S, Bessa MJ, Pasaro E, Teixeira JP & Laffon B (2016). Are iron oxide nanoparticles safe? Current knowledge and future perspectives. *J Trace Elem Med Biol,* 38: 53-63.

Valdiglesias V, Kilic G, Costa C, Fernandez-Bertolez N, Pasaro E, Teixeira JP & Laffon B (2015). Effects of iron oxide nanoparticles: cytotoxicity, genotoxicity, developmental toxicity, and neurotoxicity. *Environ Mol Mutagen,* 56: 125-48.

Villanueva A, Canete M, Roca AG, Calero M, Veintemillas-Verdaguer S, Serna CJ, Morales Mdel P & Miranda R (2009). The influence of surface functionalization on the enhanced internalization of magnetic nanoparticles in cancer cells. *Nanotechnology,* 20: 115103.

Wang R, Mikoryak C, Li S, Bushdiecker D, 2nd, Musselman IH, Pantano P & Draper RK (2011). Cytotoxicity screening of single-walled carbon nanotubes: detection and removal of cytotoxic contaminants from carboxylated carbon nanotubes. *Mol Pharm,* 8: 1351-61.

Wang X, Hu X, Li J, Russe AC, Kawazoe N, Yang Y & Chen G (2016). Influence of cell size on cellular uptake of gold nanoparticles. *Biomater Sci,* 4: 970-8.

Wang YX (2015). Current status of superparamagnetic iron oxide contrast agents for liver magnetic resonance imaging. *World J Gastroenterol,* 21: 13400-2.

Warheit DB (2008). How meaningful are the results of nanotoxicity studies in the absence of adequate material characterization? *Toxicoll Sci,* 101: 183-185.

Waters JC (2009). Accuracy and precision in quantitative fluorescence microscopy. *J Cell Biol,* 185: 1135-48.

Weinstein JS, Varallyay CG, Dosa E, Gahramanov S, Hamilton B, Rooney WD, Muldoon LL & Neuwelt EA (2010). Superparamagnetic iron oxide nanoparticles: Diagnostic magnetic resonance imaging and potential therapeutic applications in neurooncology and central nervous system inflammatory pathologies, a review. *J Cereb Blood Flow Metab,* 30: 15-35.

Westsson E & Koper GJM (2014). How to determine the core-shell nature in bimetallic catalyst particles? *Catalysts,* 4: 375-396.

Wilhelm C, Billotey C, Roger J, Pons JN, Bacri JC & Gazeau F (2003). Intracellular uptake of anionic superparamagnetic nanoparticles as a function of their surface coating. *Biomaterials,* 24: 1001-11.

Wilhelm C, Gazeau F, Roger J, Pons JN & Bacri JC (2002). Interaction of anionic superparamagnetic nanoparticles with cells: Kinetic analyses of membrane adsorption and subsequent internalization. *Langmuir,* 18: 8148-8155.

Wolfbeis OS (2015). An overview of nanoparticles commonly used in fluorescent bioimaging. *Chem Soc Rev,* 44: 4743-68.

Worle-Knirsch JM, Pulskamp K & Krug HF (2006). Oops they did it again! Carbon nanotubes hoax scientists in viability assays. *Nano Lett,* 6: 1261-1268.

Xu RL (2008). Progress in nanoparticles characterization: Sizing and zeta potential measurement. *Particuology,* 6: 112-115.

Yang H (2010). Nanoparticle-mediated brain-specific drug delivery, imaging, and diagnosis. *Pharm Res,* 27: 1759-71.

Yang WJ, Lee JH, Hong SC, Lee J, Lee J & Han DW (2013). Difference between toxicities of iron oxide magnetic nanoparticles with various surface-functional groups against human normal fibroblasts and fibrosarcoma cells. *Materials,* 6: 4689-4706.

Zhang L, Wang X, Zou J, Liu Y & Wang J (2015). DMSA-coated iron oxide nanoparticles greatly affect the expression of genes coding cysteine-rich proteins by their DMSA coating. *Chem Res Toxicol,* 28: 1961-74.

Zhang YQ, Dringen R, Petters C, Rastedt W, Koser J, Filser J & Stolte S (2016). Toxicity of dimercaptosuccinate-coated and un-functionalized magnetic iron oxide nanoparticles towards aquatic organisms. *Environ Sci-Nano,* 3: 754-767.

3 Summarizing discussion

3 Summarizing discussion

3.1 Synthesis and characterization of fluorescent iron oxide nanoparticles

The synthesized fluorescent IONPs were intensively characterized and the effect of the insertion of the fluorescence dyes into the coat of the IONPs on the accumulation of the particles by cells were investigated using C6 glioma cells as model system (chapter 2.1). Table 3.1 contains some key data obtained on the physicochemical properties of the synthesized IONPs.

Table 3.1 Characterization of fluorescent and non-fluorescent IONPs

Parameter investigated	**Method used**	**OG-DMSA-IONPs**	**TMR-DMSA-IONPS**	**BP-DMSA-IONPS**	**DMSA-IONPs**
size	TEM	5-10 nm	5-10 nm	5-10 nm	5-10 nm
size distribution	TEM/DLS	polydisperse	polydisperse	polydisperse	polydisperse
hydrodynamic diameter (nm, IB)	DLS	61 ± 7 (9)	69 ± 11 (6)	68 ± 4 (4)	60 ± 12 (8)
ζ-potential (mV, IB)	ELS	-21 ± 5 (5)	-25 ± 3 (4)	-24 ± 5 (4)	-16 ± 4 (6)
element content	EDX	iron, oxygen, sulfur	iron, oxygen, sulfur	iron, oxygen, sulfur	iron, oxygen, sulfur
λ_{max} (nm, Ex/Em)	Fluorescence spectroscopy	492/516	549/574	500/510	none
cellular iron content (nmol/ mg protein) (1h exposure of C6 cells to 1mM IONPs)					
4°C incubation in absence of serum (5)	iron assay	461 ± 92	512 ± 40	486 ± 92	417 ± 57
37°C incubation in absence of serum (5)	iron assay	255 ± 68	280 ± 61	266 ± 40	283 ± 32
Reduction in the presence of serum (5)	iron assay	80-90%	80-90%	80-90%	80-90%

Most of the data shown are derived from chapter 2.1. Additional data are included for the hydrodynamic diameter and the ζ-potential of the IONPs in IB. The numbers in brackets represent the number of independent measurements performed on individually prepared IONPs dispersions. C6 cells were exposed to IONPs for 1 h to 1 mM IONPs at 4°C and 37°C and the cellular iron contents were determined as described in chapter 2.1. The incubation in the presence of serum led to a reduction in the accumulation of IONPs measured by the cellular iron content to around 80-90% of the values obtained in the absence of serum as described in chapter 2.1.

For the synthesized fluorescent IONPs, the presence of the sulfur peak in the EDX measurements and the stability of the IONPs in the physiological medium IB confirmed the successful coating of the IONPs (Geppert *et al.*, 2011). Furthermore, for none of the

fluorescent IONPs differences in the physicochemical properties were observed in comparison to the non-fluorescent IONPs (Table 3.1). The successful insertion of the fluorescence dyes into the DMSA-coat of IONPs was confirmed by fluorescence spectroscopic analysis showing the expected excitation and emission spectra (chapter 2.1) and emission and excitation maxima (Table 3.1) recorded for the underivatized dyes (data not shown) and for the dyes coupled to DMSA, as exemplary shown for OG-IONPs and OG-DMSA (supplementary data Fig. 4.1B).

Accumulation studies in C6 glioma cells revealed that the accumulation of the DMSA-coated IONPs was not influenced by the insertion of the fluorescence dyes (Table 3.1), which is in line with comparative accumulation studies of BP-IONPs and DMSA-IONPs in oligodendroglial cells (Petters *et al.*, 2014a). Incubations of C6 glioma cells with the fluorescent IONPs at 37°C resulted in a dot like pattern for all three types of fluorescent dyes most likely due to the formation of IONPs-containing vesicles. Comparison of fluorescence intensity and stability of the three types of fluorescent IONPs demonstrated the desired higher fluorescence intensity and stability for the OG-IONPs and the TMR-IONPs, while analysis of cellular fluorescence after exposure of cell to BP-IONPs suffered from strong photo bleaching (chapter 2.1).

Charlotte Petters (Petters, 2015; personal communication) reported that after exposure of cells to BP-IONPs, BP-fluorescence was detected outside of the vesicular pattern for example in the nucleus and concluded that this may be caused by residual amounts of free fluorescent coating material or by the liberation of coating material from the IONPs over time within the cells. However, as the incubation of C6 cells with a large concentration of OG-functionalized DMSA (OG-DMSA) in the absence of any NPs did not cause any obvious cellular fluorescence (supplementary data Fig. 4.1), the dot-like fluorescence pattern observed after incubation of C6 cells with OG-IONPs is likely to result from IONP-containing vesicles, as also confirmed by the cytochemical stainings for iron that led to a similar pattern (chapter 2.2). As it is unlikely that DMSA is capable to cross the cell membrane (Aposhian and Aposhian, 1990, Zhang *et al.*, 2015a) also its fluorescent derivates may not enter the cells. Thus, the observation of BP-fluorescence (Petters, 2015) or OG-fluorescence (chapter 2.2) outside of the vesicle-structures (after extended incubation periods) is probably due to liberation of the fluorescent coat from the NPs within the cell.

Taken together, the insertion of the fluorescence dyes OG or TMR into the DMSA coat of IONPs did not alter the physiochemical properties and the colloidal stability of the IONPs nor the cellular accumulation in comparison to the non-fluorescent IONPs. However, OG- and TMR-IONPs possessed high fluorescent intensity and stability compared to BP-IONPs. Therefore, OG- and TMR-IONPs were considered as suitable tool to further investigate uptake and fate of DMSA-IONPs in neural cells by making use of the fluorescence properties suitable for the available fluorescence wide-field epifluorescence microscope.

3.2 Accumulation of fluorescent iron oxide nanoparticles in neural cells

C6 glioma cells were used in this study as model for glial cells, to characterized the newly synthesized fluorescent IONPs in comparison to the BP-IONPs and non-fluorescent IONPs and to establish conditions for an improved investigation of uptake mechanisms and intracellular trafficking.

C6 glioma cells efficiently accumulate both fluorescent and non-fluorescent DMSA-coated IONPs by a time-, concentration- and temperature dependent manner, whereby the accumulation rate slowed down with longer incubation times (chapter 2.1), which is in line with the accumulation of DMSA-coated IONPs in other brain cells (Hohnholt et *al.*, 2011, Geppert *et al.*, 2013, Petters and Dringen, 2015) or non-neural cells (Wilhelm *et al.*, 2002). This decline of accumulation with time may be caused by the saturation of available binding sites (Wilhelm *et al.*, 2002), the release of compounds from the cells, which can alter the size, charge and surface chemistry of the particles (Geppert, 2012, Petters and Dringen, 2015), and/or by the alteration of the composition of the membrane due to the binding and uptake of particles (Mahmoudi *et al.*, 2014).

As adhesion of NPs to the cell membrane is the first step during the uptake of NPs (Wilhelm *et al.*, 2002), the extracellular binding is a crucial factor in cellular uptake studies (Lesniak *et al.*, 2013, Mahmoudi *et al.*, 2014). Incubations at 4°C are often used to determine the amount of NPs extracellularly bound material (Geppert *et al.*, 2011, Smith *et al.*, 2012, Bulcke *et al.*, 2014). For C6 glioma cells a substantial adsorption of DMSA-coated IONPs at low temperature was observed which accounted for arround

70% of the iron amounts measured after incubation at 37°C (chapter 2 and Table 3.1). This is in line with data obtained in studies on astrocytes, oligodendrocytes and neurons, all reporting high specific cellular amounts of IONPs after 4°C incubations (Geppert *et al.*, 2011, Petters *et al.*, 2014a, Petters and Dringen, 2015).

In the presence of serum, the accumulation of DMSA-coated IONPs was drastically lowered down to 80-90% of the values observed in serum-free medium. This observation is consistent with the accumulation of DMSA-coated IONPs in the absence or presence of serum in other neural cells (Geppert *et al.*, 2013, Petters *et* al., 2014a, Petters and Dringen, 2015), and has also been reported for other cell types and other types of NPs (Wilhelm *et al.*, 2003, Petri-Fink *et al.*, 2008, Safi *et al.*, 2011, Lesniak *et al.*, 2013). The accumulation in the presence of serum was strongly reduced for non-fluorescent and fluorescent IONPs, suggesting that the insertion of the dye into the coat did not affect the formation and the composition of the protein corona around the IONPs. Fluorescence microscopic analysis of C6 cells exposed to fluorescent IONPs at 4°C showed hardly any fluorescence signals, whereas incubations at 37°C led to bright dotted-like fluorescence pattern. This observation strongly contrasted with the quantitative calculation of cellular iron and fluorescence content after IONP exposure. While quantification from lysates revealed a linear correlation between iron content and fluorescence content no matter if incubations were performed at 37°C or 4°C, calculation of fluorescence from microscopic pictures in correlation to cellular iron content from lysates showed a clear difference in the correlation of values obtained at 37°C and 4°C (chapter 2.1). Therefore, the calculation of cellular IONPs from fluorescence intensities in microscopic images can lead to an underestimation due to the non-visible amount of IONPs extracellularly bound. The likely explanation for this discrepancy is the limited resolution of the epifluorescence microscope used. Thus, the microscope is not able to detect the high proportion of extracellularly attached NPs, most likely to their more or less individual distribution along the cell membrane (Nazarenus *et al.*, 2014) extracellularly attached to the membrane, whereas the signal of agglomerated NPs within vesicles can be easily monitored.

The efficient acute accumulation of large amounts of iron after exposure of C6 cells to IONPs, especially in the serum-free media, did not hamper cellular viability as confirmed by determination of extracellular LDH activity and by propidium iodide staining (chapter

2.1) nor any formation of reactive oxygen species has been detected (data no shown). The lack of toxicity is in line with observations made for IONPs accumulation in astrocytes, neurons and oligodendrocytes (Geppert *et al.*, 2011, Petters *et al.*, 2014a, Petters and Dringen, 2015). Furthermore, loading the cells for 1 h with 1 mM OG-IONPs and monitoring the cellular localization of the IONPs for up to 3 days revealed no delayed cytotoxic potential as no change in cell morphology or influence on the cell proliferation in comparison to control cells was observed (supplementary data Fig. 4.2). These observations of a low toxic potential of OG-IONPs are in line with the findings for IONPs-treated astrocytes, which remained viable even 7 days after loading the cells with large amounts of DMSA-coated IONPs (Geppert *et al.*, 2012) or oligodendroglial cell line showing no loss in viability even after 3 days of culturing in continuous presence of DMSA-IONPs (Hohnholt *et al.*, 2011). In contrast, for IONPs-treated neurons a delayed toxicity was observed after 24 h (Sun *et al.*, 2013, Petters and Dringen, 2015). For microglia cells the potential toxicity is even higher, as already short time exposure with IONPs led to severe loss in viability of cultured microglia cells (Luther *et al.*, 2013, Petters *et al.*, 2016).

C6 glioma cells express astrocyte marker proteins and are often considered as model for astrocytes. The comparison of data obtained for the accumulation of IONPs in C6 cells with literature data obtained for primary astrocytes under comparable experimental conditions (Table 3.2) revealed similar results for both types of cultured cells.

For studies of IONP uptake in C6 glioma cells it was important to optimize the experimental protocol especially regarding the cell density and the unspecific binding of IONPs to the cell membrane as well as to the cell culture plates as discussed in chapter 3.3.

In contrast to confluent primary astrocytes, for C6 cells the cell cycle appears to play an important role, as a synchronization of the cell cycle by serum starvation or by application of pharmacological inhibitors led to different localization pattern of OG-IONPs within these cells (supplementary data Fig. 4.3). These observations are in line with previous studies on NPs accumulation in different cell types, showing dependency of NP uptake on the cell cycle (Kim *et al.*, 2011, Patel *et al.*, 2016). This is most likely due to changes in the membrane composition such as ratio of cholesterol and phospholipids, the expression of membrane proteins, surface antigens and receptors during the cell cycle

(Boucrot and Kirchhausen, 2007, Bregoli *et al.*, 2013, Mahmoudi *et al.*, 2014, Tang *et al.*, 2015).

Table 3.2 Accumulation of DMSA-coated IONPs in C6 glioma cells and primary astrocytes

parameters investigated	**C6 glioma cells**	**Ref.**	**primary astrocytes**	**Ref.**
iron content after incubation at 37°C (4 h, 1 mM)	1.317 ± 220 nmol iron/mg protein	[1]	1.375 ± 260 nmol iron /mg protein	[4]
iron content after incubation at 4°C (4 h, 1 mM)	825 ± 86 nmol iron/mg protein	[1]	726 ± 214 nmol iron/ mg protein	[4]
influence of serum	reduction of iron content of around 80-90%	[2,3]	reduction of iron content of around 80-90%	[4,5]
toxicity	no acute toxicity (6 h, 3 mM) no delayed toxicity (1 h, 1 mM loading, 3 days monitoring)	[1]	no acute toxicity (6 h, 3 mM) no delayed toxicity (4 h, 1 mM loading, 7 days monitoring)	[6,7]
intracellular location	perinuclear	[2,3]	perinuclear	[6,7,8]

1= unpublished data; 2= chapter 2.1; 3= chapter 2.2; 4= Hohnholt *et al.* 2011; 5= Geppert *et al*. 2013; 6= Geppert *et al*. 2012; 7= Geppert *et al.* 2011; 8= Petters *et al*. 2017

It is widely accepted that NPs are taken up by endocytotic pathways (Oh and Park, 2014, Zhang *et al.*, 2015b). Also DMSA-IONPs are internalized by endocytosis in brain cells (Geppert *et al.*, 2013, Luther *et al.*, 2013, Petters *et al.*, 2014b, Petters and Dringen, 2015). An obvious and commonly used attempt to study the role of endocytosis in the uptake of IONPs would be the inhibition of specific endocytotic pathways by pharmacological inhibitors (Iversen *et al.*, 2011) as critically discussed in chapter 2.3. Within the presented project, several attempts were made to block the uptake of fluorescent IONPs dispersed in serum-free medium into C6 glioma cells by the application of various different endocytosis inhibitors, both for continuous incubations for 1 h with 1 mM of OG-IONPs as well as for pulse-chase experiments. In none of these experiments the presence of endocytosis inhibitors caused any significant decrease of the cellular iron content or fluorescence signal monitored by fluorescence microscopy (data not shown). This confirms literature data on cultured astrocytes, oligodendrocytes and neurons showing that in the absence of serum endocytosis inhibitors did not impair IONP accumulation (Lamkowsky *et al.*, 2012, Geppert *et al.*, 2013, Petters *et al.*, 2014a, Petters, 2015, Petters and Dringen, 2015). Reasons for that could be: (1) The activation of other endocytotic pathways due to the inhibition of one specific pathway (dos Santos *et al.*, 2011). (2)

Uptake via an endocytosis pathway, that is not blocked by the used inhibitors, and (3) endocytosis-independent mechanisms leading to the uptake of IONPs in vesicular structures. The latter has for example been observed in red blood cells that do not possess an endocytosis machinery (Shang *et al.*, 2014) but are still capable to take up NPs of different size (Rothen-Rutishauser *et al.*, 2006, Wang *et al.*, 2012, Shang *et al.*, 2014). Furthermore, Lai *et al.* (2007) postulated a non-clathrin-, non-caveolae-dependent uptake mechanism that leads to non-degradative accumulation of fluorescent polystyrene NP in the perinuclear area of HeLa cell. Such a non-degradative pathway could also explain the inability of the pharmacological endocytosis inhibitors to lower IONPs accumulation in the absence of serum in C6 cells as well as in astrocytes (Lamkowsky *et al.*, 2012, Geppert *et al.*, 2013, Petters, 2015).

3.3 Nanoparticle pulse-chase experiments to improve temporal and spatial resolution of iron oxide nanoparticles uptake and trafficking

Nanoparticle pulse-chase experiments were performed in order to investigated the uptake and intracellular trafficking of IONPs with improved temporal and spatial resolution (chapter 2.3). The nanoparticle pulse-chase protocol established for the presented thesis on C6 glioma cells combined a 10 min pulse of fluorescent IONPs at 4°C to allow extracellular binding of NPs, with a subsequent chasing period to monitor internalization and subsequent intracellular trafficking (Fig. 3.1).

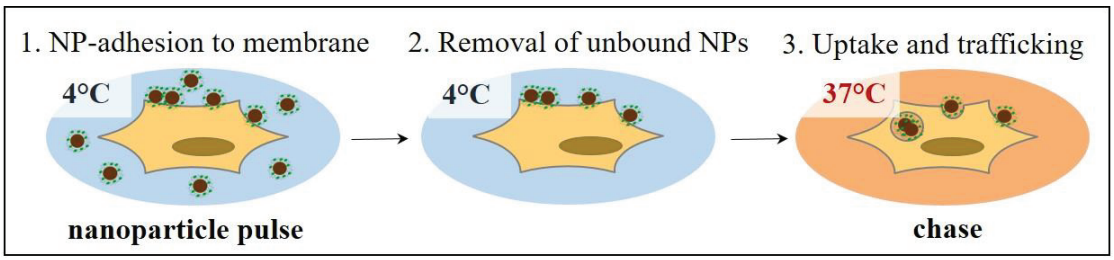

Fig. 3.1 Principle of nanoparticle pulse-chase experiments. For detailed description see chapter 2.2.

Although substantial amounts of cellular iron and fluorescence were quantified after the nanoparticle pulse (incubation at 4°C), the local density of the fluorescent IONPs extracellularly attached to the cell membrane was insufficient to detect adsorbed IONPs by fluorescence microscopy or cytochemical iron staining using the available wide-field

epifluorescence microscope. In contrast, already a few minutes after starting the chase monitoring at 37°C dot-like structures were detected, most likely representing vesicular structures that contain increased density of fluorescent IONPs. The rapid appearance of these structures is consistent with the reported rapid endocytosis and vesicle formation in the minute range (Durrbach *et al.*, 1996). Longer chase periods revealed an increase in fluorescence and iron signals and a final perinuclear localization in C6 glioma cells consistent with studies on other neural cells such as astrocytes (Geppert *et al.*, 2011) but also non-neural cells (Jarockyte *et al.*, 2016). However, the nanoparticle pulse-chase protocol revealed a loss in the fluorescence pattern already after 90 min of chasing period, whereas the perinuclear cyctochemical iron staining was preserved.

The conditions established for nanoparticle pulse-chase experiment on C6 cells were also suitable for studies on viable primary and secondary astrocyte cultures (supplementary data Fig. 4.4) revealing after exposure to OG-IONPs similar staining patterns for fluorescence and iron as found for C6 glioma cells. In contrast, for viable cerebellar granule neuron (supplementary data Fig. 4.5) no clear distinguished fluorescence pattern nor cyctochemical iron staining of the IONPs were determined and no clear perinuclear localization of IONPs was observed due to the small somata of the neurons (supplementary data Fig. 4.5) (Petters *et al.*, 2016) which makes such a localization difficult to record. For microglia, the nanoparticle pulse chase setting could not be applied as severe toxicity was observed during the chase period (supplementary data Fig. 4.6).

Double nanoparticle pulse-chase experiments in C6 glioma cells allowed to study the sequential uptake of IONPs labeled with OG and TMR (chapter 2.2) showing a rapid colocalisation of the fluorescent vesicles in the perinuclear area. For further studies confocal Laser Scanning Microscope (LSM) with a better resolution would be required to get better information about the intracellular localization of the IONPs-containing vesicles. Nevertheless, the optimized parameters for single and double nanoparticle pulse-chase could be a helpful paradigms to study the intracellular trafficking of IONPs in cultured cells with the simple wide-field epifluorescence microscope available.

3.4 Involvement of cytoskeleton in uptake and trafficking of iron oxide nanoparticles

To test for the role of actin filaments and microtubules in the uptake of IONPs in C6 glioma cells, these structure were disrupted using pharmacological inhibitors prior to the nanoparticle pulse chase experiments (chapter 2.2). The disruption of the actin filaments in C6 glioma cells drastically lowered, but not totally diminished, the internalization of IONPs consistent with studies on several types of NPs in different cell lines (dos Santos *et al.*, 2011, Iversen *et al.*, 2012, Nowak *et al.*, 2014, Prietl *et al.*, 2014). In C6 glioma cells the internalization of IONPs seems to highly depend on actin which would be in line with several studies suggesting an important role of actin in the engulfment of the membrane segment and the formation of vesicle (Durrbach *et al.*, 1996, Kumari *et al.*, 2010, Mooren *et al.*, 2012). However, the results obtained have to be carefully interpreted, due to the alteration in the shape of the C6 glioma cells after treatment with cytochalasin D, an inhibitor of actin polymerization (Mortensen and Larsson, 2003). Even though the treatment of C6 glioma cells with cytochalasin D did not cause any loss in membrane integrity during the complete nanoparticle pulse-chase experiment and the amount of IONPs extracellularly bound to the cell membrane was not affected, the effect of cytochalasin D treatment on the cell shape of C6 glioma cells under the chosen condition may also have caused unintended side effects on the cellular uptake of IONPs. Therefore, a more precise inhibition of the actin polymerization without effecting cell shape and microtubules (Durrbach *et al.*, 1996), could help to get an even better understanding of the role of actin.

While the release of vesicles from the plasma membrane into the cytosol is supported by actin, a switch from an actin-based movement to a tubulin-based movement occurs to transport the vesicle down the endocytotic pathways to their final destination (Granger *et al.*, 2014). In C6 glioma cells the disruption of the microtubules in C6 glioma cells strongly disturbed this transport as the IONPs-containing vesicle seemed to be trapped at the cell membrane. This is in line with observations made in mouse melanoma cells reporting that the disruption of the microtubules disturbed the transport of 50-100 nm microspheres from early to late endosome (Rejman *et al.*, 2004).

In conclusion, the investigation of the impact of the cytoskeleton on the OG-IONPs uptake by C6 glioma cells revealed that actin plays an essential role in the vesicle

formation and vesicle release from the membrane into the cytoplasm, whereas the microtubules are important for the subsequent intracellular transport of the vesicles to the perinuclear area (Fig. 3.2).

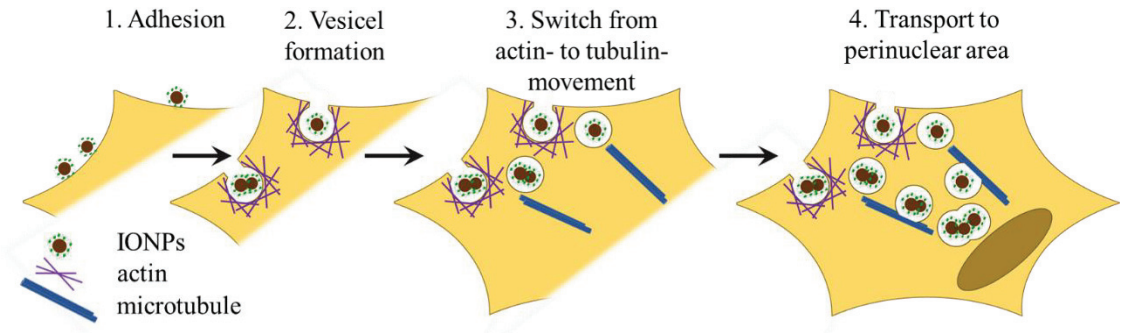

Fig. 3.2 Schematic representation of the role of actin and microtuble filaments in the uptake and intracellular trafficking of IONPs in C6 glioma cells.

3.5 Degradation of internalized iron oxide nanoparticles

The insertion of fluorescence dyes into the coat of NPs is a commonly used tool to study the uptake and intracellular fate of NPs (Bertorelle *et al.*, 2006, Kaewsaneha *et al.*, 2014, Kaewsaneha *et al.*, 2015). Several studies already stated the degradation of the coating material *in vitro* and *in vivo* (Zhang *et al.*, 2015a, Feliu *et al.*, 2016, Zhang and Liu, 2017).

During the endocytosis the particles are passed to more and more acidic vesicles following a degradative pathway (Nazarenus *et al.*, 2014, Soenen *et al.*, 2015). Several studies reported a degradation of the surface coating during trafficking of NPs in the endocytotic pathway (See *et al.*, 2009, Lunov *et al.*, 2010, Feliu *et al.*, 2016). However, also the iron core of IONPs is disintegrated over time *in vitro* and *in vivo* (Briley-Saebo *et al.*, 2006, Mazuel *et al.*, 2016) and it was observed that IONPs can be solubilized in the absence of any enzymes at a pH similar to that found in endosomes and lysosomes (Skotland *et al.*, 2002, Mazuel *et al.*, 2016, Volatron *et al.*, 2017).

Nanoparticle pulse-chase experiment revealed a separation of the fluorescence DMSA-coat and the iron-core after chasing periods longer than 90 min in C6 cells (chapter 2.3.) as well as in astrocytes cultures (supplementary data 4.4). In OG-IONPs, the DMSA forms a cage-like structure around the iron oxide core cross-linked by disulfide bridges (Fauconnier *et al.*, 1997, Valois *et al.*, 2010) containing a low number of fluorescent

molecules formed by thioether bonds (Petters *et al.*, 2014a, chapter 2.1) between the free thiol groups of the DMSA cage and the functional iodoacetamide group of the dyes. The covalent thioether link between the coating material and the fluorescent dye is relative stable, but the disulfide bridges of the DMSA cage can be easily reduced which will cause disintegration of the coat. Processes that could be involved in this degradation are acidic environments (Soenen *et al.*, 2015), enzymatic activities (Chen *et al.*, 2008, Zhang *et al.*, 2016, Zhang and Liu, 2017) and the exchange with thiol-containing endogenous biomolecules (Hong *et al.*, 2006, See *et al.*, 2009). Concerning the mechanismus involved in the separation of core and coat of internalized OG-IONPs in C6 cells preliminary experiments were performed to neutralize acidic compartments, to deplete the cellular glutathione content and to inhibit cellular transport of IONPs-containing vesicles to the lysosome (Table 3.2).

Table 3.3 Experiments to prevent degradation of the coating material

Target	**Procedure**	**Result**
Lysosome	Neutralization of lysosome using Bafilomycin A1, an inhibitor of the H^+-ATPase (Teplova *et al.*, 2007), during the pulse-chase experiment	✓Neutralization of lysosome confirmed by lysotracker staining (Petters *et al.*, 2016) ✓no toxicity × no prevention of degradation
Glutathione content	Depletion of cells on glutathione using iodoacetamide (Schmidt and Dringen, 2009) prior to the pulse-chase experiment	✓GSH depletion confirmed by GSH quantification (Tulpule *et al.*, 2014) × toxicity after 120 min chase × no prevention of degradation
Transport of vesicles to more acidic compartments	Disruption of the microtubules using colchicine prior and during the pulse-chase experiment as described in chapter 2.2	✓Microtubules disruption confirmed by immunocytochemistry ✓Inhibition of transport ✓no toxicity × no prevention of degradation

To target the lysosomes, nanoparticle pulse-chase experiments were performed as described in chapter 2.1 in the presence of 100 nM Bafilomycin A1 using TMR-IONPs. To ensure that the neutralization of the lysosome was successful, cells were incubated with 100 nM of the lysotracker DND-99 (Life technologies, Darmstadt, Germany) for 15 min, washed twice and were directly analyzed under the fluorescence microscope. To investigate the role of glutathione in the disintegration of the OG-IONPs, C6 glioma cells were incubated with 0.1 mM iodoacetamide (IAA) in IB for 30 min at 37°C to deplete the cells on glutathione, which was confirmed by GSH quantification as recently described (Tulpule *et al.*, 2014). Subsequently nanoparticle pulse-chase experiments were performed as described in chapter 2.2. The inhibition of the transport of vesicles to more acidic compartments was performed as described in chapter 2.2.

However, none of these attempts prevented the loss in cellular fluorescence signal of C6 cells that were exposed to OG-IONPs. As also the inhibition of the transport of the OG-

IONP-containing vesicles to the perinuclear area by microtubules disruption (chapter 2.2) did not prevent the degradation of the fluorescent-coat nor the separation of core and coat, quick processes seem to play a role in this separation of OG-DMSA and iron core.

In contrast to the fluorescent signals, the iron signal in C6 glioma cells after OG-IONPs exposure was rather stable throughout the complete chase period (chapter 2.2). and even three days after uptake of large amounts of IONPs in the C6 cells, the cell viability was not impaired, the cellular iron contents remained stable and clear perinuclear pattern of iron could be detected (supplementary data Fig. 4.2). Interestingly, the IONPs-containing vesicles in C6 cells were distributed during cell division to the daughter cells and the high content of IONPs did not impair the cell division, which is in line for IONPs accumulation in proliferative and endocytotic active primary-derived rat cortical astrocytes (Tickle *et al.*, 2016). As observed for cultured astrocytes (Geppert *et al.*, 2012), C6 glioma cells are highly capable to deal with an excess amount of IONPs supporting the view of a slow degradation of the iron oxide core of internalized IONPs.

An approach to study the intracellular localization of IONPs is the immunocytochemical costaining for fluorescent IONPs and intracellular marker proteins for different stages of the intracellular pathway. For example, staining for Rab7 as late endosome-/lysosome-associated small GTPase, for the lysosomal associated membrane protein 1 (LAMP1), for calnexin as integral protein of the endoplasmic reticulum or for the early endosome antigen 1 (EEA1) were done in other studies (Iversen *et al.*, 2012, Schweiger *et al.*, 2012, Granger *et al.*, 2014, Kasten *et al.*, 2014). For all these markers successful immunocytochemical stainings were observed in untreated C6 cells (data not shown), but the respective costainings failed for cells that had been exposed to OG-IONPs. The permeabilization of the cell membrane, that is necessary to allow the access of the antibodies to the desired intracellular antigen, caused rapid and almost complete loss of the fluorescence of the internalized fluorescent IONPs after paraformaldehyde fixation (Fig. 3.3A,B). This loss in OG-fluorescence was observed for all time points of the chase period, for all types of fixation and permeabilization applied as well as for conditions that caused inhibition of intracellular vesicle transport by microtubules disruption (data not shown). Several different combination of fixation and permeabilization were tested (supplementary data Table 4.1), but failed to prevent the loss in OG-fluorescence pattern. As example the fluorescence and iron staining of OG-IONPs-treated C6 cells, the most

frequently used combination of paraformaldehyde fixation and Triton X-100 permeabilization (Ohsaki *et al.*, 2005) is shown (Fig. 3.3A,B). In contrast the cyctochemical iron staining was not affected by the permeabilization procedure (Fig. 3.3E,F). Similar problems with the maintenance of the fluorescence pattern were also observed in primary rich-astrocytes cultures that had been exposed to OG-IONPs or TMR-IONPs (data not shown).

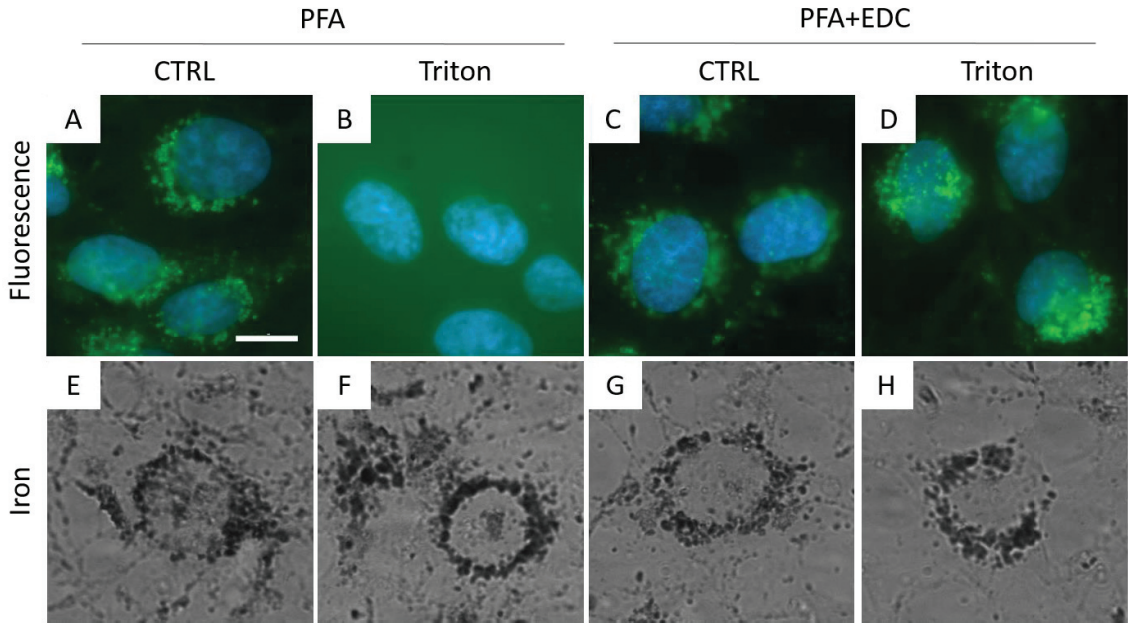

Fig. 3.3 Effects of permeablisation and fixation procedures on the fluorescence and iron pattern of accumulated OG-IONPs in C6 glioma cells. C6 glioma cells were incubated with 1 mM OG-IONPs for 1 h at 37°C. Cells were washed twice and fixation with 3.5% (w/v) paraformaldehyde (PFA) for 15 min at RT was performed (A, E). Subsequent to the PFA fixation, cells were washed twice with 0.9% NaCl (w/v) solution and additionally fixated with 2% (w/v) 1-ethyl-3-(3-dimethylaminopropyl)carbodiimide (EDC) in 0.9% (w/v) NaCl for 30 min at RT (C-G). The cells were subsequently exposed in the absence (A,E,C,G) or presence of 0.1% Triton X-100 for 5 min at RT (B,F,D,H). Fluorescence microscopy (A-D) and cytochemical iron stainings (E-H) were performed as previously described (Geppert *et al.*, 2009, chapter 2.2). The cell nuclei were stained with DAPI (blue). The size bar in panel A represents 10 µm and applies for all panels.

The loss of the fluorescence pattern from permeabilized C6 cells that had been exposed to OG-IONPs could be partially prevented by applying the cross-linking agent 1-ethyl-3-(3-dimethylaminopropyl)carbodiimide hydrochlorid (EDC) after the PFA fixation (Fig. 3.3C,D,G,H). In contrast to PFA, EDC crosslinks carboxyl groups to primary amine groups (Tymianski *et al.*, 1997), and thus the free carboxyl groups of the DMSA-coat are

likely to be coupled to proteins surrounding the particle. However, a huge drawback of this method was that the fixation with EDC led to an increased unspecific binding of the antibodies for vesicle identification despite of the use of additional blocking and washing steps (data not shown).

Taken together, these results suggest that as soon as the OG-IONPs are internalized into the cells, a rapid separation of the OG-DMSA coat and the iron core takes place which prevents immunocytochemical colocalization studies of the intact fluorescent IONPs and cellular structures.

For DMSA-coated IONPs the separation of core and coat seems to be an early event, whereas the degradation of the core is rather slow, consistent with data for non-phagocytic cells (Hohnholt *et al.*, 2011, Geppert *et al.*, 2012, Mazuel *et al.*, 2016, Petters *et al.*, 2016) and the prolonged retention of IONPs in the human body for time periods up to 11 months (Storey *et al.*, 2012, Pham *et al.*, 2018). Skotland *et al.* (2002) observed in cell-free experiments that the solubilisation of IONPs is accelerated in the present of citrate and that a low pH of 4.5 solubilized the particle in 4-7 days, while an increase to a pH of 5.5 drastically reduced and the substitution citrate with acetate inhibited the disintegration of the IONPs (Skotland *et al.*, 2002). This indicates that the composition of the vesicular environment is a crucial factor for the disintegration of the IONPs in cells. Fig. 3.4 shows a predicted mechanism of the disassembly of fluorescent DMSA-IONPs after the uptake into C6 glioma cells.

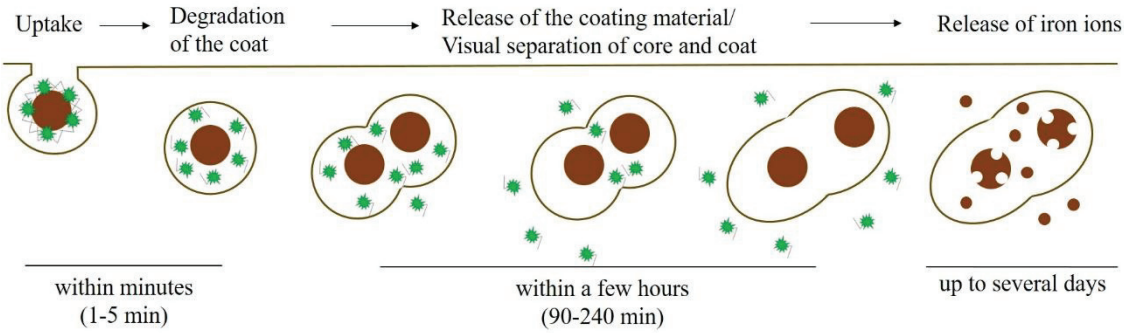

Fig. 3.4 Model of the disintegration of fluorescent DMSA-IONPs after uptake into C6 glioma cells and astrocytes. Intact fluorescent IONPs are taken up into vesicles. In an early event (1-5 min) the coat is released from the core in the vesicles and slowy permeates into the cytosol by unknow processes.The disintegration of the iorn oxide core is a slow process that takes days up to weeks (Skotland *et al.*, 2002, Geppert *et al.*, 2012, Mazuel *et al.*, 2016).

The mechanism of disintegration of the coat and the fate of the DMSA-coat after separation from the core remains to be examined. An overall cellular distribution of OG fluorescence signal was detected after more than 120 min of chase period (chapter 2.2.) and 6 h after loading the cells for proliferations studies (supplementary data Fig.4.2) suggesting a release of the disassembled coating material from the vesicles into the cytosol seems to be most likely. In line with this, Zhang *et al.* (2015) observed that the accumulation of DMSA-coated IONPs in various cell types led in the transcriptional changes of many cysteine-rich proteins coding genes presumably due to the interaction of DMSA with cytosolic cysteine-rich proteins. They predicted that the DMSA is released into the cytosol after the lysosomal thiol reductase (GLIT) disintegrated the coat of DMSA-coated IONPs that reached the lysosomes (Zhang *et al.*, 2015a). Interestingly, during the proliferation study in C6 glioma cells (supplementary data Fig. 4.2) the OG signal was still detectable within the cells after 24 h and 72 h leading to the suggestion that the components of disassembled coat may remain within in the cells and will be distributed during cell proliferation to the daughter cells.

3.6 Future perspective

The fluorescent OG- and TMR-IONPs synthesized in this thesis have been proven to be a suitable tool for the visualization of IONPs in neural cells. However, due to the disintegration of the coat, just in a limited time frame. To overcome this limitation a different approach of coating could be performed to increase the stability of the fluorescence-coat of the IONPs. A commonly used approach for fluorescent IONPs is the formation of a covalently attached and stable silica shell around IONPs, which could also be further functionalized which fluorophores (Chekina *et al.*, 2011, Kacenka *et* al., 2015). However, the non-degradability of the silica also limits the use of such particle for *in vivo* biomedical applications (Chekina *et al.*, 2011). Furthermore, the change of the surface material could also influence the uptake mechanism and the intracellular fate of the IONPs in comparison to the DMSA-coated IONPs. This possible disadvantage could be addressed by coincubation studies of fluorescent DMSA-coated IONPs and fluorescent silica-coated IONPs with fluorophores of different spectra to investigate whether the two types of fluorescent particles follow the same route of uptake and internalization.

Additionally, this attempt could also give more information about the time scale of coat and core separation in the case of DMSA-coated IONPs.

As cellular uptake mainly depends on the size of the particles and the surface chemistry (and less on the core), DMSA-coated silver NPs (AgNP) could be synthesized, as here the coat would be covalently attached to the surface through Ag-S bonds (Battocchio *et al.*, 2012). If these DMSA-coated AgNPs are taken up by the cells by identical pathways as the DMSA-coated IONPs which could be verified by colocalization studies as described above and if the fluorescence coating of the AgNPs remains with the Ag core, these particles could be used to continue the study of uptake mechanisms and the intracellular fate of DMSA-coated NPs in neural cells.

The nanoparticle pulse-chase protocols have been proven to be useful approaches to investigate the uptake and intracellular fate of IONPs in C6 glioma cells and astrocytes with an improved time and spatial resolution (chapter 2.2.). With help of this methods the importance of the cytoskeleton for IONP uptake and trafficking was demonstrated by the dependence of NP internalization on actin polymerization and the need of an intact microtubule network for the intracellular trafficking of the internalized NPs. However, as these studies were performed so far only on C6 glioma cells, a verification of these results for cultured astrocytes and other types of brain cells is required. Additionally, the establishment of the nanoparticle pulse-chase protocols for cultured microglia would be of great value, as microglia severely differ from other brain cells regarding uptake and toxicity of IONPs (Fleige *et al.*, 2001, Petters *et al.*, 2016). The nanoparticle pulse-chase experiments applied for this thesis were limited to a chasing period of maximal 8 h (data not shown). As the release of iron ions from the iron core is slow (Geppert *et al.*, 2012, Mazuel *et al.*, 2016), prolonged time frames should be applied to study the long term fate of IONPs in neural cells, also addressing the potential degradation of the core, the production of reactive oxygen species and the upregulation of the iron storage protein ferritin as reported previously (Hohnholt *et al.*, 2011, Geppert *et al.*, 2012).

The differences in uptake of IONPs in the absence or presence of serum should be investigated further. A possible approach would be a sequential pulse at 4°C with IONPs and protein-coated IONPs containing different fluorescence dyes in the DMSA-coat, followed by the simultaneous start of chase at 37°C in presence or absence of certain

inhibitors of the endocytotic pathways monitoring differences in internalization and localization of the IONPs by fluorescence microscopy.

To follow up the nanoparticle pulse-chase experiments, two questions should to be addressed: (1) the fate of the core and (2) the fate of the coating material. As long as core and coat of the IONPs are present in the same vesicles, the fluorescence signal of the coat could be used to investigate the uptake and intracellular fate of the core. This opens up a list of various possible colocalisation studies. For example, a common approach to elucidate the endocytotic pathways of NPs is the coincubation with fluorescent labeled proteins which are known as cargos of certain endocytotic pathways for example transferrin, cholera toxin B or Simian virus 40, but also here the specificity of the marker proteins has to be carefully analyzed and interpreted (Iversen *et al.*, 2011).

As immunocytochemical approaches are not suitable for colocalisation studies with OG-IONPs (chapter 3.5.), an alternative could by the transfection of cells with fluorescent labeled marker proteins of the endocytotic pathways such as the late endosome-/lysosome-associated small GTPase Rab9 or Rab7 to determine the colocalization of the OG-IONPs in certain endosomal vesicles (Sandin *et al.*, 2012).

Furthermore, the magnetic properties of the IONPs and the nanoparticle pulse-chase methodology allows subcellular compartmental isolation of endosomes and lysosomes, by a combination of homogenization, magnetic separation and ultracentrifugation (Thimiri Govinda Raj and Khan, 2016). Thereby, not only the localization of the iron-core IONPs could be determined but also the release of the coat from the IONP-containing vesicle could be investigated by isolation of the endosomal structures at different chasing time points and determination of the fluorescence of certain compartments. The distribution mechanism of the fluorescence material within the cell has not been addressed within this thesis. To gain more information about the fate of the DMSA-coat, IONPs-filled vesicles could be extracted as done for endosomes from human mesenchymal stem cells (Mazuel *et al.*, 2016) and the degradation of the iron core in these single endosomes could be monitored by measuring the magnetism over time (Mazuel *et al.*, 2016). Additionally, the leaking of the fluorescent coat of the IONPs from vesicles into the environment could be investigated to gain more information about the time scale and possible mechanisms.

During endocytosis the cargo is transported to more and more acidic environments. Using pH-dependent fluorescent dyes in the coat of the particles could provide information about the environmental pH and thereby the localization of the particle (Benjaminsen *et al.*, 2011, Nazarenus *et al.*, 2014). In this thesis two different types of fluorescent dyes were used, the pH-sensitive OG and the pH-insensitive TMR (supplier information). Simple fluorescence microscopy did not reveal striking difference in the signal intensity over time using the different fluorescence IONPs separately (data not shown). However, the usage of double labeled IONPs in combination with careful analyses of the fluorescence signals by establishing an *in vitro* calibration curve and by detailed image analysis could reveal additional information about the pH of the environment (Benjaminsen *et al.*, 2011) the particles are captured at a certain chasing periods. To investigate the fate of the DMSA-coat over time, the incorporation of pH-sensitive dyes such as SNARF1, which emits red light in alkaline and green light in acidic environments, into the DMSA-coat could also be helpful to study the release of the dye into the cytosol (Semmling *et al.*, 2008, Nazarenus *et al.*, 2014).

Very recently a Laser Scanning Microscope (LSM) with fluorescence lifetime imaging microscopy (FLIM) was purchased and is now available in our faculty. With this new equipment it is possible to perform life cell and continuous time-lapse imaging. This will increase the amount of information that can be gained and will improve the sensitivity of investigating the uptake and intracellular fate of fluorescent IONPs. Life cell studies would also avoid potential artifacts caused by fixation of cells (Schnell *et al.*, 2012). Additional the suggested colocalisation studies could be analyzed with a better resolution and robust quantification could be performed.

The adhesion of NPs to the membrane plays an important role in the cellular uptake (Lesniak *et al.*, 2013, Mahmoudi *et al.*, 2014) as 50-70% of the accumulated IONPs are absorbed to the cell membrane (chapter 2.1). Thus, the mechanism involved in the absorption should be investigated. The quantification of membrane-bound IONPs under certain conditions could be achieved by purification of the plasma membrane using the magnetic properties of the IONPs (Thimiri Govinda Raj *et al.*, 2011). The isolation of the plasma membrane at certain time points of the nanoparticle pulse-chase protocol could also be used to gain information about the time frame of uptake of the adsorbed IONPs.

The effects of IONP attachment on the morphology of the cells, could also be investigated using scanning electron microscopy (Rivet *et al.*, 2012).

Furthermore, the force of interaction between the cell surface and the IONPs could be studied by using atomic force microscopy (AFM). In a recent master thesis (Klebert, 2017), the OG-IONPs were successfully functionalized to AFM cantilevers via the coupling of free thiol-groups in the DMSA-coat to a maleimid-polyethylenglycol-N-hydoxysuccinimid linker according to a protocol developed by the Hybrid Material Interface Group of the University of Bremen. This approach could now be used to analyze the interaction of the IONPs with the cell membrane in absence or presence of serum (Pyrgiotakis *et al.*, 2014) as well as to characterize the endocytotic processes (Shan *et al.*, 2011, Ding *et al.*, 2015) and the degradation of the coating material.

3.7 References

Aposhian HV & Aposhian MM (1990). meso-2,3-Dimercaptosuccinic acid: Chemical, pharmacological and toxicological properties of an orally effective metal chelating agent. *Annu Rev Pharmacol Toxicol,* 30: 279-306.

Battocchio C, Meneghini C, Fratoddi I, Venditti I, Russo MV, Aquilanti G, Maurizio C, Bondino F, Matassa R, Rossi M, Mobilio S & Polzonetti G (2012). Silver nanoparticles stabilized with thiols: A close look at the local chemistry and chemical structure. *J Phys Chem C,* 116: 19571-19578.

Benjaminsen RV, Sun H, Henriksen JR, Christensen NM, Almdal K & Andresen TL (2011). Evaluating nanoparticle sensor design for intracellular pH measurements. *ACS Nano,* 5: 5864-73.

Bertorelle F, Wilhelm C, Roger J, Gazeau F, Menager C & Cabuil V (2006). Fluorescence-modified superparamagnetic nanoparticles: Intracellular uptake and use in cellular imaging. *Langmuir,* 22: 5385-91.

Boucrot E & Kirchhausen T (2007). Endosomal recycling controls plasma membrane area during mitosis. *Proc Natl Acad Sci,* 104: 7939-44.

Bregoli L, Benetti F, Venturini M & Sabbioni E (2013). ECSIN's methodological approach for hazard evaluation of engineered nanomaterials. *J Phys Conf Ser,* 429: 012017.

Briley-Saebo KC, Johansson LO, Hustvedt SO, Haldorsen AG, Bjornerud A, Fayad ZA & Ahlstrom HK (2006). Clearance of iron oxide particles in rat liver: effect of hydrated particle size and coating material on liver metabolism. *Invest Radiol,* 41: 560-71.

Bulcke F, Thiel K & Dringen R (2014). Uptake and toxicity of copper oxide nanoparticles in cultured primary brain astrocytes. *Nanotoxicology,* 8: 775-85.

Chekina N, Horak D, Jendelova P, Trchova M, Benes MJ, Hruby M, Herynek V, Turnovcova K & Sykova E (2011). Fluorescent magnetic nanoparticles for biomedical applications. *J Mater Chem,* 21: 7630-7639.

Chen ZP, Zhang Y, Xu K, Xu RZ, Liu JW & Gu N (2008). Stability of hydrophilic magnetic nanoparticles under biologically relevant conditions. *J Nanosci Nanotechnol,* 8: 6260-5.

Ding B, Tian Y, Pan Y, Shan Y, Cai M, Xu H, Sun Y & Wang H (2015). Recording the dynamic endocytosis of single gold nanoparticles by AFM-based force tracing. *Nanoscale,* 7: 7545-9.

dos Santos T, Varela J, Lynch I, Salvati A & Dawson KA (2011). Effects of transport inhibitors on the cellular uptake of carboxylated polystyrene nanoparticles in different cell lines. *PLoS One,* 6: e24438.

Durrbach A, Louvard D & Coudrier E (1996). Actin filaments facilitate two steps of endocytosis. *J Cell Sci,* 109 (Pt 2): 457-65.

Fauconnier N, Pons JN, Roger J & Bee A (1997). Thiolation of maghemite nanoparticles by dimercaptosuccinic acid. *J Colloid Interface Sci,* 194: 427-33.

Feliu N, Docter D, Heine M, Del Pino P, Ashraf S, Kolosnjaj-Tabi J, Macchiarini P, Nielsen P, Alloyeau D, Gazeau F, Stauber RH & Parak WJ (2016). In vivo degeneration and the fate of inorganic nanoparticles. *Chem Soc Rev,* 45: 2440-57.

Fleige G, Nolte C, Synowitz M, Seeberger F, Kettenmann H & Zimmer C (2001). Magnetic labeling of activated microglia in experimental gliomas. *Neoplasia,* 3: 489-99.

Geppert M, Hohnholt M, Gaetjen L, Grunwald I, Baumer M & Dringen R (2009). Accumulation of iron oxide nanoparticles by cultured brain astrocytes. *J Biomed Nanotechnol,* 5: 285-93.

Geppert M, Hohnholt MC, Nurnberger S & Dringen R (2012). Ferritin up-regulation and transient ROS production in cultured brain astrocytes after loading with iron oxide nanoparticles. *Acta Biomater,* 8: 3832-9.

Geppert M, Hohnholt MC, Thiel K, Nurnberger S, Grunwald I, Rezwan K & Dringen R (2011). Uptake of dimercaptosuccinate-coated magnetic iron oxide nanoparticles by cultured brain astrocytes. *Nanotechnology,* 22: 145101.

Geppert M, Petters C, Thiel K & Dringen R (2013). The presence of serum alters the properties of iron oxide nanoparticles and lowers their accumulation by cultured brain astrocytes. *J Nanopart Res,* 15: 1349.

Granger E, McNee G, Allan V & Woodman P (2014). The role of the cytoskeleton and molecular motors in endosomal dynamics. *Semin Cell Dev Biol,* 31: 20-9.

Hohnholt MC, Geppert M & Dringen R (2011). Treatment with iron oxide nanoparticles induces ferritin synthesis but not oxidative stress in oligodendroglial cells. *Acta Biomater,* 7: 3946-54.

Hong R, Han G, Fernandez JM, Kim BJ, Forbes NS & Rotello VM (2006). Glutathione-mediated delivery and release using monolayer protected nanoparticle carriers. *J Am Chem Soc,* 128: 1078-9.

Iversen TG, Frerker N & Sandvig K (2012). Uptake of ricinB-quantum dot nanoparticles by a macropinocytosis-like mechanism. *J Nanobiotechnology,* 10: 33.

Iversen TG, Skotland T & Sandvig K (2011). Endocytosis and intracellular transport of nanoparticles: Present knowledge and need for future studies. *Nano Today,* 6: 176-185.

Jarockyte G, Daugelaite E, Stasys M, Statkute U, Poderys V, Tseng TC, Hsu SH, Karabanovas V & Rotomskis R (2016). Accumulation and toxicity of superparamagnetic iron oxide nanoparticles in cells and experimental animals. *Int J Mol Sci,* 17.

Kacenka M, Kaman O, Kikerlova S, Pavlu B, Jirak Z, Jirak D, Herynek V, Cerny J, Chaput F, Laurent S & Lukes I (2015). Fluorescent magnetic nanoparticles for cell labeling: flux synthesis of manganite particles and novel functionalization of silica shell. *J Colloid Interface Sci,* 447: 97-106.

Kaewsaneha C, Jangpatarapongsa K, Tangchaikeeree T, Polpanich D & Tangboriboonrat P (2014). Fluorescent chitosan functionalized magnetic polymeric nanoparticles: Cytotoxicity and in vitro evaluation of cellular uptake. *J Biomater Appl,* 29: 761-8.

Kaewsaneha C, Tangboriboonrat P, Polpanich D & Elaissari A (2015). Multifunctional fluorescent-magnetic polymeric colloidal particles: Preparations and bioanalytical applications. *ACS Appl Mater Interfaces,* 7: 23373-86.

Kasten A, Gruttner C, Kuhn JP, Bader R, Pasold J & Frerich B (2014). Comparative in vitro study on magnetic iron oxide nanoparticles for MRI tracking of adipose tissue-derived progenitor cells. *PLoS One,* 9: e108055.

Kim JA, Aberg C, Salvati A & Dawson KA (2011). Role of cell cycle on the cellular uptake and dilution of nanoparticles in a cell population. *Nat Nanotechnol,* 7: 62-8.

Klebert E, (2017). *Untersuchung der zellulären Wechselwirkung von mit Dimercaptosuccinat ummantelten Eisenoxid-Nanopartikeln mithilfe von Kraftspektroskopie.* Master, University of Bremen.

Kumari S, Mg S & Mayor S (2010). Endocytosis unplugged: multiple ways to enter the cell. *Cell Res,* 20: 256-75.

Lamkowsky MC, Geppert M, Schmidt MM & Dringen R (2012). Magnetic field-induced acceleration of the accumulation of magnetic iron oxide nanoparticles by cultured brain astrocytes. *J Biomed Mater Res A,* 100: 323-34.

Lai SK, Hida K, Man ST, Chen C, Machamer C, Schroer TA & Hanes J (2007). Privileged delivery of polymer nanoparticles to the perinuclear region of live cells via a non-clathrin, non-degradative pathway. *Biomaterials,* 28: 2876-84.

Lesniak A, Salvati A, Santos-Martinez MJ, Radomski MW, Dawson KA & Aberg C (2013). Nanoparticle adhesion to the cell membrane and its effect on nanoparticle uptake efficiency. *J Am Chem Soc,* 135: 1438-44.

Lunov O, Syrovets T, Rocker C, Tron K, Nienhaus GU, Rasche V, Mailander V, Landfester K & Simmet T (2010). Lysosomal degradation of the carboxydextran shell of coated superparamagnetic iron oxide nanoparticles and the fate of professional phagocytes. *Biomaterials,* 31: 9015-22.

Luther EM, Petters C, Bulcke F, Kaltz A, Thiel K, Bickmeyer U & Dringen R (2013). Endocytotic uptake of iron oxide nanoparticles by cultured brain microglial cells. *Acta Biomater,* 9: 8454-65.

Mahmoudi M, Meng J, Xue X, Liang XJ, Rahman M, Pfeiffer C, Hartmann R, Gil PR, Pelaz B, Parak WJ, Del Pino P, Carregal-Romero S, Kanaras AG & Tamil Selvan S (2014). Interaction of stable colloidal nanoparticles with cellular membranes. *Biotechnol Adv,* 32: 679-92.

Mazuel F, Espinosa A, Luciani N, Reffay M, Le Borgne R, Motte L, Desboeufs K, Michel A, Pellegrino T, Lalatonne Y & Wilhelm C (2016). Massive intracellular biodegradation of iron oxide nanoparticles evidenced magnetically at single-endosome and tissue levels. *ACS Nano,* 10: 7627-38.

Mooren OL, Galletta BJ & Cooper JA (2012). Roles for actin assembly in endocytosis. *Annu Rev Biochem,* 81: 661-86.

Mortensen K & Larsson LI (2003). Effects of cytochalasin D on the actin cytoskeleton: association of neoformed actin aggregates with proteins involved in signaling and endocytosis. *Cell Mol Life Sci,* 60: 1007-12.

Nazarenus M, Zhang Q, Soliman MG, Del Pino P, Pelaz B, Carregal-Romero S, Rejman J, Rothen-Rutishauser B, Clift MJ, Zellner R, Nienhaus GU, Delehanty JB, Medintz IL & Parak WJ (2014). In vitro interaction of colloidal nanoparticles with mammalian cells: What have we learned thus far? *Beilstein J Nanotechnol,* 5: 1477-90.

Nowak JS, Mehn D, Nativo P, Garcia CP, Gioria S, Ojea-Jimenez I, Gilliland D & Rossi F (2014). Silica nanoparticle uptake induces survival mechanism in A549 cells by the activation of autophagy but not apoptosis. *Toxicol Lett,* 224: 84-92.

Oh N & Park JH (2014). Endocytosis and exocytosis of nanoparticles in mammalian cells. *Int J Nanomedicine,* 9: 51-63.

Ohsaki Y, Maeda T & Fujimoto T (2005). Fixation and permeabilization protocol is critical for the immunolabeling of lipid droplet proteins. *Histochem Cell Biol,* 124: 445-52.

Patel P, Kansara K, Senapati VA, Shanker R, Dhawan A & Kumar A (2016). Cell cycle dependent cellular uptake of zinc oxide nanoparticles in human epidermal cells. *Mutagenesis,* 31: 481-90.

Petri-Fink A, Steitz B, Finka A, Salaklang J & Hofmann H (2008). Effect of cell media on polymer coated superparamagnetic iron oxide nanoparticles (SPIONs):

Colloidal stability, cytotoxicity, and cellular uptake studies. *Eur J Pharm Biopharm,* 68: 129-37.

Petters C, (2015). *Uptake and metabolism of iron oxide nanoparticle in cultured brain cells.* Ph.D. Thesis, Univeristy of Bremen.

Petters C, Bulcke F, Thiel K, Bickmeyer U & Dringen R (2014a). Uptake of fluorescent iron oxide nanoparticles by oligodendroglial OLN-93 cells. *Neurochem Res,* 39: 372-83.

Petters C & Dringen R (2015). Accumulation of iron oxide nanoparticles by cultured primary neurons. *Neurochem Int,* 81: 1-9.

Petters C, Irrsack E, Koch M & Dringen R (2014b). Uptake and metabolism of iron oxide nanoparticles in brain cells. *Neurochem Res,* 39: 1648-60.

Petters C, Thiel K & Dringen R (2016). Lysosomal iron liberation is responsible for the vulnerability of brain microglial cells to iron oxide nanoparticles: Comparison with neurons and astrocytes. *Nanotoxicology,* 10: 332-42.

Pham BTT, Colvin EK, Pham NTH, Kim BJ, Fuller ES, Moon EA, Barbey R, Yuen S, Rickman BH, Bryce NS, Bickley S, Tanudji M, Jones SK, Howell VM & Hawkett BS (2018). Biodistribution and clearance of stable superparamagnetic maghemite iron oxide nanoparticles in mice following intraperitoneal administration. *Int J Mol Sci,* 19.

Prietl B, Meindl C, Roblegg E, Pieber TR, Lanzer G & Frohlich E (2014). Nano-sized and micro-sized polystyrene particles affect phagocyte function. *Cell Biol Toxicol,* 30: 1-16.

Pyrgiotakis G, Blattmann CO & Demokritou P (2014). Real-time nanoparticle-cell Interactions in physiological media by atomic force microscopy. *ACS Sustain Chem Eng,* 2: 1681-1690.

Rejman J, Oberle V, Zuhorn IS & Hoekstra D (2004). Size-dependent internalization of particles via the pathways of clathrin- and caveolae-mediated endocytosis. *Biochem J,* 377: 159-69.

Rivet CJ, Yuan Y, Borca-Tasciuc DA & Gilbert RJ (2012). Altering iron oxide nanoparticle surface properties induce cortical neuron cytotoxicity. *Chem Res Toxicol,* 25: 153-61.

Rothen-Rutishauser BM, Schurch S, Haenni B, Kapp N & Gehr P (2006). Interaction of fine particles and nanoparticles with red blood cells visualized with advanced microscopic techniques. *Environ Sci Technol,* 40: 4353-4359.

Safi M, Courtois J, Seigneuret M, Conjeaud H & Berret JF (2011). The effects of aggregation and protein corona on the cellular internalization of iron oxide nanoparticles. *Biomaterials,* 32: 9353-63.

Sandin P, Fitzpatrick LW, Simpson JC & Dawson KA (2012). High-speed imaging of Rab family small GTPases reveals rare events in nanoparticle trafficking in living cells. *ACS Nano,* 6: 1513-21.

Schmidt MM & Dringen R (2009). Differential effects of iodoacetamide and iodoacetate on glycolysis and glutathione metabolism of cultured astrocytes. *Front Neuroenergetics,* 1: 1.

Schnell U, Dijk F, Sjollema KA & Giepmans BN (2012). Immunolabeling artifacts and the need for live-cell imaging. *Nat Methods,* 9: 152-8.

Schweiger C, Hartmann R, Zhang F, Parak WJ, Kissel TH & Rivera Gil P (2012). Quantification of the internalization patterns of superparamagnetic iron oxide nanoparticles with opposite charge. *J Nanobiotechnology,* 10: 28.

See V, Free P, Cesbron Y, Nativo P, Shaheen U, Rigden DJ, Spiller DG, Fernig DG, White MR, Prior IA, Brust M, Lounis B & Levy R (2009). Cathepsin L digestion of nanobioconjugates upon endocytosis. *ACS Nano,* 3: 2461-8.

Semmling M, Kreft O, Munoz Javier A, Sukhorukov GB, Kas J & Parak WJ (2008). A novel flow-cytometry-based assay for cellular uptake studies of polyelectrolyte microcapsules. *Small,* 4: 1763-8.

Shan Y, Hao X, Shang X, Cai M, Jiang J, Tang Z & Wang H (2011). Recording force events of single quantum-dot endocytosis. *Chem Commun (Camb),* 47: 3377-9.

Shang L, Nienhaus K & Nienhaus GU (2014). Engineered nanoparticles interacting with cells: size matters. *J Nanobiotechnology,* 12: 1-11.

Skotland T, Sontum PC & Oulie I (2002). In vitro stability analyses as a model for metabolism of ferromagnetic particles (Clariscan), a contrast agent for magnetic resonance imaging. *J Pharm Biomed Anal,* 28: 323-9.

Smith PJ, Giroud M, Wiggins HL, Gower F, Thorley JA, Stolpe B, Mazzolini J, Dyson RJ & Rappoport JZ (2012). Cellular entry of nanoparticles via serum sensitive clathrin-mediated endocytosis, and plasma membrane permeabilization. *Int J Nanomedicine,* 7: 2045-55.

Soenen SJ, Parak WJ, Rejman J & Manshian B (2015). (Intra)cellular stability of inorganic nanoparticles: Effects on cytotoxicity, particle functionality, and biomedical applications. *Chem Rev,* 115: 2109-35.

Storey P, Lim RP, Chandarana H, Rosenkrantz AB, Kim D, Stoffel DR & Lee VS (2012). MRI assessment of hepatic iron clearance rates after USPIO administration in healthy adults. *Invest Radiol,* 47: 717-24.

Sun Z, Yathindranath V, Worden M, Thliveris JA, Chu S, Parkinson FE, Hegmann T & Miller DW (2013). Characterization of cellular uptake and toxicity of aminosilane-coated iron oxide nanoparticles with different charges in central nervous system-relevant cell culture models. *Int J Nanomedicine,* 8: 961-70.

Tang J, Liu Z, Ji F, Li Y, Liu J, Song J, Li J & Zhou J (2015). The role of the cell cycle in the cellular uptake of folate-modified poly(L-amino acid) micelles in a cell population. *Nanoscale,* 7: 20397-404.

Teplova VV, Tonshin AA, Grigoriev PA, Saris NE & Salkinoja-Salonen MS (2007). Bafilomycin A1 is a potassium ionophore that impairs mitochondrial functions. *J Bioenerg Biomembr,* 39: 321-9.

Thimiri Govinda Raj DB, Ghesquiere B, Tharkeshwar AK, Coen K, Derua R, Vanderschaeghe D, Rysman E, Bagadi M, Baatsen P, De Strooper B, Waelkens E, Borghs G, Callewaert N, Swinnen J, Gevaert K & Annaert W (2011). A novel strategy for the comprehensive analysis of the biomolecular composition of isolated plasma membranes. *Mol Syst Biol,* 7: 541.

Thimiri Govinda Raj DB & Khan NA (2016). Designer nanoparticle: Nanobiotechnology tool for cell biology. *Nano Converg,* 3: 22.

Tickle JA, Jenkins SI, Polyak B, Pickard MR & Chari DM (2016). Endocytotic potential governs magnetic particle loading in dividing neural cells: Studying modes of particle inheritance. *Nanomedicine (Lond),* 11: 345-58.

Tulpule K, Hohnholt MC, Hirrlinger J & Dringen R (2014). Primary cultures of astrocytes and neurons as model systems to study the metabolism and metabolite export from brain cells. *In:* Hirrlinger J & Waagepetersen HS (eds.) Brain Energy Metabolism. New York: Springer.

Tymianski M, Bernstein GM, Abdel-Hamid KM, Sattler R, Velumian A, Carlen PL, Razavi H & Jones OT (1997). A novel use for a carbodiimide compound for the

fixation of fluorescent and non-fluorescent calcium indicators in situ following physiological experiments. *Cell Calcium,* 21: 175-83.

Valois CR, Braz JM, Nunes ES, Vinolo MA, Lima EC, Curi R, Kuebler WM & Azevedo RB (2010). The effect of DMSA-functionalized magnetic nanoparticles on transendothelial migration of monocytes in the murine lung via a beta2 integrin-dependent pathway. *Biomaterials,* 31: 366-74.

Volatron J, Carn F, Kolosnjaj-Tabi J, Javed Y, Vuong QL, Gossuin Y, Menager C, Luciani N, Charron G, Hemadi M, Alloyeau D & Gazeau F (2017). Ferritin protein regulates the degradation of iron oxide nanoparticles. *Small,* 13.

Wang TT, Bai J, Jiang X & Nienhaus GU (2012). Cellular ptake of nanoparticles by membrane penetration: A study combining confocal microscopy with FTIR spectroelectrochemistry. *ACS Nano,* 6: 1251-1259.

Wilhelm C, Billotey C, Roger J, Pons JN, Bacri JC & Gazeau F (2003). Intracellular uptake of anionic superparamagnetic nanoparticles as a function of their surface coating. *Biomaterials,* 24: 1001-11.

Wilhelm C, Gazeau F, Roger J, Pons JN & Bacri JC (2002). Interaction of anionic superparamagnetic nanoparticles with cells: Kinetic analyses of membrane adsorption and subsequent internalization. *Langmuir,* 18: 8148-8155.

Zhang L & Liu Y (2017). Research of an iron oxide nanoparticles and potential application. *Toxicology Open Access,* 3: 3.

Zhang L, Wang X, Zou J, Liu Y & Wang J (2015a). DMSA-coated iron oxide nanoparticles greatly affect the expression of genes coding cysteine-rich proteins by their DMSA coating. *Chem Res Toxicol,* 28: 1961-74.

Zhang S, Gao H & Bao G (2015b). Physical principles of nanoparticle cellular endocytosis. *ACS Nano,* 9: 8655-71.

Zhang YQ, Dringen R, Petters C, Rastedt W, Koser J, Filser J & Stolte S (2016). Toxicity of dimercaptosuccinate-coated and un-functionalized magnetic iron oxide nanoparticles towards aquatic organisms. *Environ Sci-Nano,* 3: 754-767.

4. Appendix

4.1 Supplementary data

4.1.1 Potential uptake of coating material

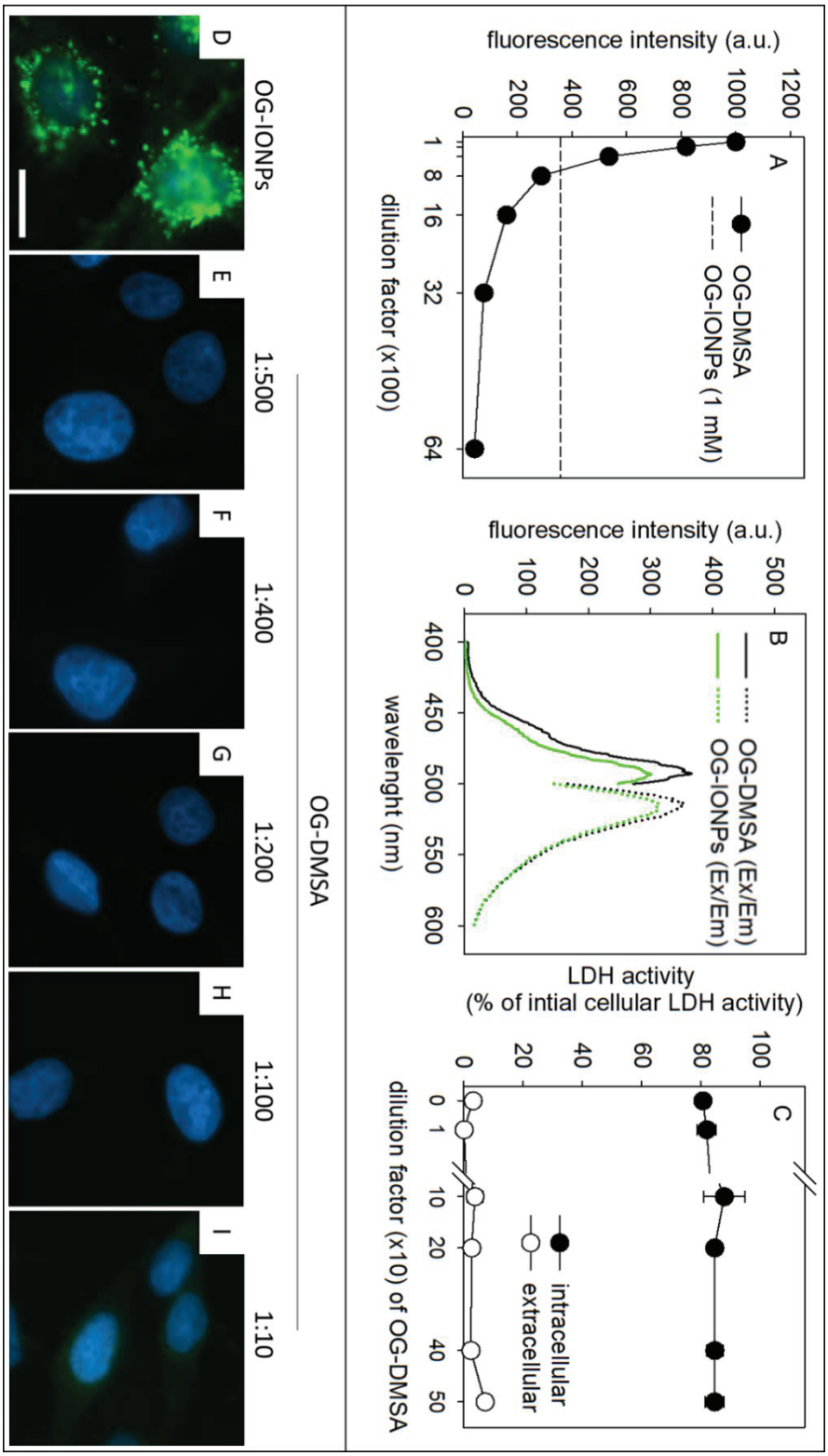

Fig. 4.1 Comparison of fluorescent OG-DMSA and OG-DMSA-IONPs. OG-DMSA (142.5 µM of OG) was synthesized as described (chapter 2.1), diluted in 50 mM NaOH and fluorescence intensities of the different dilutions were compared to the fluorescence intensity of 1 mM OG-IONPs in 50 mM NaOH (A). A dilution of the coating material of 1:500 in NaOH (28.5 nM dye) led to a similar fluorescence signal as that determined for 1 mM OG-IONPs. The excitation (emission at 516 nm) and emission (excitation at 492 nm) spectra of OG-DMSA (1:500 diltued) and OG-IONPs (1 mM) were recorded showing no differences in the excitation or emission peaks (B). C6 glioma cells were incubated with OG-DMSA in dilution up to 1:500 of the OG-DMSA in IB for 1 h at 37°C and intra- and extracellular LDH activity was measured as previously described (Dringen *et al.*, 1998, Tulpule *et al.*, 2014) showing no compromised viabilty compared to the control cells (C). Fluorescence microscopy picture were taken for cells exposed as previously described (chapter 2.1) for 1 h at 37°C to 1 mM OG-IONPs (D) or the given dilutions of OG-DMSA (E-I). Even incubation of C6 glioma cells with the highest concentration of OG-DMSA (I) did not cause any fluorescence staining in contrast to a strong perinuclear fluorescence pattern as observed in OG-IONPs treated cells (D). The cell nuclei were stained with DAPI (blue). The size bar in panel D represents 10 µm and applies for the panels D-I.

4.1.2 Influence of IONPs on C6 glioma cell proliferation

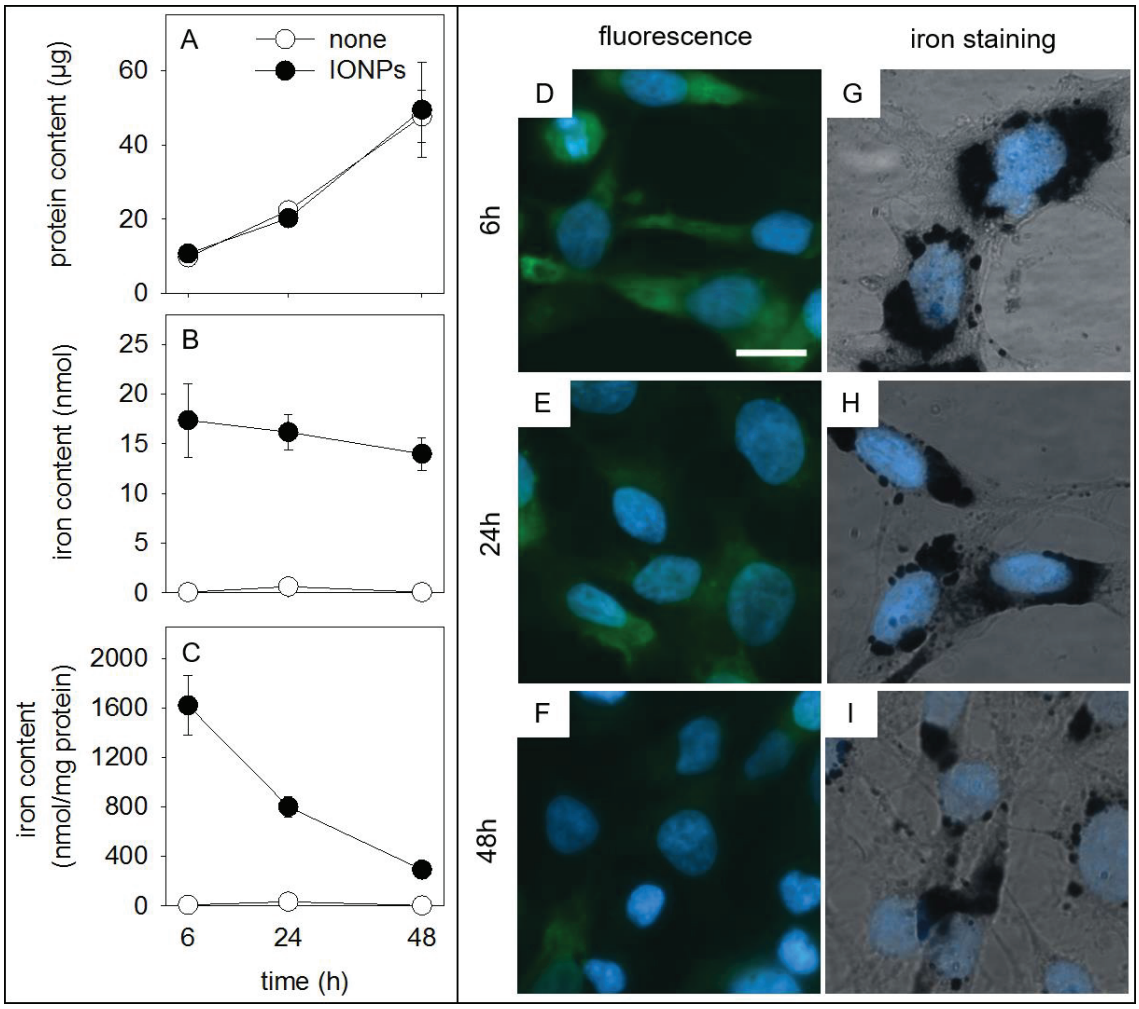

Fig. 4.2 C6 glioma cells were seeded in a density of 25.000 cells/well and grown for 24 h. Cells were washed with IB, incubated with 1 mM OG-IONPs in IB for 1 h at 37°C, washed twice with IB and cultured for 6 h, 24 h or 48 h in IONP-free DMEM containing 10% FCS at 37°C. Protein content (A) and iron content (B) were measured as previously described (Lowry *et al.*, 1951) (Geppert *et al.*, 2009) and the specific cellular iron content was calculated (C). Cellular localization of OG was monitored by fluorescence microscopy (D-F) and the localization of cellular iron was analyzed by cyctochemical staining as previously described (Geppert *et al.*, 2009, Rastedt *et al.*, 2017) (G-I). The cell nuclei were stained with DAP (blue) (chapter 3.2.). The size bar in panel D represents 10 µm and applies to the panels D-I. The data shown are means ± distance to the indivivual values of results obtained in two individual experiments.

4.1.3 Influence of cell cycle on IONPs distribution in C6 glioma cells

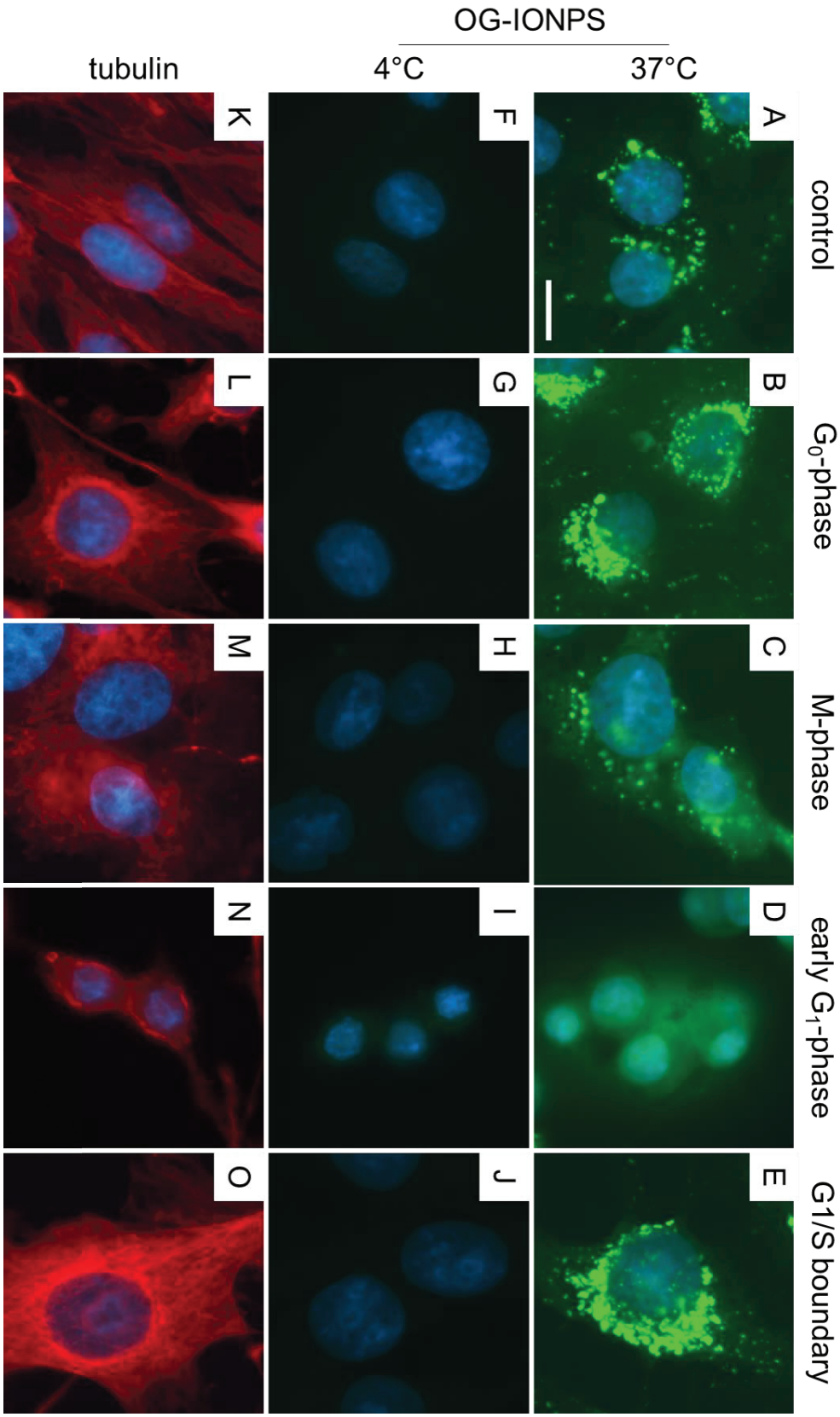

Fig. 4.3 Cell cylce and accumulation of OG-IONPs in C6 glioma cells. The cells were preincubated for 24 h under appropiate conditions to capture the cells in certain cell cycle state prior to the incubation with 1 mM OG-IONPs in IB for 1 h at 37°C (A-E) and 4°C (F-J) as described in chapter 2.1. The preincubation in DMEM containing 10% FCS (A,F,K) functioned as control for normal cell culture conditions. Alternatively, the cell were arrested in the G0 phase by preincubation without serum (0% FCS) (B,G;L), in the M phase by preincubation in 0.05 µM colchicine in DMEM/FCS (C,H,M), in the early G1 phase by preincubation in 2.5 µM simvastatin in DMEM/FCS (D,I,N) and at the G1/S boundary by preincubation in 1 mM hydroxyurea in DMEM/FCS (E,J). The cellular localization of OG was monitored by fluorescence microscopy (A-K) and cell morphology alteration were analyzed by immunohistochemistry staining as previously described (Stapelfeldt et al., 2017) against α-tubulin using a mouse anti-alpha-tubulin antibody (cloneDM1A) from Sigma-Aldrich (Steinheim, Germany) and the Cy3-conjugated goat anti mouse anitbody from Jackson ImmunoResearch (West Grove, Pennsyvania, USA) (K-O). The cell nuclei were stained with DAPI (blue). The size bar in panel A represents 10 µm and applies for all panels. Panels show representative images from two individually preformed experiments.

4.1.4 Nanopaticle pulse-chase experiment on astrocyte cultures

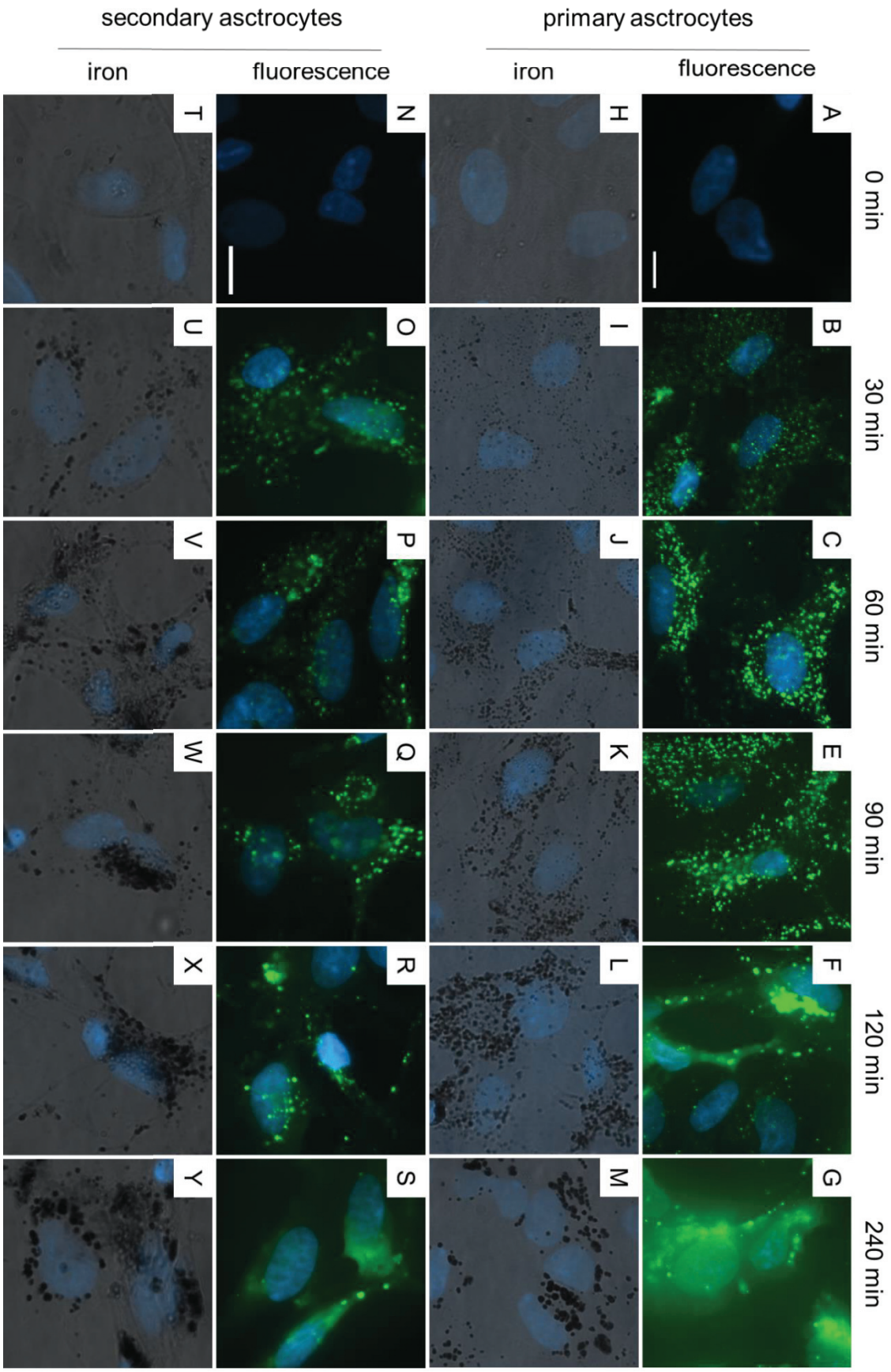

Fig. 4.4 Nanoparticle pulse-chase experiments with OG-IONPs on astrocyte-rich primary and secondary cultures. Astrocyte-rich primary and secondary cultures were obtained as previously described in (Petters and Dringen, 2014, Tulpule *et al.*, 2014) and nanoparticle pulse-chase experiments were performed as previously described (chapter 2.2). The cells were incubated with 1 mM OG-IONPs for 10 min at 4°C (nanoparticle pulse), unbound IONPs were removed by washing and the cultures were incubated (chase period) for up to 240 min. At the indicated time points the cellular OG fluorescence (A-G; N-S) was visualized using fluorescence microscopy and the localization of cellular iron by cytochemical staining (H-M, T-Y) as previously described (chapter 2.2). The cell nuclei were stained with DAPI (blue). The size bars in panels A and N represent 10 µm and apply for the panels A-M and N-Y, respectively.

4.1.5 Nanoparticle pulse-chase experiment on neuron cultures

Fig. 4.5 Nanoparticle puls-chase experiments with OG-IONPs on primary neurons. Cerebellar granule neuron cultures were prepared as recently described (Tulpule *et al.*, 2014) and nanoparticle pulse-chase experiments with OG-IONPS were performed as described in chapter 2.2. Extracellular LDH activity was determined as previously described (Dringen *et al.*, 1998) (A) and no loss in membrane integrity was detected during the 240 min of chase period. Cellular localization of OG was monitored by fluorescence microscopy (B-F) and the localization of cellular iron was analyzed by cyctochemical staining (G-K) as previously described (chapter 2.2). The cell nuclei were stained with DAP (blue) .The size bar in panel B represents 10 µm and applies to

4.1.6 Nanopaticle pulse-chase experiment on microglia cultures

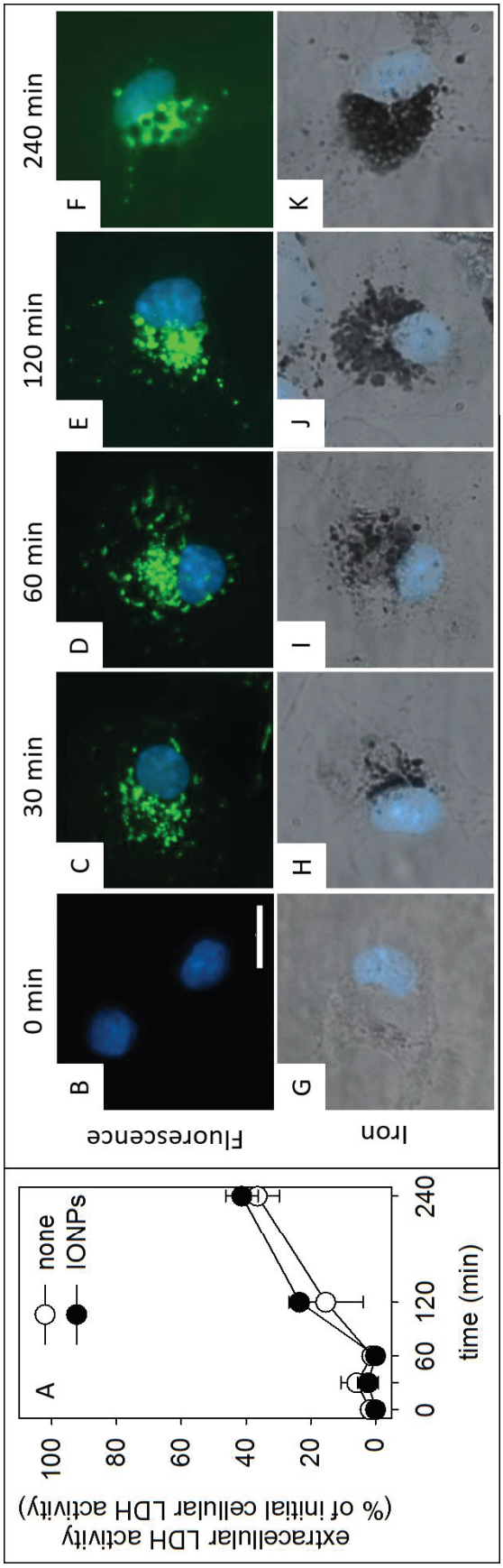

Fig. 4.6 Nanoparticle pulse-chase experiments with OG-IONPs on primary microglia. Microglia cultures were prepared as recently described (Luther et al., 2013) and nanoparticle pulse-chase experiments with OG-IONPS were performed as described in chapter 3.2. Extracellular LDH activity was determined as previously described (Dringen *et al.*, 1998) (A) and severe impairment of the membrane integrity was observed after 120 min of chase period in the presence as well as in the absence of IONPs during the pulse period. Cellular localization of OG was monitored by fluorescence microscopy (B-F) and the localization of cellular iron was analyzed by cytochemical staining (G-K) as previuosly described (chapter 2.2). The cell nuclei were stained with DAP (blue) (chapter 3.2.). The size bar in panel B represents 10 µm and applies to the panels (B-K). The data displayed represents data obtained in two individual experiments.

4.1.7 Fixation and permeabilization methods in immunocytochemistry

Table 4.1 Fixation and permeabilization methods applied for immunocytochemical colocalization studies

Fixation		**Permeabilization**
Mechanism	**Procedure**	
Cross-linking	3.5% (w/v) paraformaldehyde in PBS, 15 min, RT	0.1% Triton X-100 in PBS, 5-10 min, RT
		0.01% Digitonin, 30 min, RT
		100% Methanol, 5-10 min, -20°C
		70% Ethanol, 5-10 min, RT
		100 % Acetone, 5-10 min, -20°C
	3.5% (w/v) paraformaldehyde + 0.05% (w/v) glutaraldehyde in PBS,15 min, RT	0.1% Triton X-100 in PBS, 5-10 min, RT
		0.01% Digitonin in PBS, 30 min, RT
Dehydration/ precipitation	100% Methanol, 10 min, -20°C	no additional permeabilization step
	100% Acetone, 30 sec, -20°C	

To ensure good immunocytochemical stainings at least three main factors have to be address: (1) Preservation of the cell structure, (2) excess of the antibody to the desired antigen and (3) specific recognition of antibody and antigen to prevent unspecific background signal. For the preservation of the cell structures commonly used methods are based either on the cross-linking of proteins by using formaldehyde or glutaraldehyde or on the dehydration, and thereby precipitation of the proteins using organic solvents like alcohols and acetone (Van Ewijk *et al.*, 1984, Williams *et al.*, 1997, Glynn and McAllister, 2006). The fixation by cross-linking agents also requires an additional permeabilization step, whereas organic solvents already make the membrane permeable for small molecules like antibodies by dissolving membrane lipids (Ohsaki *et al.*, 2005, Jamur and Oliver, 2010).

4.1.8 References

Dringen R, Kussmaul L & Hamprecht B (1998). Detoxification of exogenous hydrogen peroxide and organic hydroperoxides by cultured astroglial cells assessed by microtiter plate assay. *Brain Res Brain Res Protoc,* 2: 223-8.

Geppert M, Hohnholt M, Gaetjen L, Grunwald I, Baumer M & Dringen R (2009). Accumulation of iron oxide nanoparticles by cultured brain astrocytes. *J Biomed Nanotechnol,* 5: 285-93.

Glynn MW & McAllister AK (2006). Immunocytochemistry and quantification of protein colocalization in cultured neurons. *Nat Protoc,* 1: 1287-96.

Jamur MC & Oliver C (2010). Permeabilization of cell membranes. *Methods Mol Biol,* 588: 63-6.

Lowry OH, Rosebrough NJ, Farr AL & Randall RJ (1951). Protein measurement with the Folin phenol reagent. *J Biol Chem,* 193: 265-75.

Luther EM, Petters C, Bulcke F, Kaltz A, Thiel K, Bickmeyer U & Dringen R (2013). Endocytotic uptake of iron oxide nanoparticles by cultured brain microglial cells. *Acta Biomater,* 9: 8454-65.

Ohsaki Y, Maeda T & Fujimoto T (2005). Fixation and permeabilization protocol is critical for the immunolabeling of lipid droplet proteins. *Histochem Cell Biol,* 124: 445-52.

Petters C & Dringen R (2014). Comparison of primary and secondary rat astrocyte cultures regarding glucose and glutathione metabolism and the accumulation of iron oxide nanoparticles. *Neurochem Res,* 39: 46-58.

Rastedt W, Thiel K & Dringen R (2017). Uptake of fluorescent iron oxide nanoparticles in C6 glioma cells. *Biomed Phys Eng Expr,* 3: 035007.

Stapelfeldt K, Ehrke E, Steinmeier J, Rastedt W & Dringen R (2017). Menadione-mediated WST1 reduction assay for the determination of metabolic activity of cultured neural cells. *Anal Biochem,* 538: 42-52.

Tulpule K, Hohnholt MC, Hirrlinger J & Dringen R (2014). Primary cultures of astrocytes and neurons as model systems to study the metabolism and metabolite export from brain cells. *In:* Hirrlinger J & Waagepetersen HS (eds.) *Brain Energy Metabolism.* New York: Springer.

Van Ewijk W, Van Soest PL, Verkerk A & Jongkind JF (1984). Loss of antibody binding to prefixed cells: Fixation parameters for immunocytochemistry. *Histochem J,* 16: 179-93.

Williams JH, Mepham BL & Wright DH (1997). Tissue preparation for immunocytochemistry. *J Clin Pathol,* 50: 422-8.

4.2 Curriculum vitae

Personal information

Name	**Wiebke Willmann (Maiden name: Rastedt)**
Birthday	25/05/1988 in Barßel, Germany

Education and work experience

04/2015 – 04/2018	**PhD thesis "Synthesis and Characterization of Fluorescent Iron Oxide Nanoparticles to Study Uptake and Intracellular trafficking of Nanoparticles in Neural Cells" in the research group of Prof. Ralf Dringen, Neurobiochemistry, University of Bremen, Germany**
07/2013 – 03/2015	Research assistant at Paul-Ehrlich-Institute (PEI), Federal Institute of Vaccines and Biomedicines, Langen, Germany Research topic: "Entry mechanism fo Hepatitis B Virus" in the research group of Prof. Eberhard Hildt, Virology, PEI
10/2010 – 02/2013	Master studies in Biochemistry (M.Sc.) at Medizinische Hochschule Hannover (MHH), Germany Master thesis: "Viral Determinants for Utilization of Claudin Proteins for Cell Entry by Hepatitis C Virus." in the research group of Prof. Thomas Pietschmann, Virology, Twincore
10/2011 – 03/2010	ERASMUS internship at the University of Dundee, Scotland Topic of research: "Characterizing the Role of GPR55 in Energy Metabolism" in the research group of Prof. Hari Hundal, Molecular Physiology, College of Life Science, University of Dundee
10/2007 – 09/2010	Bachelor studies in Biochemistry (B.Sc.) at the Leibniz University of Hannover (Germany) Bachelor thesis: "Analyses of Lipotoxicity in Insulin-Producing Cells." in the research group of Prof Sigurd Lenzen, Institute for Clinical Biochemistry, Medizinische Hochschule Hannover
06/2007	Graduation (Abitur) at the Albertus Magnus Gymnasium, Friesoythe, Germany

List of publications

Willmann W & Dringen R. How to study the consequences of an exposure of cultured neural cells to nanoparticles: The Dos and Don't forgets. *Submitted for publication*.

Willmann W & Dringen R. Monitoring of the cytoskeleton-dependent intracellular trafficking of fluorescent iron oxide nanoparticle in C6 glioma cells by nanoparticle pulse-chase experiments. *Submitted for publication*.

Rastedt W, Thiel K & Dringen R (2017). Uptake of fluorescent iron oxide nanoparticles in C6 glioma cells. *Biomed Phys Eng Expr,* 3: 035007.

Rastedt W, Blumrich EM & Dringen R (2017). Metabolism of mannose in cultured primary rat neurons. *Neurochem Res*, 42: 2282-2293.

Stapelfeldt K, Ehrke E, Steinmeier J, **Rastedt W** & Dringen R (2017). Menadione-mediated WST1 reduction assay for the determination of metabolic activity of cultured neural cells. *Anal Biochem,* 538: 42-52.

Joshi A, **Rastedt W**, Faber K, Schultz AG, Bulcke F & Dringen R (2016). Uptake and toxicity of copper oxide nanoparticles in C6 glioma cells. *Neurochem Res,* 41: 3004-3019.

Zhang YQ, Dringen R, Petters C, **Rastedt W**, Koser J, Filser J & Stolte S (2016). Toxicity of dimercaptosuccinate-coated and un-functionalized magnetic iron oxide nanoparticles towards aquatic organisms. *Environ Sci-Nano,* 3: 754-767.

Lipina C, **Rastedt W**, Irving AJ & Hundal HS (2013). Endocannabinoids in obesity: brewing up the perfect metabolic storm? *WIREs Membr Transp Signal* 2: 49-63.

Lipina C, **Rastedt W**, Irving AJ & Hundal HS (2012). New vistas for treatment of obesity and diabetes? Endocannabinoid signalling and metabolism in the modulation of energy balance. *Bioessays* 34(8): 681-91

4.3 Versicherung an Eides Statt

Ich, Wiebke Willmann (geb. Rastedt), Lange Straße 10, 26169 Friesoythe

Versichere an Eides Statt durch meine Unterschrift, dass ich die vorstehende Arbeit selbständig und ohne fremde Hilfe angefertigt und alle Stellen, die ich wörtlich dem Sinne nach aus Veröffentlichungen entnommen habe, als solche kenntlich gemacht habe, mich auch keiner anderen als der angegebenen Literatur oder sonstiger Hilfsmittel bedient habe.

Ich versichere an Eides Statt, dass ich die vorgenannten Angaben nach bestem Wissen und Gewissen gemacht habe und dass die Angaben der Wahrheit entsprechen und ich nichts verschwiegen hab.

Die Strafbarkeit einer falschen eidesstattlichen Versicherung ist mir bekannt, namentlich die Strafandrohung gemäß § 156 StGB bis zu drei Jahren Freiheitsstrafe oder Geldstrafe bei vorsätzlicher Begehung der Tat bzw. gemäß § 161 Abs. 1 StGB bis zu einem Jahr Freiheitsstrafe oder Geldstrafe bei fahrlässiger Begehung.

_____ _____

Ort, Datum Unterschrift